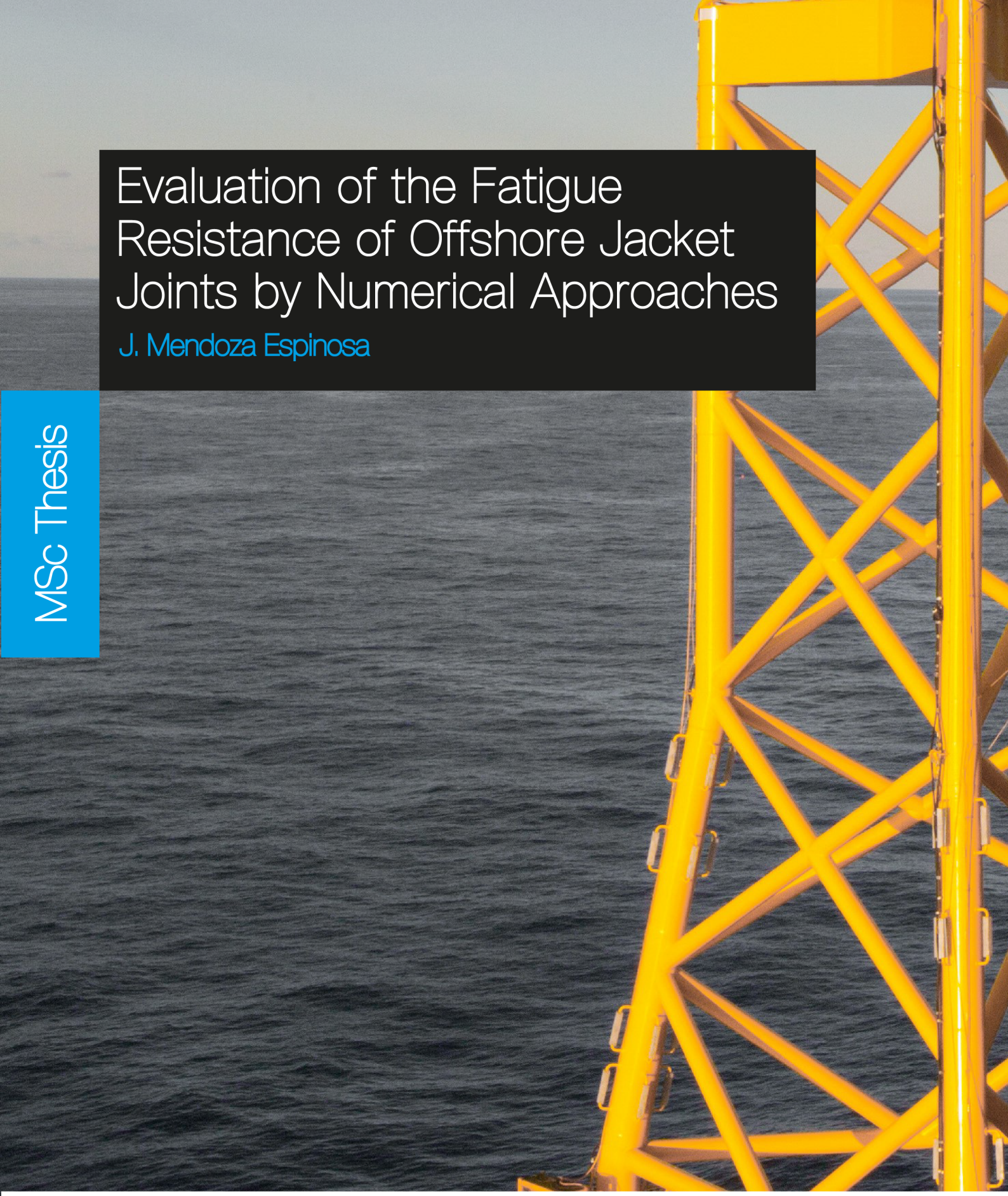

Evaluation of the Fatigue Resistance of Offshore Jacket Joints by Numerical Approaches

J. Mendoza Espinosa

MSc Thesis

EWEM

TU Delft

NTNU

RAMBOLL

Offshore Engineering

Evaluation of the Fatigue Resistance of Offshore Jacket Joints by Numerical Approaches

As a partial requisite for obtaining the degree of MSc in Offshore and Dredging Engineering at the Delft University of Technology and the MSc in Technology-Wind Energy at the Norwegian University of Science and Technology.

Jorge Mendoza Espinosa

September 27, 2017

MSc Thesis

Department of Offshore Engineering (TU Delft)
Department of Civil and Environmental Engineering (NTNU)
Department of Marine Technology (NTNU)

Chairman: Prof. Dr.-Ing. Andrei Metrikine
Chairman: Prof. Dr. Michael Muskulus
Supervisor at the TU Delft: Dr.-Ing. Eliz-Mari Lourens
Supervisor at Ramboll: Dr.-Ing. Marc Voßbeck

Abstract

Jacket support structures are a preferred solution for offshore wind turbines in deeper waters. The lattice structure has advantages over other types of support structures, such as the high strength to weight ratio and the inherent property of the tubular members minimizing hydrodynamic forces. Extensive knowledge exists in relation to its construction technique as well as its crucial components, but due to considerable cost pressure, continued optimization is essential for the future competitiveness of the concept in the offshore wind business. A significant share of the overall production costs of jacket structures is related to the joints connecting the tubular members. Hence, these joints along with their complex welds are of special interest in terms of cost reduction.

The design of tubular joints is generally driven by the fatigue resistance. The hot-spot method, as described in standards (e.g. DNV or IIW), is commonly used in practice. Parametric formulae for several joint situations have been developed by some authors in order to estimate the Stress Concentration Factors (SCF) at the connections. However, the size, complexity and cost of these joints lead engineers to perform analyses with detailed FE models in order to assess their fatigue resistance.

When defining a numerical model, assumptions have to be made. These decisions influence the obtained output. Several aspects that have an impact on the results of the models are identified. The following topics are found to require further research and are going to be investigated within this project: (1) influence of using solid elements versus shell elements in the modelling of the joint members; (2) degree of accuracy of the Efthymiou equations; (3) influence of the carry-over effect in multiplanar KK-joints; (4) differences in the fatigue life predictions between the hot-spot and the effective notch stress methods.

Guidelines recommend the use of both solid and shell theories for the definition of the FE models used in the hot-spot fatigue assessment. Both options are compared in terms of accuracy of the results and computational time. Generally speaking, significant differences are found between both models. The background of the differences is studied. Moreover, it is investigated in which cases the use of solid elements can be beneficial in terms of the optimization of the joint.

The employment of the Efthymiou formulae is common in practice. These equations provide the SCF at the locations around the weld where they are found to be maximum. The stress is found as the superposition of the hot-spot stress obtained due to several load cases. Therefore, the use of this approach carries two sorts of uncertainty. One is directly related to the values that the equations predict. The second one stems from the lack of information on the results at the other positions around the weld. The output of this approach is compared with the results of numerical models. The validity of its use is quantified.

Offshore wind jacket joints are mainly multiplanar KK-joints. Loading in the braces of one face of the jacket may yield significant carry-over effects on the out-of-plane braces connected to the same joint. FE models are built for different multiplanar KK-joint situations to investigate the accuracy of modelling the joint as a planar K-joint. In general, it is found that the carry-over effect cannot be neglected and the assumption is not accurate.

The fatigue assessment of tubular joints by means of the hot-spot method is subjected to several assumptions that limit the optimization of the members. The notch concept is a more realistic method that is presented as an alternative. However, this method is not widely used in engineering practice. Its main drawbacks are the difficulties in building the numerical model and the required high computational times. An algorithm to carry out the effective notch stress assessment, based on the sub-modelling technique, is proposed. An example of a full SCF assessment of a K-joint is provided, giving an insight into the feasibility of the implementation of this method in the routines of engineering consulting companies. A comparison of the fatigue life prediction, between the hot-spot and the effective notch methods, is carried out. The latter method is found to predict a higher fatigue life for many of the situations tested. Since this method allows for a more detailed modelling, the weld profile can also be designed in order to optimize the fatigue resistance. A parametric investigation of the influence of the weld slope is performed. This parameter is found to have a significant impact on the results.

Preface and Acknowledgments

This MSc Thesis is conducted for the purpose of achieving the MSc Offshore Engineering and Dredging degree at the TU Delft and the MSc Technology-Wind Energy degree at the NTNU. The studies have been part of the Offshore Engineering track of the European Wind Energy Masters.
The work here presented has been carried out at the Ramboll offices in Hamburg during the months of February to August of the year 2017. The preliminary work was done as part of the TMR 4590 Specialization Project at the NTNU, in Trondheim. The outcome of that project was summarized in the paper *J. Mendoza (2017)* [1].
I would like to express my gratitude to my supervisors Dr.-Ing. M. Voßbeck (Ramboll), Dr.-Ing. E. Lourence (TU Delft), Prof. M. Muskulus (NTNU) and Ing. S. Schafhirt (NTNU) for their assistance and guidance throughout the development of this project.
This master's programme has been a great experience. I have broaden my horizons and I became a more tolerant and complete person. I have shared this time with ambitious and talented people that have the honest desire of using their knowledge to change and improve the world. I want to acknowledge the moral support that my family and friends have provided me during all these months. I want to thank in particular to Tuna Baydın for her love and patience, that she showed to me everyday. Also, I want to mention my fellow students, with whom I have shared so many moments during these two years: J. Norbruis, C. Owen, M.B. Rhomberg, I. Rivera and V. Van de Putte.
Finally, I want to appreciate the people working at Ramboll in Stadtdeich for their kind attitude and the always welcoming feeling. It has been a pleasure working closely with Marc; the good discussions and his experience are imprinted on this work.

Jorge Mendoza Espinosa

Ramboll Wind & Towers
Technical University of Delft
Norwegian University of Science and Technology

Hamburg, August 29, 2017

Contents

Nomenclature

Greek

β	Non-dimensional diameter	[-]
γ	Solidity ratio, i.e. ratio between the chord radius and its thickness	[-]
σ_k	Effective notch stress	[Pa]
σ_s	Structural stress	[Pa]
σ_x	Normal stress due to axial internal force	[Pa]
σ_{my}	Normal stress due to in-plane bending moment	[Pa]
σ_{mz}	Normal stress due to out of plane bending moment	[Pa]
τ	Non-dimensional thickness	[-]
θ	Relative angle between chord and brace	[Degree]
ζ	Dimensionless gap	[-]
S_x	Normal stress in the x direction referred to a specified local coordinate system	[Pa]

Roman

$\log \overline{a}$	Intercept of the x-axis of the SN-curve	[-]
NSCF_{eqv}	Equivalent notch stress concentration factor	[-]
SCF_{eqv}	Equivalent hot-spot stress concentration factor	[-]
a	Crack length	[m]
a_i	First extrapolation point at brace i	[m]
a_N	Notch SN-curve constant	[-]
a_T	T-curve constant	[-]
a_{0C}	First extrapolation point at the chord crown	[m]
a_{0S}	First extrapolation point at the chord saddle	[m]
a_c	Critical crack length	[m]
b_i	Second extrapolation point at brace i	[m]
b_{0C}	Second extrapolation point at the chord crown	[m]
b_{0S}	Second extrapolation point at the chord saddle	[m]
d_0	Chord diameter	[m]
d_1	Brace diameter	[m]
e	Total eccentricity	[m]
e_i	Eccentricity related to brace i	[m]
g	Total gap	[m]

g_i	Part of the joint gap related to brace i	[m]
K	Stress intensity factor	[MPa$\sqrt{\text{m}}$]
k	Thickness exponent	[-]
k_w	Weld shape factor	[-]
K_c	Fracture toughness	[MPa$\sqrt{\text{m}}$]
N	Number of cycles to failure for a given stress range	[-]
n_{tt}	Number of solid elements across the wall thickness of a member	[-]
r_0	Chord radius	[m]
r_1	Brace radius	[m]
S	Nominal stress range	[Pa]
S_y	Yield strength	[Pa]
t_0	Chord thickness	[m]
t_1	Brace thickness	[m]
t_{ref}	Reference thickness	[m]

List of Abbreviations

BAL	=	Balanced Axial Load
CAPEX	=	CAPital EXpenditures
CHS	=	Circular Hollow Section
CPU	=	Central Processing Unit
DOF	=	Degrees of Freedom
DWT	=	Distance to the Weld Toe
ET	=	Element Type
FE	=	Finite Element
FEA	=	Finite Element Analysis
FEM	=	Finite Element Method
FLS	=	Fatigue Limit State
GCS	=	Global Coordinate System
HSS	=	Hot-Spot Stress
IPB	=	In-plane Bending
LC	=	Load Case
LCS	=	Local Coordinate System
MPC	=	Multi-Point Constraint
MRC	=	Mesh Reference Code
MSc	=	Master in Science
NSCF	=	Notch Stress Concentration Factor
OPB	=	Out-of-plane Bending
OPEX	=	OPerational EXpenditure
OWT	=	Offshore Wind Turbine
SCF	=	Stress Concentration Factor
SCF_{AC}	=	Stress Concentration Factor due to axial internal force
SCF_{MIP}	=	Stress Concentration Factor due to in-plane bending moment
SCF_{MOP}	=	Stress Concentration Factor due to out of plane bending moment
ULS	=	Ultimate Limit State
WT	=	Weld Toe
std	=	standard deviation

1 | Introduction

While the offshore wind energy industry keeps on growing, so does the market pressure for making it price competitive with the other energy alternatives. 97% [2] of the offshore wind turbines installed in Europe in 2015 were founded on monopiles, often the simplest and cheapest alternative for shallow and intermediate waters (water depths up to around 30 m) together with gravity base concepts. Although the offshore environment may look immense, the space allocated for the development of offshore wind farms is reduced. Moreover, the areas where monopile foundations are suitable alternatives are even more limited. Therefore, other alternatives, such as jacket structures or floating concepts, require further development and optimization in order to suit the demand of offshore wind farms. The remaining 3% of the support structures installed in 2015 were jacket type.

Jackets are lattice truss steel support structures constituted by tubular circular hollow section (CHS) beams welded together and founded to the sea bed on piles, suction buckets or gravity base foundations[1]. This solution provides, using a minimum amount of steel, a high moment of inertia to compensate the environmental overturning moments. However, the main drawback of this material saving solution is the amount of weldings to be performed in order to assemble the tubular beams. This yields high costs in the fabrication and uncertainty in the structural analysis. The design of these joints are generally driven by fatigue failure. Therefore, further studies in the fatigue assessment of welded tubular joints are motivated by two main reasons: on the one hand, optimizing the joints themselves and on the other hand, avoiding non-conservative designs resulting from an insufficient understanding of the fatigue phenomena.

The jacket concept has been widely used in the Oil & Gas offshore industry during the last decades. However, the risk management of structures, i.e. the agreement between safety and costs, usually results in over-engineered designs that do not satisfy the requisites of the offshore wind market. Nevertheless, a large literature related to the fatigue assessment of tubular joints exists and a thorough review of the state of the art is essential for this project.

1.1 Research topic and goals

The goal of this work is to gain a better understanding of the various methods used in the fatigue assessment of tubular joints. Several research topics have been identified to require further research. This work is going to address four topics, answering the following research gaps:

1. ***Are plate elements a valid alternative for the hot-spot assessment using numerical methods?*** DNV-GL [3] allows the use of both volume and shell elements for the fatigue assessment of tubular joints following the hot-spot methodology. No clear guidelines are given for when to use which type of method, or about the differences between both ways of modelling. A comparison between using volume and shell elements is to be carried out. First of all, the assumption of having a linear through thickness stress field at the read-out points is to be studied. A comparison of the stress field normal to the weld, predicted by the solid and shell models, is to be performed at several locations and for various load cases. The SCF are to be compared and the background of the differences discussed. In order to broaden the validity of the conclusions made, the investigation is to be performed within a parametric study, covering several combinations of chord and brace diameter, thickness and inclination angle.

2. ***What is the degree of accuracy of the Efthymiou equations?*** In the original papers published by *Efthymiou et al. (1985)* [4] and *Efthymiou (1988)* [5], the widely used parametric

[1] Originally the concept jacket was attributed to the truss-frame structures whose piles are driven through the legs and welded above sea level. However, nowadays it is common to use the name jacket, as well, to call the tower truss-frame structures, whose piles are connected to sleeves around the legs at the base of the structure.

formulae were introduced and their fitting to the FE models was discussed. Nevertheless, the SCF formulae for K-joints were given for the hot-spot positions only. This means that the SCF at the other positions around the weld is not given and it can only be estimated in a conservative way. Therefore, the superposition principle, which is used in the computation of the structural stress, would result in a different degree of inaccuracy on the conservative side. An investigation and discussion of these equations is to be carried out. The results of the parametric study mentioned in the previous point is to be completed with the output of these equations. A quantitative study of their applicability and the degree of conservatism implicit in their use is to be discussed.

3. ***Can multiplanar KK-joints be modelled as planar K-joints?*** In reality, jacket joints are constituted by the assembly of multiplanar joints, most of them being the KK-type. The concepts of influence functions and carry-over effect were introduced by *Efthymiou (1988)* [4], covering the multiplanar joints case. Nevertheless, DNV-GL [3] do not include formulae for multiplanar KK-joints and therefore, the fatigue assessment of these joints is considered by the planar K-joints analogues. Further optimization of the members is sought after in order to make jackets cost competitive. A quantitative study of the differences between the solutions obtained by the two methods is to be performed. Different KK-joint configurations are to be generated and compared for various load cases. This will create an overview of the degree of inaccuracy implicit in the assumption of modelling a KK-joint as a K-joint. Guidelines are to be given for when this assumption is not acceptable.

4. ***Can the effective notch stress method be a feasible alternative for the assessment of tubular joints?*** As mentioned at the beginning of this chapter, jackets are not a popular support structure for offshore wind. Further optimization is required to make them cost competitive with monopiles for the intermediate water depths where monopiles are still a feasible solution. The optimization of the jackets mainly focuses on their tubular joints, whose design is generally driven by fatigue. The general assumptions of the hot-spot method limit the optimization of these joints. More advanced methods are generally not used in practice due the numerical modelling challenges and the lack of knowledge of the potential material savings. Little experience exists in the use of this method for the assessment of tubular joints. An algorithm for the employment of this approach in a practical way is to be developed. The assumptions and decisions made for the execution of the approach are to be reported. The notch concept is a more detailed and accurate way of assessing the stresses at the weld, where the highest concentration factors are found. This model will provide a better understanding of the stress distribution at the jacket joints. This is to be used as a benchmark for the comparison of the other fatigue assessment methods. The differences in the SCF, obtained by the notch and hot-spot methods, are to be compared.

1.2 Thesis layout

In Chapter 2, a theoretical background that serves as a basis for this Thesis is presented. The literature review of the topics relevant for the investigations covered in this work is given in Chapter 3. The investigation of the use of solid and shell elements for the hot-spot method is carried out in Chapter 4. The results of that investigation are compared with the ones obtained using the Efthymiou equations in Chapter 5. The carry-over effect of the out-of-plane braces in multi-planar KK-joints is studied in Chapter 6. In Chapter 7, an algorithm for the assessment of the effective notch stress in tubular joints is developed. An example of the employment of that algorithm applied to a K-joint is included. The results of the parametric investigation of the hot-spot method are compared with the ones from the effective notch stress concept. A summary of the project and the general conclusions that are drawn from the results of the investigations are reviewed in Chapter 8. Finally, the future work that can be followed from this project is discussed.

2 | Review of the Fatigue Theory

Offshore wind jacket structures are lattice structures that consist of the assembly of Circular Hollow Section (CHS) tubular members. This typology of beams is used due to two main facts:

1. Their good behavior against the given environmental conditions, i.e. a CHS yields small drag from the wave and current actions and its symmetry provides a similar resistance for the variable wind and wave headings.

2. Their small exposed area optimizes the material performance in terms of corrosion and fire resistance and therefore, the maintenance. In the development of offshore wind farms, the OPEX is a crucial part of the total cost, i.e. ca. 20% of the CAPEX [11].

Offshore wind jacket structures are mainly loaded by wind, waves and current; which induce high static loading, dynamic effects and fatigue during the whole lifetime of 20 years. Fatigue is the driving failure mechanism of the welded connections of the tubular members that constitute the jackets. A summary of the fatigue theory focused on tubular joints is described in this chapter.

2.1 Fatigue of Tubular Joints

A metallic structural component that is subjected to a cyclic loading below the yield strength is still susceptible to fail. The phenomenon that causes failure when the cyclic loading is acting long enough, i.e. for a certain amount of cycles, is called fatigue. The way of approaching fatigue in engineering practice does not often reflect the physics behind.

Fatigue failure is caused by crack propagation and therefore, by the reduction in strength when a crack is long enough. The nature of the fatigue failure is completely different than the Ultimate Limit State (ULS) failure. Due to that, the variation of basic parameters, such as the member thickness and diameter, the steel class, etc., affects the Fatigue Limit State (FLS) in a different way than the ULS. In fact, it would sometimes be non-intuitive if the nature of the phenomenon was disregarded. An example of this is the influence of the yield strength in the fatigue life. It can be observed in Figure 2.1, that increasing the yield strength has a minor effect in the fatigue resistance. The tendency is almost a horizontal line, particularly for butt welds. The improvement in the production of steels and the increase in the yield strength, especially in the naval and offshore businesses, resulted in fatigue being one of the main driving mechanisms of failure. When designing a naval component to optimality for the ULS using high strength steels, there is a point in which the ULS is not the driving failure mechanism anymore.

The effect of varying the wall thickness is another technological factor whose effect is contrary to what could be expected. Increasing the cross section of a component actually leads to a smaller fatigue resistance. This effect has been widely investigated [13, 14, 15]. It can be explained by the fact that, while increasing the wall thickness, the quality of the steel decreases and there is a higher likelihood for defects to be present. Thus, the probability of crack initiation also increases. Moreover, the initial crack will experience a lower stress in a thinner plate [12]. The thickness effect is covered in guidelines [3, 16, 17], as it will be shown later in this chapter.

Welded joints are specially prone to fail due to fatigue when cyclic loading is acting. The welding methods inevitably introduce imperfections, where the cracks tend to initiate. Slag intrusions in the order of 0.1 mm tend to appear in the fusion line. Moreover, the weld geometry itself means a stress concentration. When designing the weld, the ULS and the FLS have to be analyzed. However, the goal and design parameters are quite different between both kinds of tests. The main objective when designing a weld due to ULS is to assure that the weld joint will resist as much as the parent material.

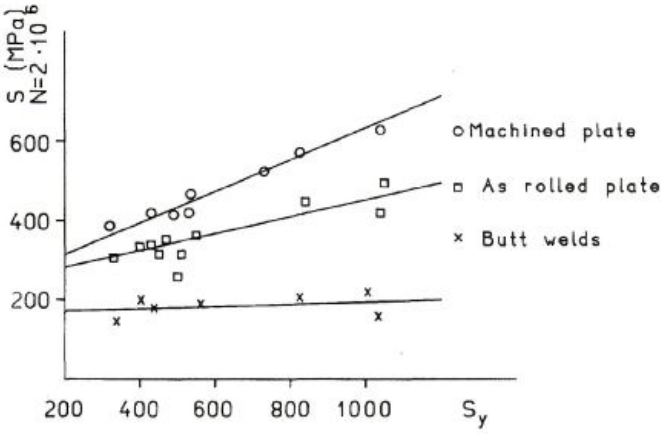

Figure 2.1: *Effect of increasing the steel yield strength on the fatigue strength (resistance at* $2 \cdot 10^6$ *cycles in the SN-curve) for machine plate, as rolled plate and butt welds. Picture taken from [12].*

As a result, the weld throat is defined. However, this philosophy is not feasible for the FLS. The fatigue failure takes place at the locations where the stresses are the highest. The weld joint is assumed to be the weakest link under fatigue considerations. The stress concentration at the joint is dependent on the geometry and the dimensions of the joint. Hence, the effort is rather concentrated on the design of other parameters, such as the diameter and thickness of the members that constitute the welded union. These parameters can be varied in the vicinity of the joint if necessary. Furthermore, the radius of curvature of the weld ρ, shown in Figure 2.2, is crucial due to the notch effect in an area where local stresses are naturally high. However, this parameter is not generally designed using mathematical models, but by recommended practice based on experience.

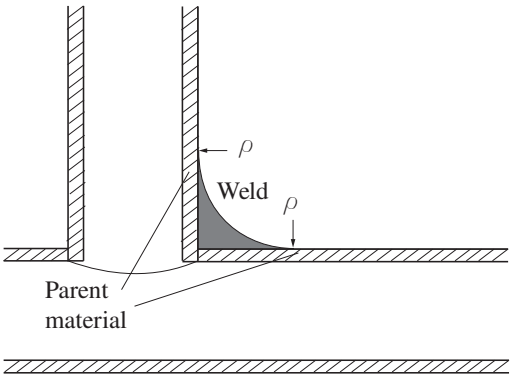

Figure 2.2: *Schematic representation of a tubular welded joint.*

In practice, the fatigue resistance is assessed by four main approaches, i.e. fracture mechanics, nominal stress, structural stress and notch stress. A brief description of the these methods is presented hereafter.

Fracture mechanics approach

Although this method is not going to be used in this work, it is going to be briefly discussed in this chapter, since it gives a good understanding of the physics behind the fatigue failure. The fatigue crack growth of steel in air shows three distinguishable regions, as sketched in Figure 2.3:

1. The Region (I) is the threshold region, where the crack initiates. It can be considered as a transient part before the crack growth rate becomes relatively stable during the finite life region. The crack initiates at the threshold value ΔK_{th}. In this region, the crack growth rate is driven by the micro-structure of the material, the mean stress and the environmental conditions.

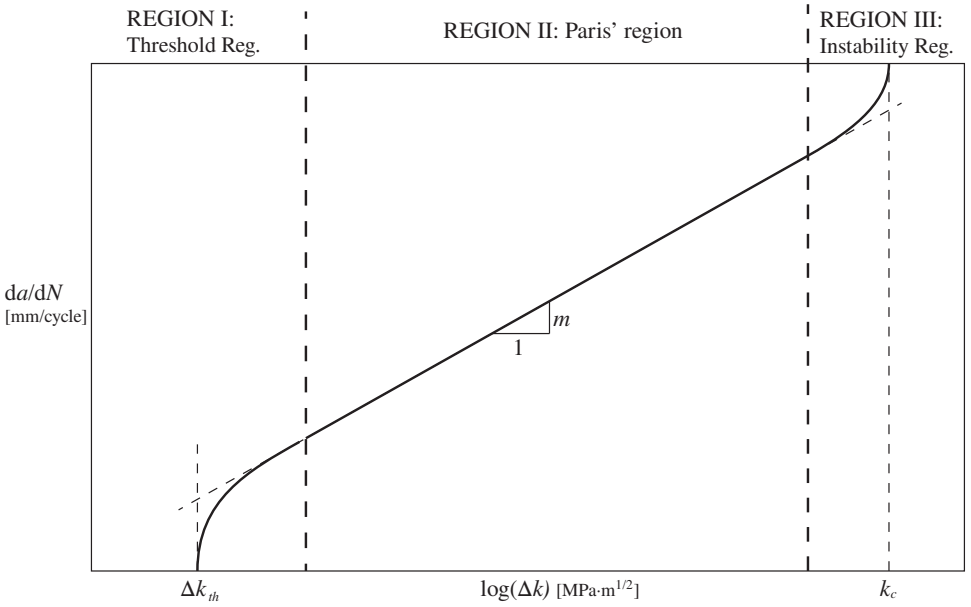

Figure 2.3: *Generic sketch of the fatigue crack growth rate curve for steel in air.*

2. The Region (II) is the finite life region, also known as the Paris' region. For configurations such as welded joints, most of the fatigue life happens in this region. The Paris' law in Eq. (2.1) applies. The slope of the line m is the same as in the SN-curves, explained later in this chapter. C is a fitting parameter whose dimensions depend on the value of m.

$$\frac{\mathrm{d}a}{\mathrm{d}N} = C(\Delta K)^m \tag{2.1}$$

3. The Region (III) is the instability region. It is characterized by a fast crack growth and an imminent failure. The loads and the crack length have overcome the fracture toughness K_c of the material and therefore, the critical crack length a_c. This results in an unstable crack growth, which is not driven by the environmental conditions but by the micro-structure and the mean stress.

In practice, this approach is not used for the design of structures due to fatigue. This can be explained by three main reasons:

1. The assessment depends on the crack initial geometry, i.e. the crack length a and the crack shape, which either is not known or is difficult to model realistically. Moreover, the model is very sensitive to the initial crack length a_i, which is not always possible to be measured with enough accuracy.

2. A significant part of the fatigue life happens in the threshold region, where the crack growth strongly depends on the micro-metallurgy. Furthermore, the fracture mechanics approach uses an extrapolation of the Paris' law within that region, which is a quite conservative assumption.

3. Elastic fracture mechanics is valid for crack lengths $a < 2.5(\frac{K}{S_y})^2$. This implies that the theory is not valid for small cracks, i.e. cracks in the order of 0.1 mm.

A case in which fracture mechanics has applicability is in the design of maintenance strategies of aerospace and offshore structures and in the calculation of the residual fatigue life. When designing a structure based on the fail safe philosophy, crack initiation is allowed and corrective maintenance occurs when the crack length reaches a certain threshold. Therefore, the modelling of the crack propagation is crucial to estimate when the corrective actions ought to be taken, based on the preventive maintenance observations. Another application of this method is found for the assessment of the fatigue failure for

cracks initiating at the weld root [18]. The SN-curves are defined under the assumption of cracks initiating at the weld toe. The root failure has been found to be relevant [19]. It can only be assessed, alternatively, by corrections of the nominal and hot-spot methods or by the notch concept, which requires rather complex FE models.

Nominal stress method

The nominal stress method is the most common approach for the fatigue assessment. It is a semi-empirical method used for predicting the lifetime of a structural component. Given a stress range and a cycle history, SN-curves are used to determine the fatigue resistance and thus, the remaining fatigue lifetime or failure of the situation under study. The SN-curves are regression curves of empirical data obtained by intensive campaign of destructive fatigue testing of scaled specimens. The stress range S is plotted in the y-axis, while the x-axis shows the number of cycles to failure, also called endurance. Notice that although in [3] the stress range uses the nomenclature $\Delta\sigma$, in this text S will be used for consistency. The Greek character σ will be used for the local stress. Eq. (2.2) shows the expression of the SN-curve given in [3].

$$\log N = \log \overline{a} - m \log \left(S \left(\frac{t}{t_{ref}} \right)^k \right) \tag{2.2}$$

It should be noted that it is accounted for the thickness effect through a penalty factor on the stress range. For tubular joints, the reference thickness t_{ref} is 16 mm. When following the T-curve, the thickness exponent k is set to 0.25. In order to understand the magnitude of this effect, let t be 30 mm. This would yield an increment of 17% in the applied stress range, meaning a 60% reduction in the fatigue life.

Notice that the influence of the mean stress is considered negligible and thus, the stress range S suffices to characterize the stress state. This fact is supported by evidence and it has been widely studied [12, 7]. Only when post-welding treatments are applied and the structure is free of secondary stresses, it may be advantageous to account for the mean stress correction [20].

The SN-curves account for the scatter in the fatigue tests through $\log \overline{a}$, i.e. the intercept of the curve with the x-axis. If $\log a$ is related to the regression line of the scatter test data, $\log \overline{a}$ is $\log a - 2 \cdot \text{std}$. Where, std is the standard deviation of the scatter data. This consideration reduces the uncertainty to approximately 2.3% probability of failure [21]. If the logarithmic scale is used, these curves become straight lines, whose slopes are rounded to an integer for ease in computation. The curves are divided in two parts. The first part is related to low cycle fatigue and the second part to high cycle fatigue. The transition between both parts occurs at the so called fatigue limit. If only constant amplitude stress history is considered, a stress range lower than the fatigue limit would result in infinite life. For variable amplitude stress history, DNV-GL [3] follows the Haibach correction [22]. All the SN-curves but the B-curves have a slope of three during the first part of the curve. Below the fatigue limit, the slope is set to $2m - 1$, hence five for all the curves but for the B-curves.

SN-curves are categorized for several tabulated situations. 15 SN-curves are defined in total: B1, B2, C, C1, C2, D, E, F, F1, F3, G, W1, W2, W3, T; cf. Figures 2.4 and 2.5. Since all the curves from C to T have the same slope, similarity of the results is found by scaling with a linear factor [21]. Only the nominal stress is considered since some of the local stress magnifications are accounted for implicitly in the SN-curves, depending on the tabulated details. It can be concluded that the accuracy of this procedure is limited. Conservative assumptions have to be made to match equal SCF for different details and structural connections.

Fatigue damage can be estimated by combining the stress time series with an SN-curve. The time series can be decomposed in cycles and half-cycles of equal stress range by applying cycle counting methods

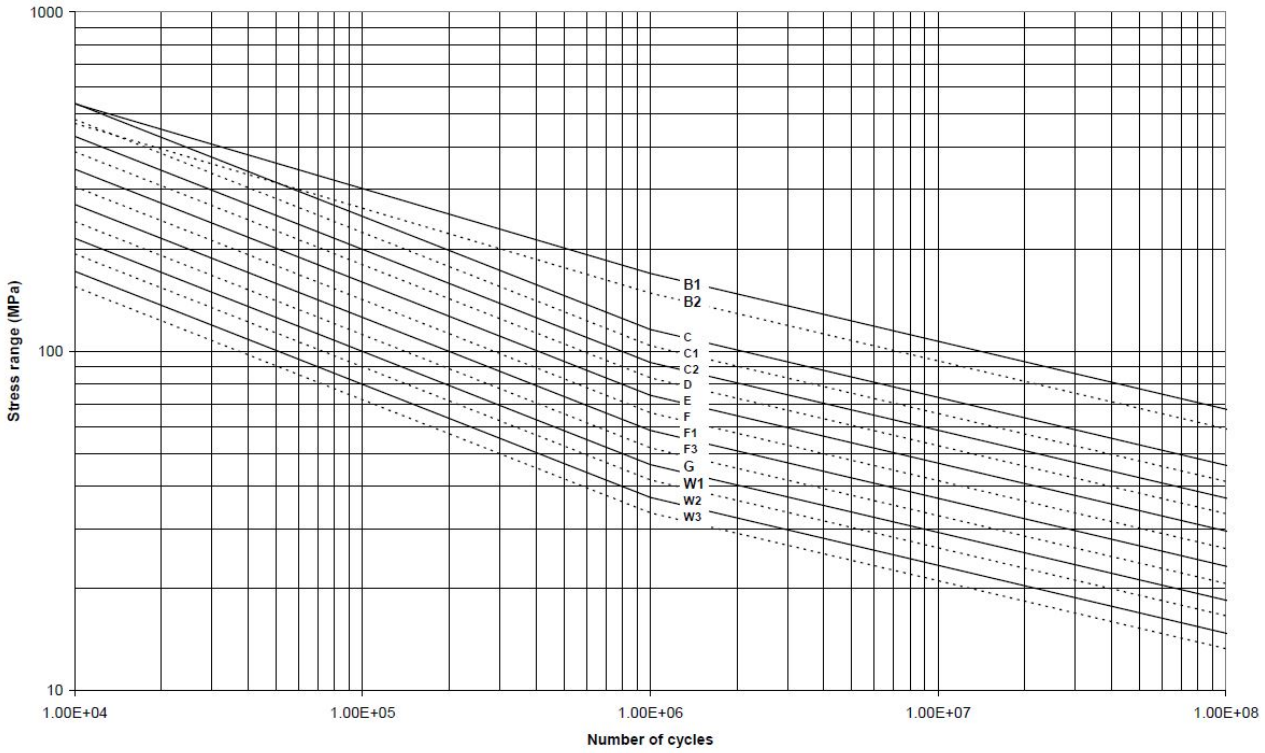

Figure 2.4: *SN-curves as presented by DNV-GL. Picture taken from [3].*

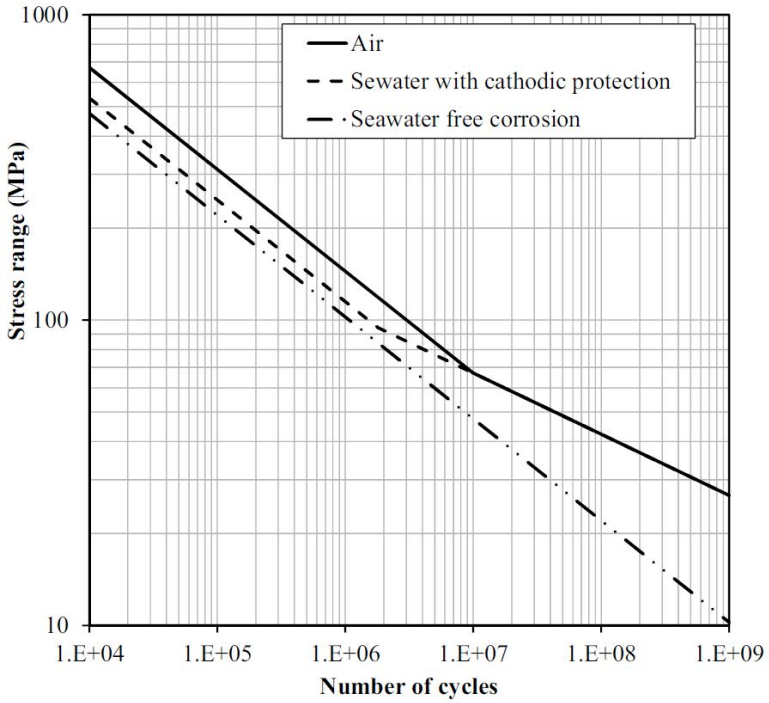

Figure 2.5: *T-curves as presented by DNV-GL. Picture taken from [3].*

such as the rain-flow algorithm. Using the linear cumulative damage model of Palmgren-Miner in Eq. (2.3), the total damage can be computed. In that equation, the index k is the total number of different stress ranges counted and n_j is the number of cycles for the range j. The model predicts failure when $D \geq 1$. However, evidence shows that this may be non-conservative for some cases, cf. Chapter 4.3.1. of [17].

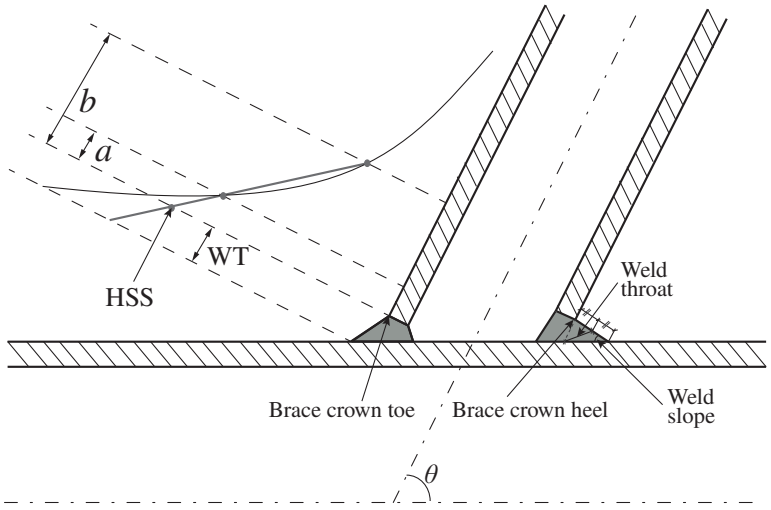

Figure 2.6: *Illustration of the hot-spot stress method, using linear extrapolation of the structural stress to the weld toe, WT.*

$$D = \sum_{j=1}^{k} \frac{n_j}{N_j} \tag{2.3}$$

Structural stress method

The structural stress method, also known as the hot-spot stress method, is a more detailed approach for the fatigue assessment of a connection. The hot-spot stress (HSS) is the local stress, whose magnitude depends on the external actions, the local geometry and the material properties. Nevertheless, it should be noted that the stress concentration due to small discontinuities in the geometry is included implicitly in the definition of the fatigue resistance, i.e. in the SN-curve. Thus, it is excluded in the definition of the hot-spot stress, cf. Figure 2.6. The weld notch, the material roughness or the material imperfections are considered as small discontinuities. Therefore, the hot-spot stress cannot be obtained directly from a numerical model. In order to capture the linear structural stress tendency, the results are to be regarded where the notch concentration does not have influence on the results. The difference between the nominal stress and the structural stress is caused mainly by the bending and ovalization of the members that conforms the connection. Afterwards, this tendency is to be extrapolated to the intersection point. The relation between the HSS and the nominal stress is the so called Stress Concentration Factor (SCF) cf. Eq. (2.4).

The way of assessing the fatigue resistance with this method is similar as for the nominal stress approach. However, instead of using the nominal stress and several SN-curves, depending on the tabulated joint classifications, it uses the structural stress and an SN-curve related to a stress concentration factor of 1, i.e. the D and T curves in [3]. Since this approach allows for the direct computation of the SCF instead of matching a case with similar tabulated situations, a higher accuracy can be obtained. Moreover, it does not require a high level of detailed modelling. Those two reasons explain why it is the preferred method for the fatigue assessment of the tubular jacket joints.

$$\text{SCF} = \frac{\text{HSS}}{S} \tag{2.4}$$

In practice, it is very common to use parametric formulae, such as the Efthymiou equations [5]. Their extended use is explained due to their parametric formulation, which adapts to many tubular joint situations, avoiding the need of generating FE models. More information about the development of this formulae can be found in the following Chapter 3. These equations estimate the HSS as a linear

superposition of axial forces and bending (in plane and out of plane) moments that are to be evaluated at at least eight points (hot spots) around the circumference that constitutes the welded joint (σ_1 to σ_8), cf. Eqs. (2.5). It requires matching the case under study with tabulated geometry situations. Therefore, the accuracy that can be obtained using these equations is limited.

$$\begin{aligned}
\sigma_1 &= \mathrm{SCF_{AC}} \cdot \sigma_x + \mathrm{SCF_{MIP}} \cdot \sigma_{my} \\
\sigma_2 &= \frac{1}{2}(\mathrm{SCF_{AC}} + \mathrm{SCF_{AS}}) \cdot \sigma_x + \frac{1}{2}\sqrt{2}\mathrm{SCF_{MIP}} \cdot \sigma_{my} - \frac{1}{2}\sqrt{2}\mathrm{SCF_{MOP}} \cdot \sigma_{mz} \\
\sigma_3 &= \mathrm{SCF_{AC}} \cdot \sigma_x - \mathrm{SCF_{MOP}} \cdot \sigma_{mz} \\
\sigma_4 &= \frac{1}{2}(\mathrm{SCF_{AC}} + \mathrm{SCF_{AS}}) \cdot \sigma_x - \frac{1}{2}\sqrt{2}\mathrm{SCF_{MIP}} \cdot \sigma_{my} - \frac{1}{2}\sqrt{2}\mathrm{SCF_{MOP}} \cdot \sigma_{mz} \\
\sigma_5 &= \mathrm{SCF_{AC}} \cdot \sigma_x - \mathrm{SCF_{MIP}} \cdot \sigma_{my} \\
\sigma_6 &= \frac{1}{2}(\mathrm{SCF_{AC}} + \mathrm{SCF_{AS}}) \cdot \sigma_x - \frac{1}{2}\sqrt{2}\mathrm{SCF_{MIP}} \cdot \sigma_{my} + \frac{1}{2}\sqrt{2}\mathrm{SCF_{MOP}} \cdot \sigma_{mz} \\
\sigma_7 &= \mathrm{SCF_{AC}} \cdot \sigma_x + \mathrm{SCF_{MOP}} \cdot \sigma_{mz} \\
\sigma_8 &= \frac{1}{2}(\mathrm{SCF_{AC}} + \mathrm{SCF_{AS}}) \cdot \sigma_x + \frac{1}{2}\sqrt{2}\mathrm{SCF_{MIP}} \cdot \sigma_{my} + \frac{1}{2}\sqrt{2}\mathrm{SCF_{MOP}} \cdot \sigma_{mz}
\end{aligned} \tag{2.5}$$

If the HSS is computed using the FEM, the following has to be considered. The D-curve accounts for the notch effect due to the weld itself. This avoids the need of using small solid elements to capture such a small detail. In contrast, shell elements can be defined in a relatively non-mesh dependent model. The HSS is not defined in the weld toe itself. It is the linear extrapolation to the weld toe position of the stresses computed at two characteristic positions. These positions are also called the extrapolation points, a and b. The region between these points is called the extrapolation region. Guidelines [3, 17] give recommendations for the definition of these points for three different situations, cf. Eqs. (2.6), (2.7) and (2.8). These positions are illustrated in Figure 2.7.

- Along the brace surface:

$$\begin{aligned}
a_{1,2} &= 0.2\sqrt{r_1 t_1} \\
b_{1,2} &= 0.65\sqrt{r_1 t_1}
\end{aligned} \tag{2.6}$$

- Chord surface at the crown position:

$$\begin{aligned}
a_{0C} &= 0.2\sqrt{r_0 t_0} \\
b_{0C} &= 0.4\sqrt[4]{r_1 t_1 r_0 t_0}
\end{aligned} \tag{2.7}$$

- Chord surface at the saddle position:

$$\begin{aligned}
a_{0S} &= 0.2\sqrt{r_0 t_0} \\
b_{0S} &= 2\pi\frac{r_0}{36}
\end{aligned} \tag{2.8}$$

For tubular joints, it is recommended to use the so called T-curve. It should be noticed that there is a significant difference in the definition of the T-curve between the 2011 [23] and 2016 [3] editions. In the earlier version, the T-curve is identical to the D-curve except for the thickness effect correction, which is more severe, i.e. 0.25-0.30 instead of 0.20. In the 2016 edition, the T-curve is more beneficial, in the sense that it enables a higher utilization of the material, i.e. the curve is shifted up $\log 14.46$ MPa. By way of example, let the stress range be of constant amplitude and equal to 100 MPa. The thickness factor is set to 0.25. This results in a fatigue life of 580,764 cycles according to the 2011 version and to 3,019,951 cycles according to the 2016 version. Therefore, the new version predicts a fatigue life which is more than five times longer. It should be noticed that a safety factor of around 1.5 is built into the T-curve due to bi-axiality in the stresses in the vicinity of the intersection.

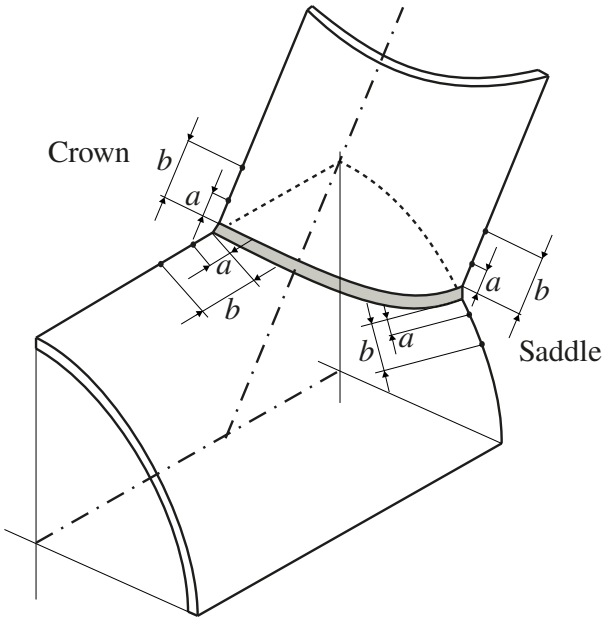

Figure 2.7: *Sketch of the extrapolation points .*

Notch stress method

The fatigue failure of tubular joints is dominated by the notch stress at the weld toe. The notch stress method consists of assessing this peak stress. Its applicability is practically restricted to numerical modelling, since the experimental testing of the notch stress is unpractical for most situations. Nevertheless, parametric formulae exist as well. The hot-spot method is then understood as an intermediate solution between the nominal and the notch concepts. The fatigue strength is assessed by DNV-GL [3] similarly as in those methods, i.e. with SN-curves. The SN-curves to be used allow for a better material utilization. By way of example, the fatigue class, i.e. the fatigue resistance at two million cycles, of the T-curve in air conditions is 115 MPa, while the notch curve is 225 MPa. Hence, a fatigue class ca. two times higher. This means that if the Notch Stress Concentration Factor (NSCF) is smaller than approximately 1.95 SCF, following this method will allow for material optimization. It should be noticed that the NSCF can be understood as a magnification of the hot-spot SCF factorized with the nonlinear contribution due to the weld itself, i.e. the weld stress concentration factor k_w, cf. Eq. (2.9). This factor is also known as the weld shape factor or the notch factor. σ_k and σ_s are the effective notch stress and the structural stress, respectively. The difference between both of them is exemplified in Figure 2.8.

$$k_w = \frac{\sigma_k}{\sigma_s} \tag{2.9}$$

Only the weld throat and the weld slope are given by the designer, cf. Figure 2.6. However, this parameters are not enough to recreate the local model of the joint. Infinitely high stresses are found at sharp corners when assuming elastic material behavior. A smoothing of the singularity is done by implementing an effective notch, which is modelled by an arc. Arcs of 1 mm radius are employed by DNV-GL [3]. This consideration was elaborated in *D. Radaj (1990)* [24].

For highly inclined braces, the weld slope tends to get closer to the brace inclination, resulting in a mild-notch. Thus, the situation gets closer to the case of having a butt-weld with little weld overfill. This yields a small notch factor k_w, regardless of the small notch radius. In spite of the benefits on the reduction of the effective notch stresses σ_k, the fatigue resistance decreases. This phenomenon is addressed by IIW in *W. Fricke (2010)* [25]. A lower bound of the weld concentration factor k_w of 1.6 is proposed, to account for the fatigue resistance reduction. The structural stress σ_k can be estimated

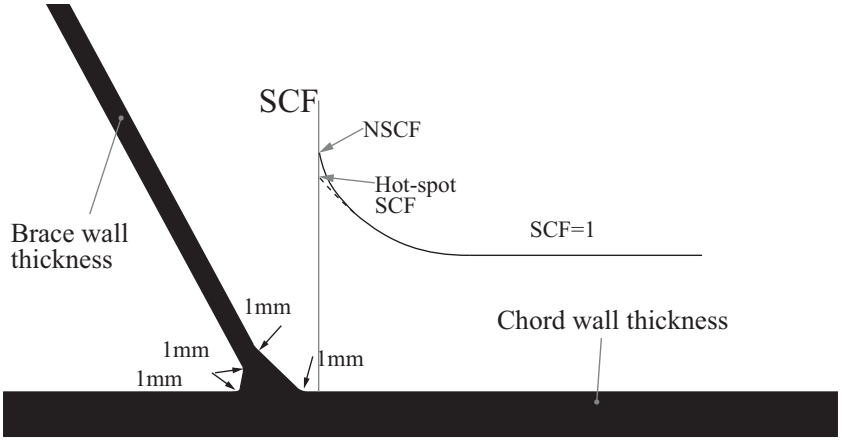

Figure 2.8: *Sketch of the effective notch model, showing the definition of the hot-spot stress concentration factor SCF and notch stress concentration factor NSCF.*

directly from the notch model by reading the stress at a distance of 2 mm from the tangent point of the effective notch arc. Moreover, it is recommended, in that same document, to not account for the thickness correction.

2.2 Basic Tubular Connections in OWT Jackets

Jackets structures were originally developed to support Oil & Gas platforms. The concept has been extended to support wind turbines in intermediate waters. However, the design had to be adapted to the new specific conditions. Raisers, caissons and horizontal frames, whose functions were to provide support to the wells, are no longer needed. Furthermore, the same batter angle is set in all four legs, since no well drilling is to be performed by a jack-up vessel that has to be founded close to the jacket piles. No distinction exists between broadside and end-on faces, since wind loading is of higher importance and its main heading can vary due to the yaw actuator of the rotor. The width is also significantly narrowed since instead of a top-side, there is a turbine, with a ca. 7 m tower bottom diameter supported in the center. A transition piece between the tower and the jacket has to be carefully designed to assemble two structures, whose behavior against environmental loading are very distinct. With the given order of magnitude of the members dimensions and the absence of horizontal bracing, redundancy in the diagonals (X-bracing) is of common use. A generic design of the mentioned general practice is sketched in Figure 2.9.

The fatigue design of the joints influences the design of an area around them. This project is going to focus on the analysis of these areas. Three types of joints can be differentiated: (1) K-joints, (2) X-joints and (3) Y-joints. (1) Two braces intersect at a given angle with respect to the chord. According to [3], at least 10% of one brace axial force should be balanced with the other brace. (2) One brace intersects with the chord at a given angle yielding mainly beam shear in the chord. (3) A combination of four braces or two braces and one continuous chord intersect in the same union. The steel of the union has to withstand and carry through the loading between the beams. Within this project, the definition of these joints is purely based on geometry. However, depending on the loading conditions, it may be convenient to treat a K-joint as a Y-joint, e.g. if one of the braces was not loaded. A schematic representation of the mentioned joint classification is shown in Figure 2.9.

2.3 Summary

In this chapter, a summary of the fatigue theory background in which this work is based on is presented. Various methods used in the fatigue assessment of welded connections are elaborated. Finally, the tubular joints that are employed in the assembly of OWT jackets are described.

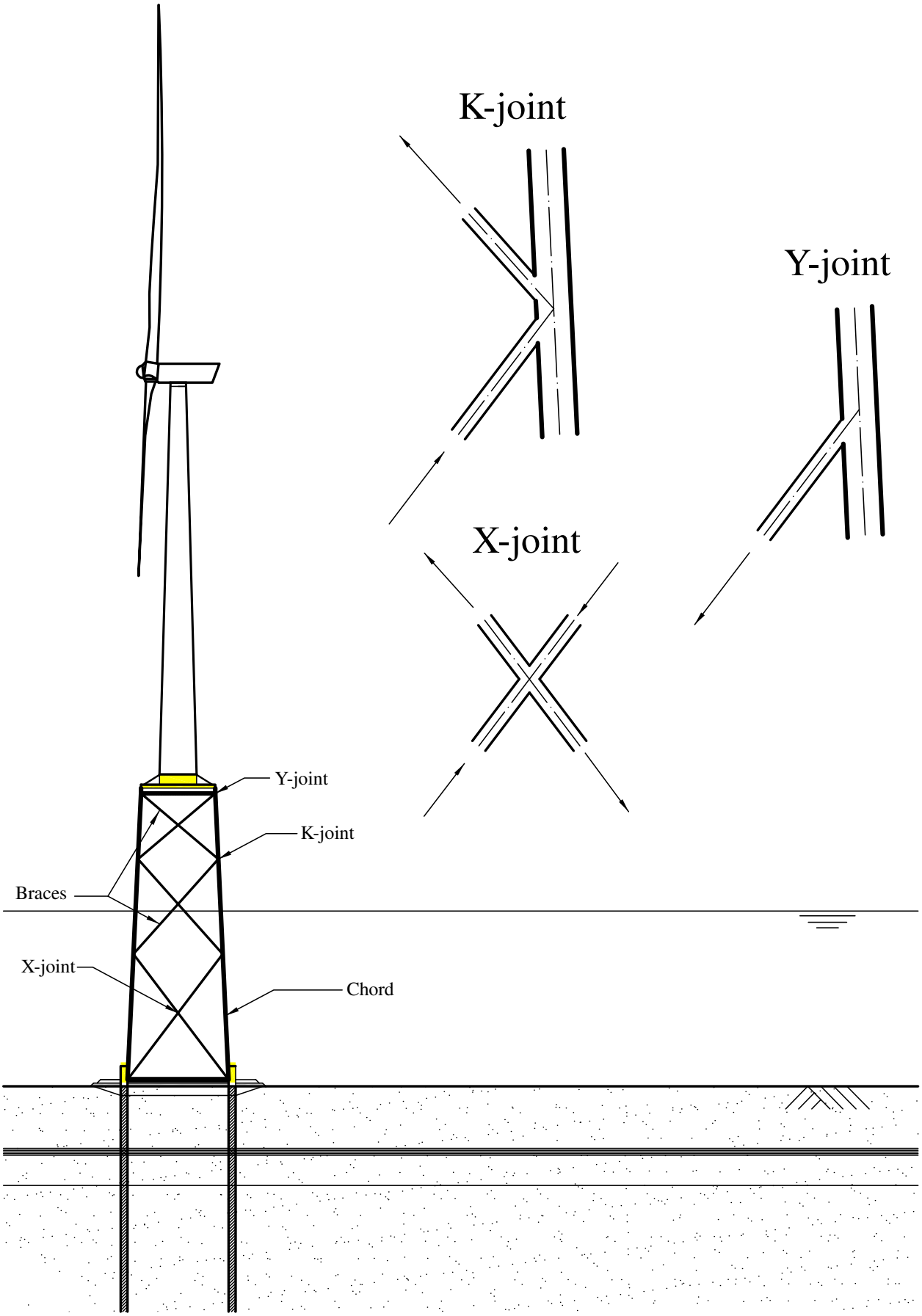

Figure 2.9: *Types of tubular joints in OWT jackets.*

3 | Literature Review

Prolific work has been done on the fatigue of tubular joints due to their importance in the offshore support structure solutions for the Oil & Gas industry. Most of the papers and technical reports are from the 80s and 90s. The current guidelines and papers contain small variations from those works, e.g. the DNV-GL [3] philosophy is the same as in *T.R. Gurney (1976)* [21]. *S.J. Maddox (1969)* [7] already covers the fundamental theory of the fatigue assessment of welded connections. Since then, additional work has been done for completeness and to satisfy the demand of the current market.

Safety used to be the main requisite in the design of offshore structures. The wind market has pushed the cost optimization requirements to be one of the driving criteria, if not the most important one. Nevertheless, the fatigue assessment guidelines for offshore structures have not been adapted to that requirement. Large safety margins follow the assessment of the fatigue resistance. Some examples of this are: the two standard deviations off-set to the safe side of the empirical scattered results that constitutes the SN-curves; the tabulated categorization of the structural details used when following the nominal stress approach, which recommends the use of the same SN-curve for different details; the built-in safety factor in the T-curve due to the bi-axial stress state close to the welded connection of tubular joints; the notch stress concentration due to the weld itself, which is derived conservatively to be applicable to a diverse range of situations [26].

Many topics, regarding the fatigue of tubular joints, have been addressed during the past decades. However, there is still research interest on this area, which is decisive in the development of jacket structures in terms of cost and safety. Some of the challenges that are still of interest to the industry are covered in this project. In Section 3.1, firstly, these challenges are briefly introduced and a motivation for addressing them is given. For each of them, the background literature and the state of the art are reviewed.

3.1 State of the art in the fatigue assessment of tubular joints

1. ***Validity of the use of shell instead of solid elements in the fatigue assessment of tubular joints using the FEM***. DNV-GL [3] does not give a clear guidance of whether it is more convenient to use solid or shell elements for the modelling of tubular joints by means of the hot-spot method. As seen in Chapter 2, the prediction of the fatigue life of steel tubular joints is highly sensitive to small variations in the estimation of the SCF. Therefore, it is expected to find significant variations in the results obtained by both ways of modelling the joint. This is to be quantified. Furthermore, a better understanding of the background of the differences is sought after within this project. The influence of the meshing density and element type, applied to T- and X-joints, is covered by *A. Romeijn (1994)* in [27]. In *Doerk et al. (2003)* [28] a mesh parametric study for two plates welded together is carried out, showing that the stress evaluation close to the weld toe is affected by the element size and type. The influence of three mesh features, i.e. the mesh regularity, the element size and the shell element type, is investigated in *J. Mendoza et al. (2017)* [1]. Recommendations for the FE aspects of the hot-spot method are given in *W. Fricke (2002)* [29], where the influence of the element type and size and the stress evaluation techniques are studied. Additional recommendations regarding the numerical modelling are provided in *I. Huther et al. (1999)* [30].

2. ***Validity of the Efthymiou equations [5]***. These equations are used in the hot-spot approach by many guidelines, such as DNV-RP-C203 [3]. They are generally used in practice due to their parametric formulation, which avoids developing computationally intense FE models. These equations estimate the hot-spot stress (HSS) as a linear superposition of axial forces and bending (in-plane and out-of-plane) moments that are to be evaluated in at least eight points (hot spots) around the circumference that constitutes the welded joint. The structural stress is computed

from the SCF, which is computed using equations of the form presented in Eq. (3.1), where γ, β, τ, ζ and θ are the non-dimensional joint parameters defined in Figure 4.1. Therefore, the SCF depends on the geometry, which is defined by non-dimensional joint parameters and the applied actions. It requires to match the joint type with given tabulated situations. In some cases, this results in making rough assumptions. Further quantitative and qualitative understanding of the applicability of these equations is therefore relevant for the safety and optimization of the jacket joints. The hot-spot method, as described in standards such as [3] or [17] is commonly used in practice. Parametric formulae have been developed by several authors for the most common joint types. The most famous are *Efthymiou (1988)* [5] and *Wordsworth and Smedley (1997)* [31]. They allow to estimate the SCF at discrete locations around the weld. There is evidence [32] pointing out that the results depend on the number of points where the HSS is evaluated. In some cases, it is found that using only 8 points around the weld is non-conservative. Furthermore, it is demonstrated that, under different basic load combinations, the maximum peak can be found at any position along the intersection [33]. *S. Yong-Bo* has written extensive literature about the stress field distribution around the weld, e.g. [34]. Comparison of the parametric formulation with FEA has been carried out [35, 36, 28], as well as their extension and modifications [37]. Moreover, experimental tests exist in this research line [38, 39].

$$\text{SCF} = K \cdot \gamma^{m1} \cdot \beta^{m2} \cdot \tau^{m3} \cdot \zeta^{m4} \cdot \sin\theta^{n} \tag{3.1}$$

3. ***Relevance of the carry-over effect in multiplanar KK-joints***. The previously mentioned SCF parametric equations in [3] are given for planar K-joints. However, the joints of the OWT jackets are in most cases multiplanar KK-joints. The *carry-over* effect has been studied quantitatively using *influence functions* for in-plane configurations of braces. In engineering practice, their use is also extended to the assessment of multiplanar joints. Therefore, it is interesting to study the SCF for multiplanar KK-joints in comparison to the planar K-joints solutions. Parametric formulae for multiplanar joints and FEA have been developed by several authors. The first publications date back to late 1980s. The amount of combinations of multiplanar joints that are built in practice allows the authors to continue with this task up to now. Examples of parametric equations for multiplanar joints are *Wordsworth (1987)* [40] for TT-joints, *Wingerde et al. (2001)* [41] for KK-joints, *Karamanos et al. (2002)* [42] for DT-joints, and *Ahmadi et al. (2016)* [43] for KT-Joints. *A. Romeijn (1994)* covers in his PhD [27], the formulation for XX-joints and a parametric study of the influence of several aspects, such as the extrapolation path or the weld shape. However, little effort has been given so far on defining the influence of the carry-over effect of the out-of-plane braces. *Efthymiou (1988)* [5] extended the use of this formulation for K-joints to the multiplanar case by the definition of influence functions. This extension is however not adopted by DNV-GL [3]. He reported that the impact of not including the multiplanar effect yielded $\pm 15\%$ differences. This degree of inaccuracy is not enough for the OWT jackets requirements. Furthermore, it is not covered for which cases the highest differences are found.

4. ***Application of the effective notch stress method for tubular joints***. So far, all challenges stated in this chapter refer to the hot-spot approach. The optimization that can be achieved following this method is limited by its intrinsic assumptions. For instance, the stress concentration due to the weld detail is implicit in the SN-curve use for assessing the fatigue resistance. This inevitably includes some conservatism in order to extend the applicability of the method to most joint situations. If further optimization is pursued, the effective notch concept is the method that allows a more detailed modelling of the joint. However, this method has not been researched in depth up to now. Furthermore, it has not been applied to tubular joints in general engineering practice. *D. Radaj (1990)* collects in [24] the fundamentals of the effective notch stress concept. In *H. Petershagen et al. (1991)* [44], the motivation for the use of the local approach is emphasized. The method developed by Radaj is used to compute the stress concentration due to the weld notch and to derive SN-curves that are valid for the structural stress method. A notch model is built for the doubler plate ending detail type. *W. Fricke et al. (2001)* [45] compares the use of the local

approach and the hot-spot method (with linear and quadratic extrapolations). A comparison between the hot-spot and the notch approaches is covered in *W. Fricke et al. (2004)* [46] for a bracket detail. In *D. Radaj et al. (2006)* [47], the results from tests, which were performed on a K-joint, were reported. These results are used in *J. Schönherr (2009)* [48] for a comparison with the ones obtained using the structural and the notch stress methods. Both approaches predicted remarkably conservative results. The hot-spot method estimated a lifetime of less than 40% of the one found experimentally. Moreover, the local approach predicted an even shorter lifetime, lower than 40% of the one estimated by the hot-spot method. Nevertheless, it should be noted that this example covered one single case and only one position around the weld. Therefore, the conclusions cannot be extended to a broader understanding. The importance of the root crack failure is reported in *W. Fricke (2013)* [19]. Guidelines are given for the assessment of the weld toe and the weld root cracks by means of the notch and crack propagation methods. The notch approach is also used for the assessment of the notch stress intensity factor. Recommendations on how to build the meshes are given as well. A study of the influence of the weld shape is covered in *A. Romeijn (1994)* [27].

3.2 Summary

In this chapter, the research gaps that are going to be investigated within this work are briefly described. For each of these topics, a study of the state of the art is presented. The fatigue of tubular members has been extensively addressed due to its relevance in the offshore Oil & Gas industry. Due to that, a solid foundation is found for the further research that is to be performed within the following chapters.

4 | Use of Plate and Solid Models

In the paper *J. Mendoza et al. (2017)* [1], three shell mesh features are investigated, i.e. the mesh regularity, the mesh refinement and the element type. Within this chapter, this study is extended to the influence of using volume elements instead of plate elements. The layout of this chapter has the following structure. First of all, the problem is introduced in Section 4.1. The methods used to investigate the problem are elaborated in Section 4.2. The characteristics of the models used to apply this methodology are described in Section 4.3. Finally, the results are presented and discussed in Section 4.4. In Chapter 5, this study is combined with a comparison of the results computed using the Efthymiou formulae. A complete analysis of the results is covered in that chapter.

4.1 Introduction to the problem

There is no unique way of defining a numerical model. The use of beam, shell or solid element types may be preferred for the definition of the FE model depending on the type of analysis, desired output and given geometry. Generally speaking, solid elements are used when beam and shell elements are not appropriate for the purpose of the mathematical model. For the given case of assessing the stress concentration of a jacket joint, beam elements are dismissed, since they can only provide information about the nominal stress distribution. Therefore, shell or volume elements are to be used in order to compute the SCF at the joint. DNV-GL [3] recommends to use one of these element types. No guidelines are given regarding when to use solid elements instead of shell, except for the following consideration: thin shell elements are to be avoided when calculating the SCF if it is expected to find the hot-spot near the brace-ring crossing point.

On the one hand, when computing the SCF following the hot-spot methodology, a plate model will provide, in general, good solutions for a lower computational cost than the analogue solid model. Moreover, regular meshes are easier to be built when using shell elements. For instance, when using solid elements, a regular mesh is achieved when the geometry is discretized by hexahedron elements. This can only be achieved when bodies are sweepable, i.e. when all bodies assembled in the model are constituted by six faces and twelve edges. Sweepable bodies are not easy to isolate from complex geometries. Therefore, tetrahedral elements are used at some locations, decreasing the mesh quality. If a good mesh is not achieved when using solid elements, the solutions obtained with a shell model can be more trustworthy for some situations.

On the other hand, using solid elements allows the geometry of the joint to be modelled more accurately, recreating the local stiffness with more fidelity. This assertion is true even when using one single solid element through-thickness. The stress field close to the joint includes tensile and compressive stresses in the through-thickness direction. This cannot be captured by following first order plate theories. Moreover, OWT jacket joints are constituted by reinforced thick plates welded together. At some point, a high refinement in a shell mesh results into out-bounding the model from the shell theory assumptions. For instance, when the element size is smaller than the member wall thickness, the quality of the solution becomes doubtful, specially considering the real through-thickness stress distribution.

The investigation carried out in this chapter covers the study of the differences in the results from using the shell and solid types of modelling. An explanation of what causes these differences is to be searched. Recommendations on when it is better to use each alternative are given regarding the accuracy of the solution and computational time.

4.2 Problem approach

The investigation of this problem is divided into two parts. First of all, the through-thickness stress field close to the hot-spot is going to be investigated. This will serve to understand why and when solid elements are to be used and how many elements should be used within the plate thickness. For completeness of the work, axial, in-plane and out-of-plane actions are considered. Moreover, brace and chord crown (toe and heel) and saddle positions are regarded. To carry out this study, FE models are developed and the normal stress fields across the thickness are investigated in the aforementioned positions at four distances from the weld in the brace and chord axis directions, i.e. at the joint intersection, at the read-out points a and b, and at a position far from the joint, cf. Figure 4.2(b). Furthermore, the deformed shapes are compared between the solid and the shell models. Various mesh densities through the wall thickness are considered in Section 4.3.4 in order to study its influence on the results.

The second part of the investigation is the comparison of the computed SCFs by following the two different theories. Pairs of analogue numerical models are built. The stress fields normal to the weld toe and the differences in the SCF are compared. Again, the same actions and positions around the weld are regarded. Only normal stresses are considered for the sake of simplicity. It is found that this approximation is accurate enough, with the differences between the principal stress[1] S_1 and the stress normal to the weld being negligible at the crown position and lower than 10% at other positions [27, 37]. A parametric study of the non-dimensional geometry parameters β, τ and θ, which are defined in Figure 4.1, is performed in order to make the investigation more rigorous.

As mentioned above, several FE models are built to carry out this study. The general characteristics of these models are described in the following section.

4.3 Characteristics of the models

The decisions and assumptions made during the definition of the models are summarized in this section. The FE models are defined sequentially in ANSYS© Workbench as follows: (1) the geometry is defined from key-points, lines, areas and volumes; (2) the materials are specified; (3) the element types that are used are defined; (4) the areas are meshed; (5) the boundary conditions are applied; (6) the type of analysis to be performed is stated; (7) the simulation of the FE model is executed; and (8) the post-processing of the results is carried out.

Even though the model is defined sequentially, all the steps have to be regarded as a whole in an integral prior plan. The outcome of a FE model is a mathematical model that partially represents some physical aspect of the reality under some given simplifications and assumptions. For instance, the geometry to be defined in step (1) may vary, depending on the type of the elements, set in step (3). The mentioned steps of the model are elaborated in detail in the following subsections.

As mentioned above, ANSYS© Workbench is used for this part of the project, instead of APDL. This software fits the aim of this investigation better due to two main reasons. First of all, complex meshes are built. This software allows for an easier control of the definition of the mesh. Secondly, an extensive post-processing is to be performed, where the solutions are read at numerous positions. The better interface of Workbench is more suitable to accomplish that.

4.3.1 Geometry

The geometry is defined parametrically through the non-dimensional joint parameters, cf. Figure 4.1. All the parameters are directly or indirectly related to only one dimensional parameter, i.e. the chord

[1] The principal stress S_1 is defined as the maximum component of the stress tensor, when the reference is rotated such that the shear components become zero.

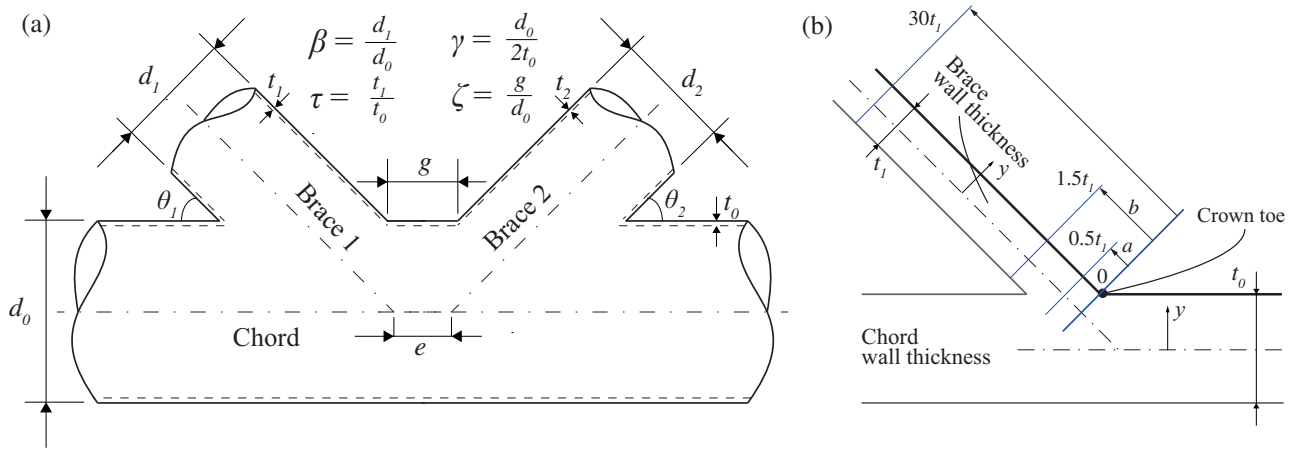

Figure 4.1: *(a) Reference CHS K-joint under study. (b) Sketch of the positions where the results are regarded for the investigation carried out in Section 4.4.1.*

outer diameter, which is set to a typical dimension for OWT jackets of 1 m. The variation of these parameters lies within the ranges stated in Eq. (5.1). The ranges are given in DNV-GL for typical dimensioning due to extreme statics, dynamics, global and local stability, and global fatigue analysis. The range of θ is, however, given by weldability of the joint. A systematic variation of these parameters is carried out in order to investigate their impact on the results.

Within this chapter, the upper and lower braces are called Brace 1 and Brace 2, respectively. The Cartesian GCS origin is set at the mid-point of the braces axes intersection with the chord axis, cf. Figure 4.1. The x-axis is aligned with the chord axis, being positive when pointing from Brace 1 to Brace 2. The y-axis is defined so that the members axes lay in the xy-plane, being positive when moving from the chord to the braces. A Local Coordinate System (LCS) is defined for each tubular member. The local x-axis is set in the direction of the members revolution axes. The local y-axis is set in the GCS xy-plane in such a way that the z local axis goes in the same direction as the GCS z-axis.

In practice, truss frames do transfer moments at the joints. Due to the dimensions of the tubular members and for fabrication purposes, a gap is usually set between the braces for tubular K-joints. This may result, in some cases, in an eccentricity between the points where the braces and the chord axes intersect. The gap can be formulated as a function of the eccentricity and the joint dimensions, cf. Eq. (4.1). This equation is easily derived applying basic trigonometry from the case sketched in Figure 4.2(a), where r_0 and $r_{1,2}$ are the radii of the chord and the braces, respectively. Notice that the gap g is the sum of g_1 and g_2, i.e. the parts of the gap related to the Braces 1 and 2, respectively. The non-dimensional gap ζ is defined as the ratio between the gap g and the chord thickness d_0, cf. Eq. (4.2).

$$g_{1,2} = e_{1,2} - \frac{r_{1,2}}{\sin\theta_{1,2}} + \frac{r_0}{\tan\theta_{1,2}} \tag{4.1}$$

$$\zeta = \frac{g}{d_0} = \frac{g_1 + g_2}{d_0} \tag{4.2}$$

Table 4.1: *Steel properties that define the material used in the FE model.*

Property	Value	SI unit
E_s	$2.10 \cdot 10^{11}$	[N/m^2]
ρ_s	7850	[kg/m^3]
ν_s	0.3	[-]

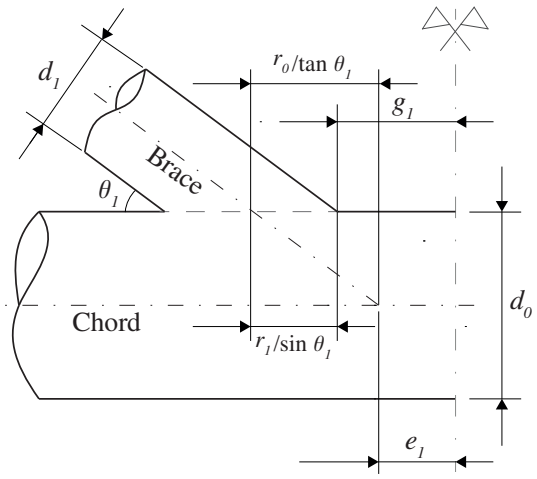

Figure 4.2: *Relation between gap and eccentricity.*

4.3.2 Materials

The hot-spot stress philosophy neglects the non-linear stress peak due to the weld itself, i.e. only the structural stress behaviour is regarded. The hot-spot method avoids the stress singularity at the intersection by extrapolating the structural stress from a region out of the influence of the sharp intersection. This justifies the use of linear elastic material behaviour. The same standard steel is set for all elements. This type of material is defined by three properties, i.e. Young or elastic modulus E_s, density ρ_s and Poisson modulus ν_s. The values that are used are summarized in Table 4.1. Notice that the yield strength is not an input of the model. It would have to be checked in the post-processing and analysis of the results if a ULS check was performed. All units input in ANSYS© are according to the SI system.

4.3.3 Element type

Depending on the type of element, the properties to be defined vary. The element types are chosen regarding the recommendations in DNV-GL [3]. First of all, the element types employed in the shell model are described. After that, the same is done for the solid model. The main relevant characteristics of the chosen element types are compiled in Table 4.2 and sketched in Figure 4.3.

For the plate model, SHELL181 is used. This element has identical properties as the 4-node SHELL43 element, which was used in the investigation reported in the paper *J. Mendoza et al. (2017)* [1]. For this element type, the thickness is set as a real constant. This element type follows the first order shear deformation theory, also called Mindlin-Reissner plate theory [49, 50], which is an extension of the Kirchhoff-Love plate theory [51]. This theory is, at the same time, an adaptation of the Euler-Bernoulli beam theory [52]. The Mindlin-Reissner theory is valid for thick plates, i.e. when the plate thickness is in the order of ten times the planar dimensions. Hence, it accounts for the shear deformation and a section does not necessarily remain perpendicular to the mid-plane. In the element formulation, the non-linear stress field across the thickness is accounted for. Therefore, it uses the formulation derived by *Reissner (1945)* [49]. Moreover, plane stress condition is assumed, which neglects the stress in the through-thickness direction.

Regarding the solid model, DNV-GL recommends the use of 20-node elements for the hot-spot approach, to capture the steep gradients and to account for the linear stress distribution through-thickness due to the plate bending. When developing the guideline, the possibility of using one single element through-thickness was searched for. This consideration was made due the computational time limitations, which at the time the method was developed were obviously stronger than nowadays. Two solid element types are used for the solid modelling in this chapter, i.e. SOLID186 and SOLID187. SOLID187 element is the tetrahedral version of the SOLID186 element, with ten nodes instead of twenty.

Table 4.2: *Main properties of the elements SHELL181 and SOLID186.*

SHELL181	**SOLID186**
Defined by four nodes	Defined by twenty nodes
One at each corner of the element	One at each corner and mid-sides of the edges
Six DOF at each node	Three DOF at each node (translations at x, y and z directions)
Linear deformation at both in-plane directions	Quadratic displacement behavior
Mixed interpolation of tensorial the components in the out-of-plane direction	-

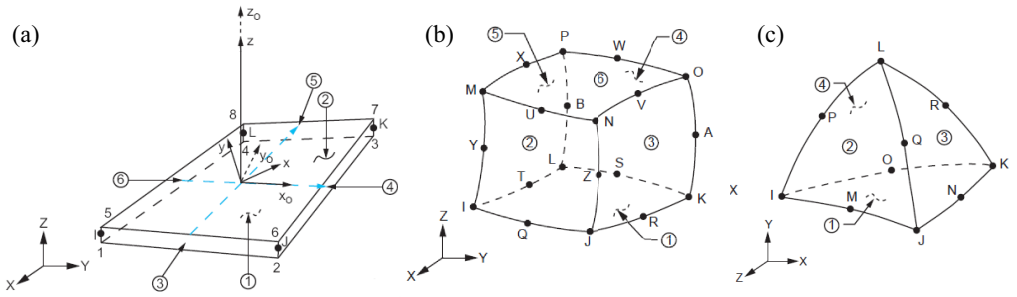

Figure 4.3: *Sketch of the element types [53]: a) SHELL181; b) SOLID186 and c) SOLID187.*

The integration scheme is set to reduced integration. This consideration does not have much influence when using several elements through-thickness. However, when using one single element, this conditions the stress field to be linear trough thickness, since only two Gaussian points per element are employed in the integration. In DNV-GL [3], it is assumed that the stress field through-thickness is linear at the read-out points and thus, only one element is needed to capture the distribution, for minimum computational time.

4.3.4 Meshing

A parametric shell mesh study was carried out in a preliminary study, which is described in *J. Mendoza (2017)* [1]. An efficient shell mesh was developed. It was seen that, considering the accuracy of the results and computational time, an element size of half the member thickness is in general the best refinement for the assessment of K-joints by means of the hot-spot method. The characteristics of the shell mesh are collected in Table 4.3 under the Mesh Reference Code (MRC) SHM. A parametric study of the solid mesh is carried out and described in this section. Four mesh layouts with various refinements across the thickness are tested. Each mesh is designated by an MRC. SM1 refers to the model with one single element through-thickness. SM2 to SM4 are the models with multiple elements through-thickness, SM4 being the one with the finest mesh, used as a benchmark for calibration of the other meshes. The characteristics of these meshes are summarized in Table 4.3. Note that n_{tt} is the number of elements across the thickness and t_{CPU} is the computational time employed in running a simulation. It should be noted that, a parametric study is carried out for the investigation in Section 4.4.2 and thus, the geometry is varied. Therefore, the numbers should be understood as an orientative measurement of the characteristics. The techniques used during the meshing process are described hereafter for the shell and solid models. Afterwards, the description, results and conclusions of the solid mesh parametric study are presented.

The mesh of the shell model (SHM) is built with an element size in the order of $t_1/2 \times t_1/2$ at the hot-spot area. A sketch of the shell mesh layout is shown in Figure 4.5. It should be noted that, the element thickness is set from the outer part of the members. This way, the results are read at the same points of the geometry as for the solid model. The geometry is partitioned in order to obtain elements with a regular shape at that region. The partitions, as sketched in Figure 4.4, are of two kinds:

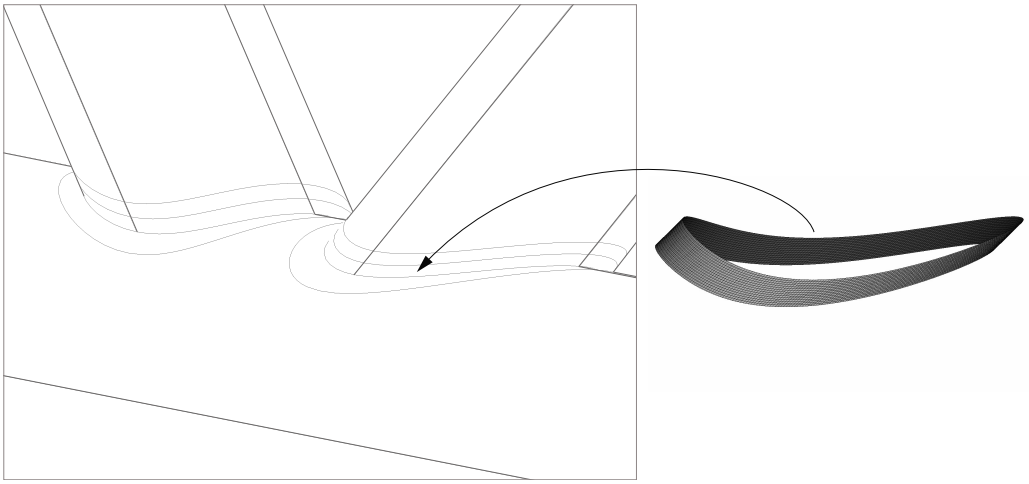

Figure 4.4: *Sketch of the partitions made to build the shell mesh.*

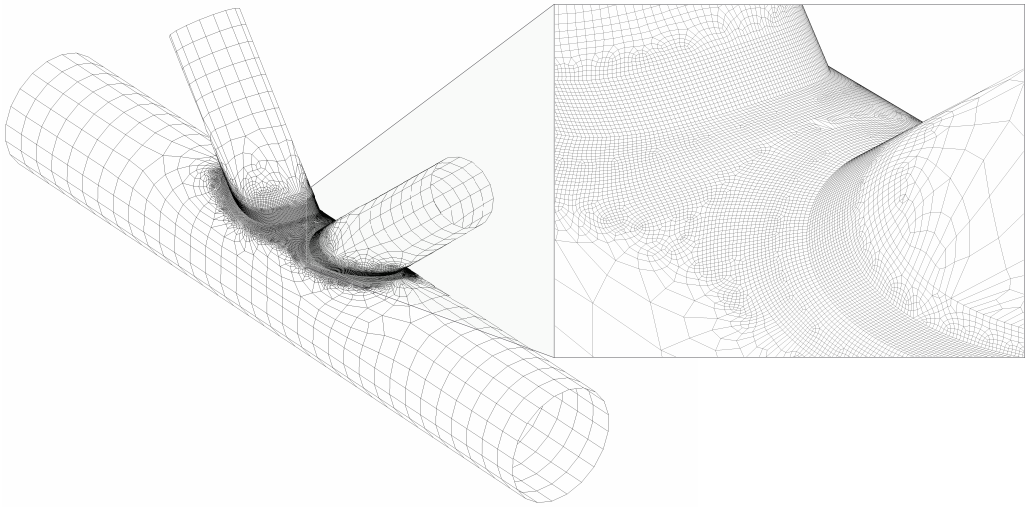

Figure 4.5: *Shell mesh layout including a detail of the local refinement at the vicinity of the weld.*

1. In the braces, the partitions are equal and parallel to the brace-chord intersection curve. This is achieved by intersecting a brace with a cylinder similar to the chord but displaced in the y-direction. The offset from the chord axis is set as a parameter, which was varied to study its influence on the hot-spot computation. It was concluded that increasing this area of influence more than $4t_1$ does not provide any benefit in the accuracy of the computation of the SCF.
2. In the chord, the partitions are dilations of the brace-chord intersection. This is achieved by intersecting the chord with a cylinder whose central axis is the same as the brace axis but with a higher radius. The radius of that cylinder is set to $\frac{3}{5} g_1 \sin\theta_1$ which was investigated to provide enough area for the purpose of mesh generation but also good stability for the parametric study.

In order to build the solid mesh, bodies are partitioned so that all parts are sweepable. A sketch of the partitions made is shown in Figure 4.6. A regular mesh is then built at each region using the sweeping technique. The same element size as in the shell mesh is used in the direction perpendicular to the weld. A sketch of the solid mesh layout is shown in Figure 4.7. Some issues were faced in the definition of the areas at the intersection between the chord and the braces. All bodies were combined in a single part, so a continuous model was built. However, the common lines between chord and braces were automatically partitioned, making the definition of sweepable bodies unfeasible. This was solved by having the braces and chord as three independent parts. The nodes at the common areas were merged with a tolerance of $t_{1,2}/(2n_{tt})$. Note that this tolerance is approximately equal to the distance between nodes, for elements with mid-side nodes.

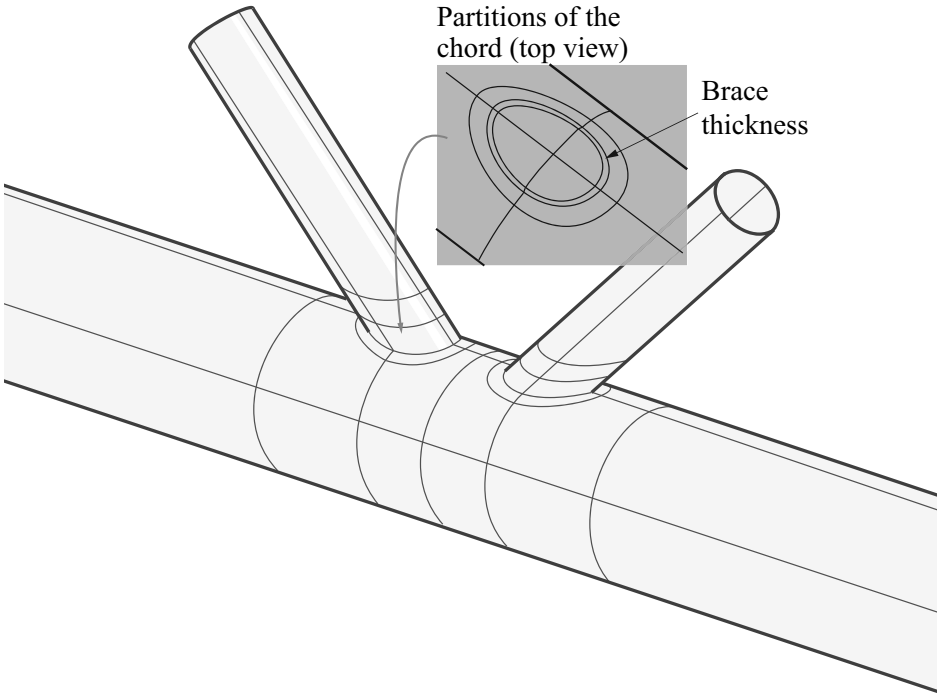

Figure 4.6: *Sketch of the geometry of the solid model, including the partitions made for the generation of a regular mesh layout.*

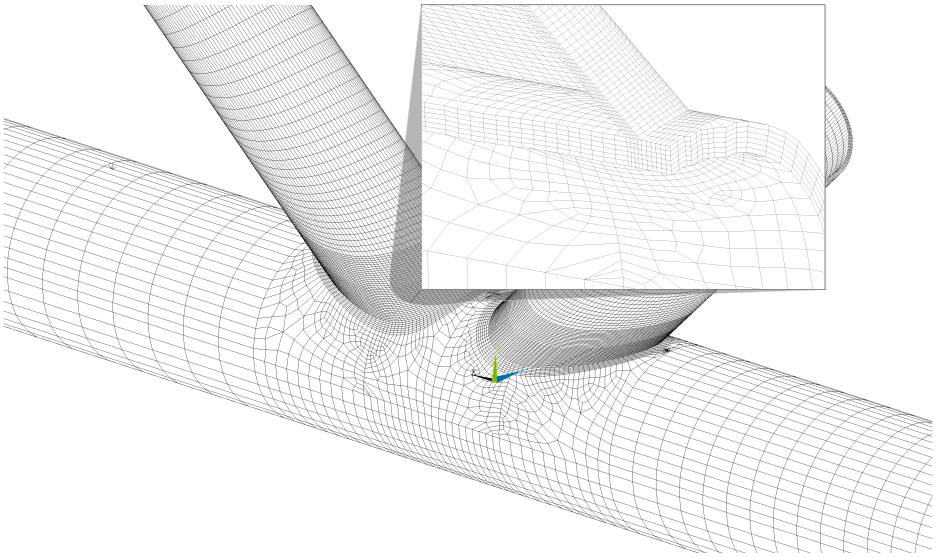

Figure 4.7: *Solid mesh layout, including a detail of the mesh across the thickness. The SM2 layout (cf. Table 4.3) is used in this picture.*

A mesh parametric study of the solid mesh is carried out in order to find an adequate mesh refinement for the investigations done in Sections 4.4.1 and 4.4.2. First of all, the normal stress S_x across the section is regarded, in the toe and heel positions, at three distances to the weld, i.e. $x_{T,H} = 0{,}0.5 \times t_1$ and $1.5 \times t_1$, cf. Figure 4.1. $x_{T,H}$ are the distances to the weld, measured from the toe and heel positions, respectively. The results are presented in Figure 4.8. It is seen that the number of elements across the thickness has a great influence on the computation of the stress field across the section. The stress at the edge singularity ($x_{T,H} = 0$ and $y/t_1 = 0.5$) is theoretically infinite. Thus, an increasing tendency is found for increasing the number of elements through-thickness. A reasonable match is found between the results given by SM3 and SM4 for the other two distances. The solutions obtained from the use of SM2 are not accurate enough for the through-thickness investigation. Therefore, SM3 is chosen for that purpose due to the reasonable accuracy and computational time.

Table 4.3: *Summary of the characteristics of the FE models used in the mesh parametric study. The values are rounded.*

MRC	ET	Brace n_{tt} [#]	Chord n_{tt} [#]	Elements [#]	Nodes [#]	t_{CPU} [s]
SHM	SHELL181	1	1	32,600	32,650	20
SM1	SOLID186	1	1	50,600	321,900	82
SM2	SOLID186	4	6	138,000	677,500	325
SM3	SOLID186	5	8	240,100	1,080,500	1,220
SM4	SOLID186	12	15	1,200,000	5,500,000	8,900

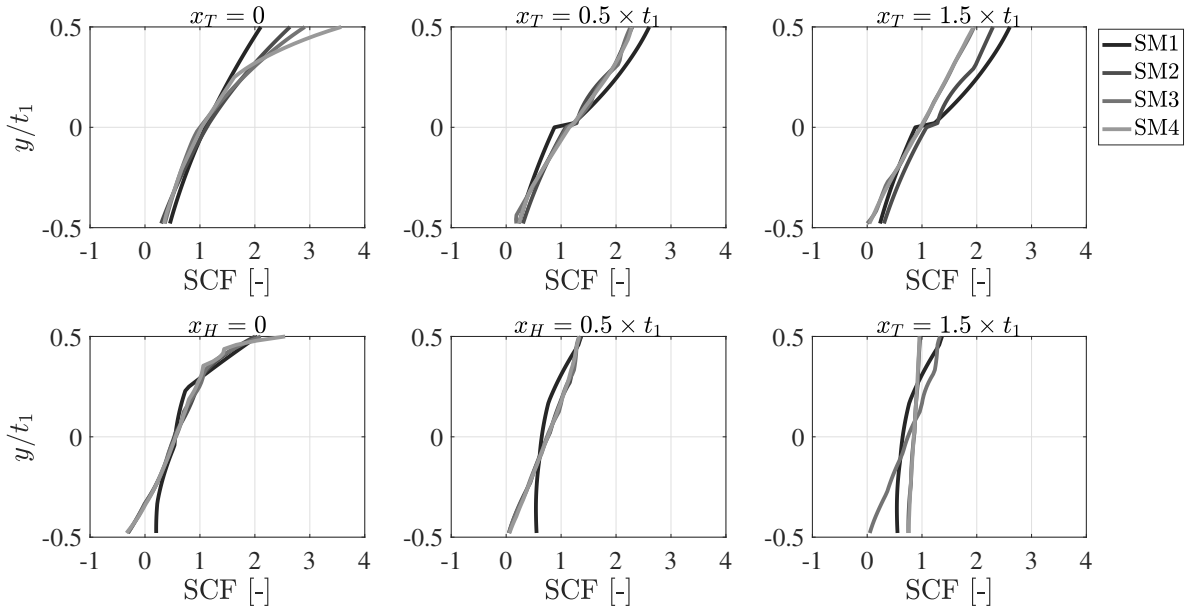

Figure 4.8: *Solid mesh parametric study. SCFs along paths across the thickness. The characteristics of the FE meshes SM1 to SM4 are collected in Table 4.3. The coordinates refer to the brace LCS. BAL are applied. The following non-dimensional parameters are used to create the data:* $\beta = 0.4$, $\tau = 0.4$, $\gamma = 10$, $\theta = 45°$, $\zeta = 0.434$.

Secondly, the normal stress along the paths perpendicular to the weld at the toe and heel positions are compared for the four meshes. This is presented in Figure 4.9. Furthermore, the SCFs are computed and compared to the SCFs obtained with SM4, cf. Table 4.4. It is observed that the differences are, in average, higher at the toe position. A local phenomenon is identified to occur close to that position. This is going to be investigated in more depth in Section 4.4.2. SM1 does not capture this effect. Thus, this mesh refinement is not sufficient. A great amount of simulations are to be run within the parametric investigation carried out in Section 4.4.2. For that reason, a good balance between computational time and accuracy is to be pursued. It is concluded that SM2 is the most suitable mesh for the investigations in that section.

4.3.5 Boundary conditions

The modelling of the boundary conditions has a great influence on the SCF results. The use of several boundary conditions has been discussed in the literature [27], e.g. clamped or hinge ends of braces or chord. In this study, the boundary conditions are simplified to simple supports at the chord ends (pinned-pinned). The chord length L_0 is defined as the distance between the brace-chord intersection and the chord cross-section where boundary conditions are applied. It is chosen so that, when it is extended, the stress field near the joint does not change significantly [3]. Figure 4.10 shows the influence of the chord length in the computation of the SCF. As can be seen, it has little influence. Even for small values of L/d_0, the difference between the computed SCFs and the value reached for $L/d_0 = 10$ is no higher than 2%. It should be noted that the solution does not perfectly converge to

Table 4.4: *Solid mesh parametric study. SCFs computed for the four meshes described in Table 4.3, using the same inputs as in Figure 4.9. The third and fifth columns refer to the difference with respect to the finest mesh, i.e. SM4.*

MRC	SCF at heel [-]	Diff. at heel [%]	SCF at toe [-]	Diff. at toe [%]
SM1	1.60	5.68	3.13	28.30
SM2	1.64	7.88	2.52	2.97
SM3	1.58	4.46	2.46	0.75
SM4	1.52	0.00	2.44	0.00

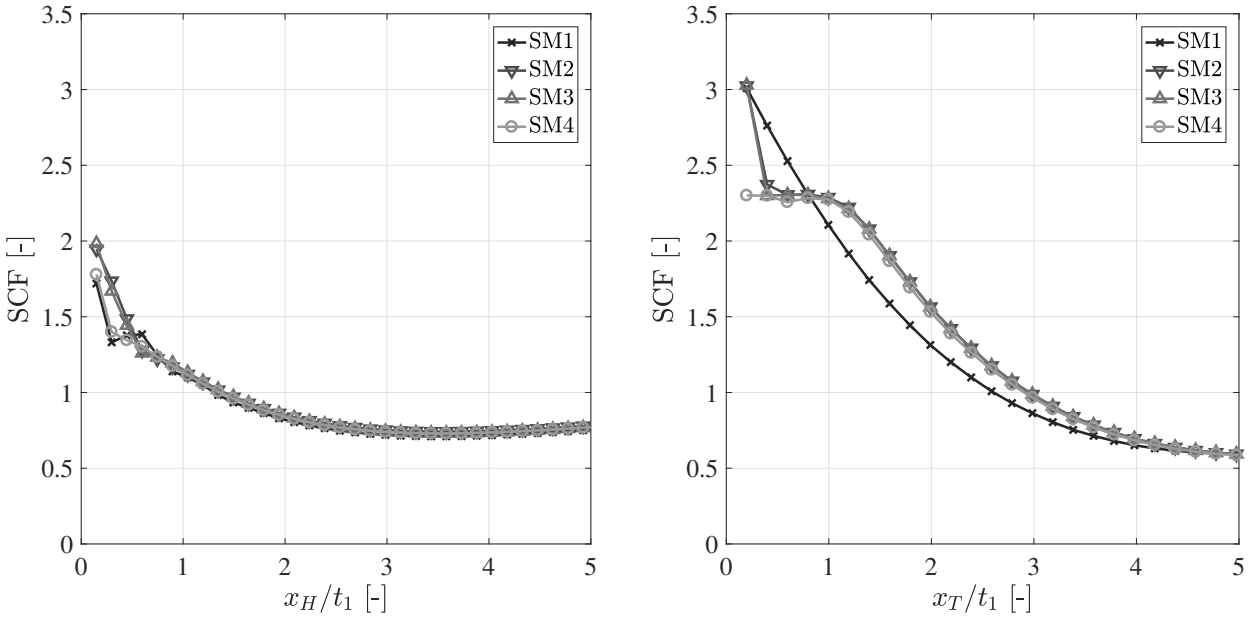

Figure 4.9: *Solid mesh parametric study. SCFs along paths normal to the weld at the heel and toe positions. The characteristics of the FE meshes SM1 to SM4 are collected in Table 4.3. BAL are applied. The following non-dimensional parameters are used to create the data:* $\beta = 0.4$, $\tau = 0.4$, $\gamma = 10$, $\theta = 45°$, $\zeta = 0.434$.

a constant value for increasing chord length. Nevertheless, the influence of the chord length becomes negligible for $L/d_0 > 3$ for the case investigated in Figure 4.10. Since this study has not been performed extensively by covering more cases and the computational repercussion of increasing the chord length is not exceedingly relevant, a ratio of $L/d_0 = 5$ is taken for all simulations within this chapter.

The loads are applied at the ends of the braces by setting a Multi-point Constraint (MPC). Three load cases are considered. They coincide with the cases (1), (2) and (3) depicted in Figure 5.2.

- Balanced Axial Loads (BAL). Brace 1 is compressed and Brace 2 is tensed by the application of axial forces F_a;
- In-plane Bending moments (IPB). Moments M_0 are applied in the negative z-direction considering the braces LCS;
- Out-of-plane Bending moments (OPB). Moments M_0 are applied in the positive x-direction considering the braces LCS.

4.3.6 Post-processing

For the investigation carried out in Section 4.4.1, the results are read from paths in the through-thickness direction at four distances from the weld, as was previously mentioned. The element solution is interpolated at a discrete number of points that are read into Matlab©. The read-out points are defined as for the generic hot-spot method [3], i.e. at 0.5 t and 1.5 t, cf. Figure 4.11. This is chosen for

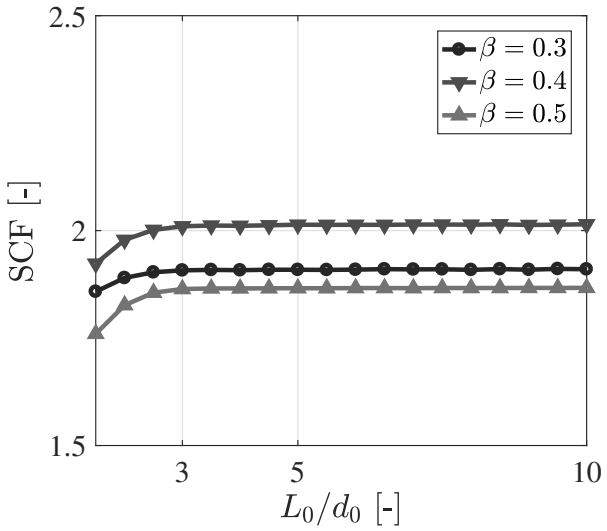

Figure 4.10: *Influence of extending the chord length in the computation of the SCF. Shell elements and the following non-dimensional parameters are used to generate the data:* $\tau = 0.5$, $\gamma = 10$, $\theta = 45°$, $\zeta = 0.4$.

simplicity in the presentation of the results. Nevertheless, for tubular members of high diameter, that formulation and the one presented in Chapter 2.1 present minor differences. Additional paths are set at the intersection points and at a point far from the joint, i.e. at 30 t.

For the post-processing done in Section 4.4.2, the results are read along paths perpendicular to the weld. The stresses are then interpolated at the read-out points and linearly extrapolated to the weld toe, afterwards, in order to compute the HSS. The SCF is then computed as the HSS divided by the nominal stress. The nominal stress at the braces due to BAL is computed as in Eq. (4.3). The nominal stress in the chord due to load case BAL is computed as in Eq. (4.4). The nominal stress at the braces due to IPB and OPB is computed using Eq. (4.5), with $I_{y1,2}$ defined as in Eq. (4.6). The coordinates refer to the regarded member LCS.

$$S = \frac{4F_a}{\pi d_{1,2}^2} \tag{4.3}$$

$$S = \frac{8F_a}{\pi d_0^2}(\cos\theta_1 + \cos\theta_2) \tag{4.4}$$

$$S = \frac{M_0}{I_{y1,2}} y \tag{4.5}$$

$$I_{y1,2} = \frac{\pi}{64}(d_{1,2}^4 - (d_{1,2} - 2t_{1,2})^4) \tag{4.6}$$

4.4 Discussion of the results

The results are organized in two sections. In Section 4.4.1, the through-thickness stress field investigation is presented. In Section 4.4.2, the comparison between the plate and solid models is elaborated.

4.4.1 Through-thickness behavior

In this section, the normal stress field across the plate thickness is studied using the solid model SM3, cf. Table 4.4. The following matters are to be assessed. First of all, the validity of using one single element through-thickness is going to be studied. As mentioned before, DNV-GL [3] suggests the use of a single element across the thickness and reduced integration. This recommendation is given with the purpose of saving computational time. However, this assumption is only valid if the aforementioned

stress field is linear. Additionally, any variation that is different from the linear distribution will not be captured using the plate theory. Thus, this would yield additional differences between the solutions obtained by using solid and plate theories.

The stress field normal to the weld is here denoted S_x, x referring to the LCS of the member under study. In Figure 4.11, S_x is plotted at the region close to the weld crown toe position for the BAL case. It can be observed that the stress distribution becomes linear across the wall thickness when moving further from the intersection point. At the extrapolation region, the distribution is approximately linear. This is especially true for the chord plate. When getting closer to the intersection point, the stress approximates to a singularity and the distribution through-thickness becomes non-linear. As can be observed, the solid model fulfills, in this studied case, the assumption implicit in the hot-spot method, which states that the structural stress behavior is linear along paths perpendicular to the weld, and across the thickness.

The normal stress fields S_x, computed using the SM1 and SM3 mesh refinements, are compared in Figure 4.12, along paths across the thickness. The results are computed at four paths at the crown toe position in the Brace 1 and in the chord. Regarding the results at the chord, it is observed that the variation at the read-out points is approximately linear. Moreover, the results obtained using one single element through-thickness reproduce the behavior accurately. As was previously discussed, the stress field at the intersection point is theoretically infinite. Nevertheless, this affects a relatively small region and does not affect the extrapolation region. The stress field, at a distance of $30 \times t_0$ from the intersection point, presents a noticeable deviation from the nominal stress. This is expected, since the gap between the two braces is short, i.e. 0.480 m in comparison with the 1 m chord diameter. Thus, the stress field does not have enough space to recover its tendency to the nominal situation.

Regarding the results at the brace plate, a poor matching between the two mesh refinements is seen. The solutions of SM1 and SM3 only converge for the path at $30 \times t_1$ from the intersection. At this distance, they both match the nominal stress distribution. The poor representation given by the SM1 mesh is primarily due to the distortion of the element shape. In order to build a regular continuous mesh, the elements at the brace plate are of trapezoidal shape. It is seen that this affects the results to a great extent. Thus, a great refinement in the trough thickness direction is to be set to compensate. It is therefore recommended to use more than one element through-thickness.

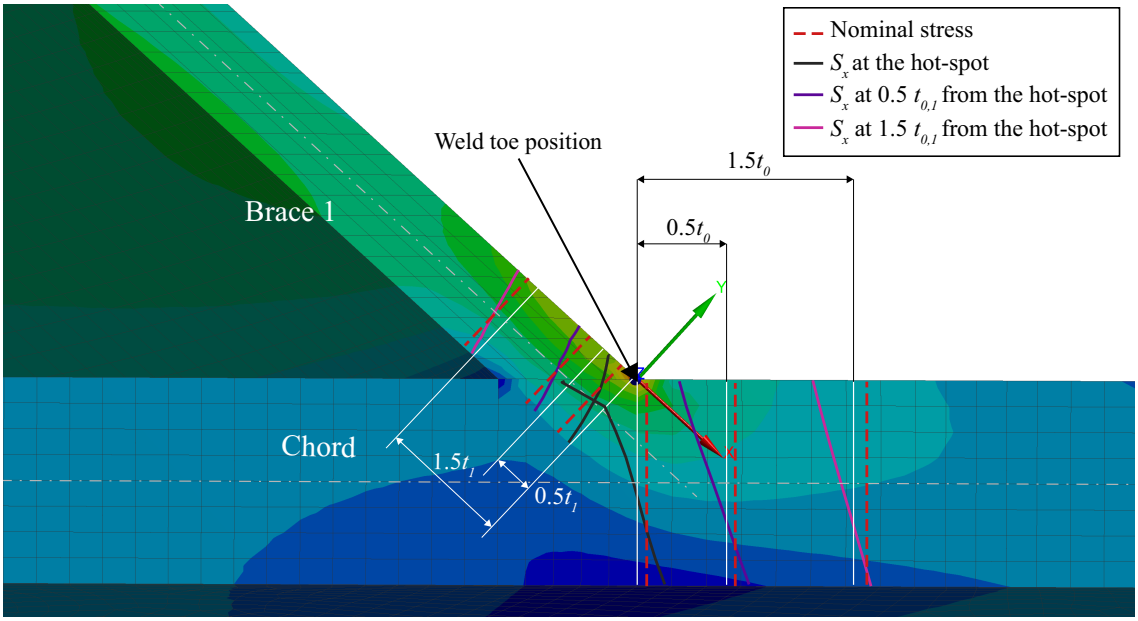

Figure 4.11: *Schematic representation of the normal stress S_x across the brace and chord thickness due to BAL. The following non-dimensional parameters are used: $\tau = 0.45$, $\beta = 0.45$, $\gamma = 10$, $\theta = 40°$, $\zeta = 0.48$.*

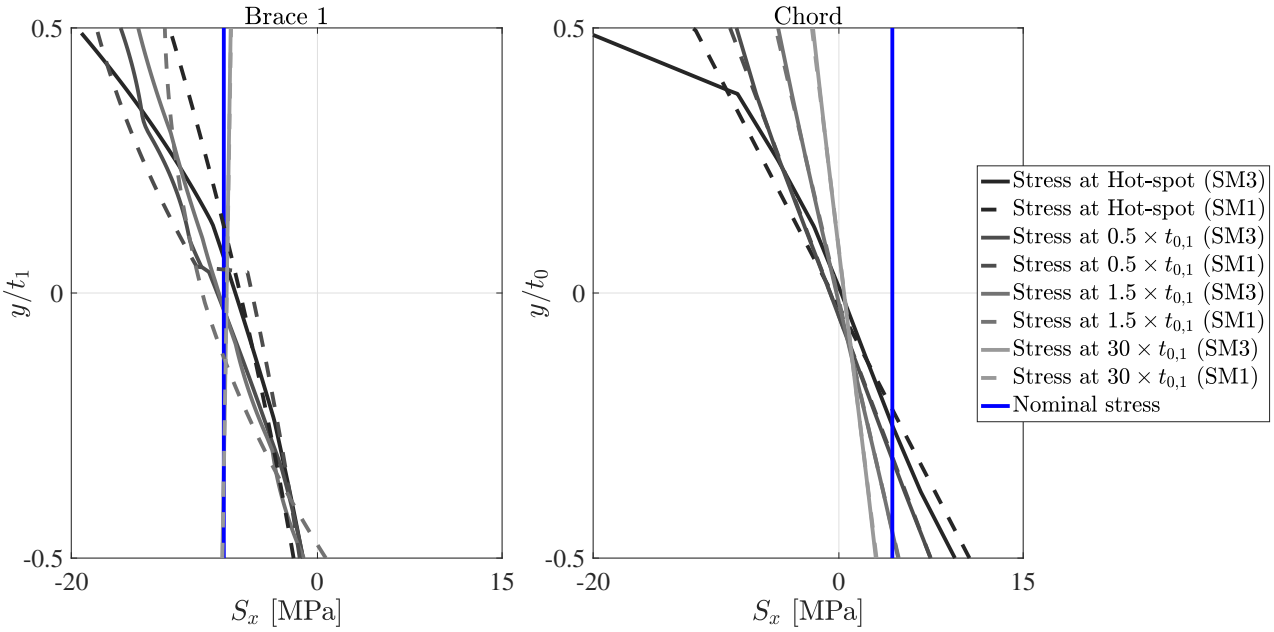

Figure 4.12: *Through-thickness normal stress field S_x at four different locations of the Brace 1 and chord toe positions. The coordinates refer to the LCS of the members. The same non-dimensional parameters as in Figure 4.11 are employed.*

Additionally, the deformed shapes, obtained by using the solid and shell models, are compared. The contour diagrams are plotted on the deformed shapes for both the solid and shell models, at the vicinity of the hot-spot positions, for the BAL, IPB and OPB cases in Figure 4.13. The more complex deformed shape is given by the BAL case. The differences between both models deformed shapes are also the highest for this case. This case is marked by a pronounced bending of the chord plate. The brace plate has to adapt to this deformation, suffering a tensile elongation in the through-thickness direction at the nearby of the connection. It can be appreciated that the shell model cannot capture this behavior. The shell model predicts high shear deformations of the chord plate, whose section does not remain perpendicular to the mid-plane. Moreover, for the shell model, the curvature of the brace plate increases continuously up to the intersection point, where it is found to be maximum. This is not the case for the solid model. A turning point of the vertical displacement field is found at a certain distance from the intersection point. The best matching between the models is found for the IPB case. For this case, the deformed shape is marked by mild changes in the curvature of the members plates. For the OPB case, the deformed shapes that both models predict are reasonably similar. Nevertheless, the solid model estimates a slightly higher bending of the brace plate.

It can be appreciated for the shell model that, the required mesh refinement yields a poor ratio between the members thickness and the element size. This has a strong influence on the results. Particularly, when using shell elements that account for the shear deformation. Moreover, it is observed that the shell model fails to represent the local stiffness of the connection. Therefore, it is expected to find poor matching between the results of both models, particularly for members of high thickness to diameter ratios.

4.4.2 Path perpendicular to the weld

In this section, the outcome of the hot-spot method using the solid and the shell models is compared. A parametric study is performed to generate a wider overview that is applicable to most situations. This section follows the following structure. First of all, the extension of the parametric study is defined. Secondly, the obtained results are presented. A local phenomenon is identified from the analysis of the results. This effect is studied and lastly, its repercussion in the results is investigated.

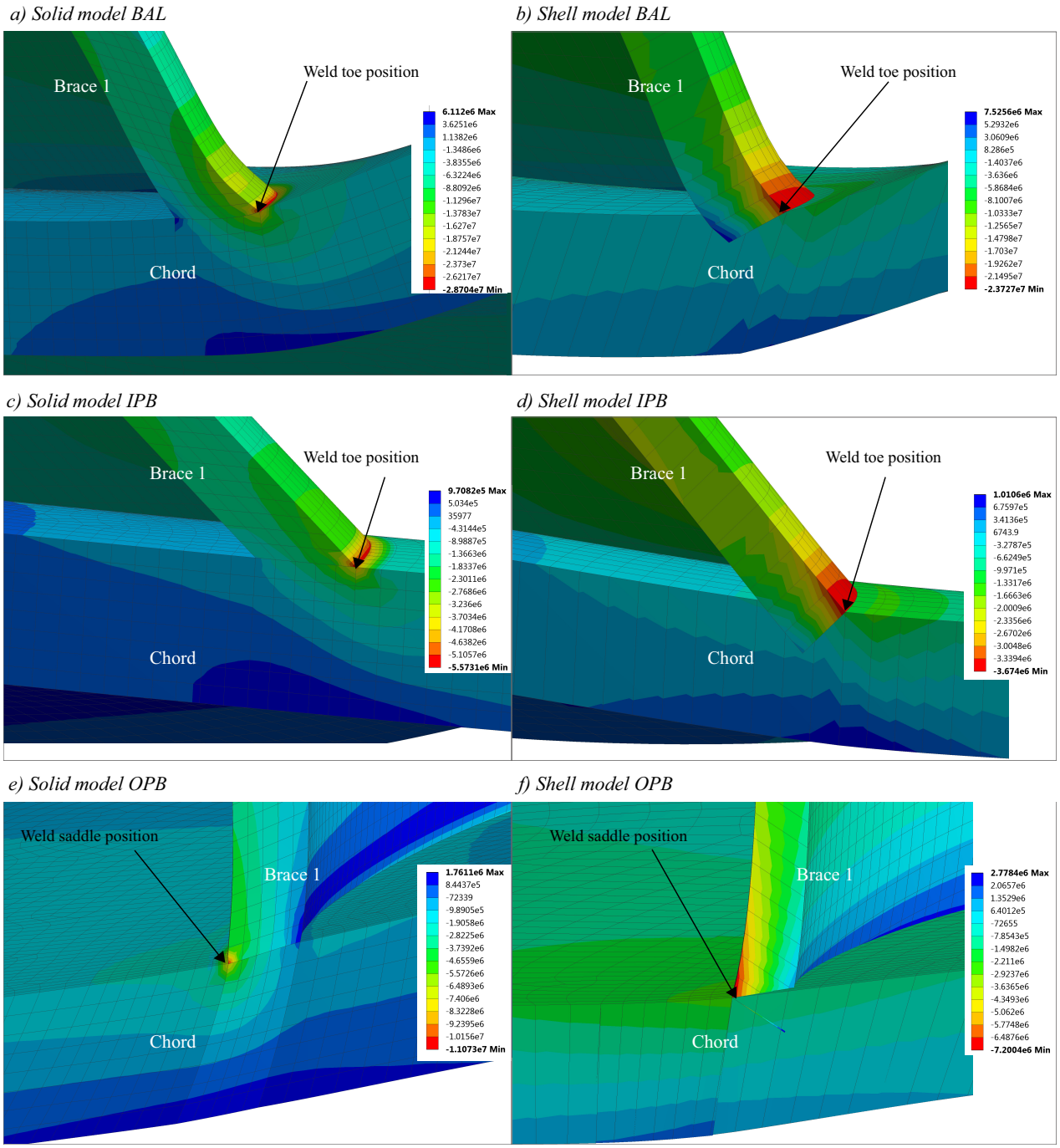

Figure 4.13: *Comparison between the solid and the shell models of the stress normal to the weld S_x at the Brace 1 toe position due to BAL, IPB and OPB actions. The deformed shape is scaled by a factor of $3.1 \cdot 10^3$. The same non-dimensional parameters as in Figure 4.11 are employed.*

Extension of the parametric study

A parametric study is carried out in order to extend the applicability of the conclusions drawn. Initially, the model is defined by 9 independent parameters, as shown in Figure 4.1. The braces are kept identical in all the built models, i.e. $\tau_1 = \tau_2$, $\beta_1 = \beta_2$, $\theta_1 = \theta_2$ and $\zeta_1 = \zeta_2$. The subscripts are not included from this point on, for simplicity. The influence of γ in the SCF is reasonably low, as it was shown in *J. Mendoza (2017)* [1]. For simplicity, this parameter is kept constant within this investigation and equal to 10 for all cases. A small eccentricity is defined for the cases which have high β values in order to avoid the braces from overlapping. Considering the four constraints due to brace symmetry and neglecting the influence of ζ and γ, the parametric study is performed regarding three parameters only, i.e. β, τ and θ.

Various cases are built, aiming to minimize the amount of FEM simulations that are run. Seven cases are chosen to generate the general overview, i.e. three cases per parameter; one low value, one intermediate value and one high value. A general case, which is used in the investigations of the three parameters, is defined by $\beta = 0.4$, $\tau = 0.4$, $\theta = 45°$. This case is here designated by the name CASE 1. From this general case, two more cases per studied parameter are created. To study the influence of β, this parameter is varied to 0.6 and 0.8, keeping the other parameters as in CASE 1. To study the influence of τ, this parameter is varied to 0.6 and 0.8, keeping the other parameters as in CASE 1. To study the influence of θ, this parameter is varied to 35° and 55°, keeping the other parameters as in CASE 1. A clear overview of the seven cases is presented in Table A.1 in Appendix A.

Considering the seven geometry cases, and that three load situations are tried for the two types of models (solid and shell), a total of 42 simulations are performed within this investigation. Taking into account that the results are read for the two braces at three positions around the weld, a total of 252 result files are produced for post-processing in Matlab©.

Presentation of the results

The normal stress field S_x is read in paths perpendicular to the weld at three positions, i.e. the toe, heel and saddle positions. This is plotted for both, the solid and shell models, in Figures A.1 to A.7 in Appendix A. When analyzing the results, a phenomenon is observed to be present only for the solid models and at certain positions around the weld. The effect is characterized by a sudden change in the slope of the normal stress field, in the area close to the intersection. This can be observed in Figure 4.14. This effect happens specially at the toe position and, to a lesser extent, at the saddle and intermediate positions. However, the effect does not occur at the heel position.

It is observed that the effect has a strong dependency on the brace inclination θ, cf. Figure 4.15. The higher the inclination is, i.e. the lower θ is, the greater the extension of the effect is. It can also be appreciated in the same plot that, as mentioned above, this effect does not appear at the heel position. When defining a path perpendicular to the brace wall at the weld crown toe area, the brace thickness is

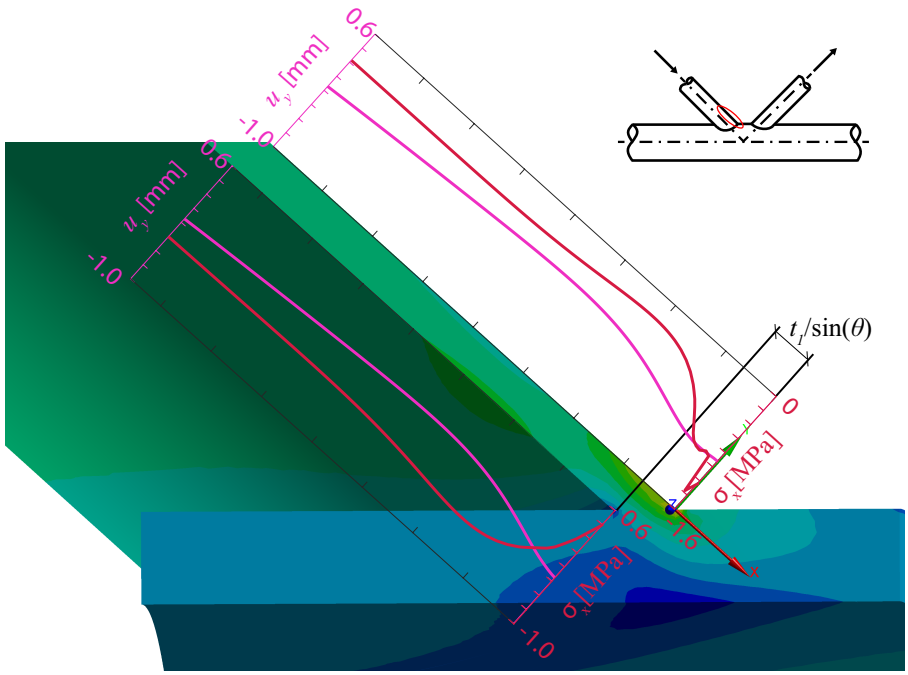

Figure 4.14: *Effect of the local clamping of the brace plate. The normal stress S_x and the vertical displacement u_y are plotted at the outer and inner walls of the brace at the crown toe position. BAL are applied at the braces ends and the following non-dimensional parameters are used: $\tau = 0.45$, $\beta = 0.45$, $\gamma = 10$, $\theta = 40°$, $\zeta = 0.48$.*

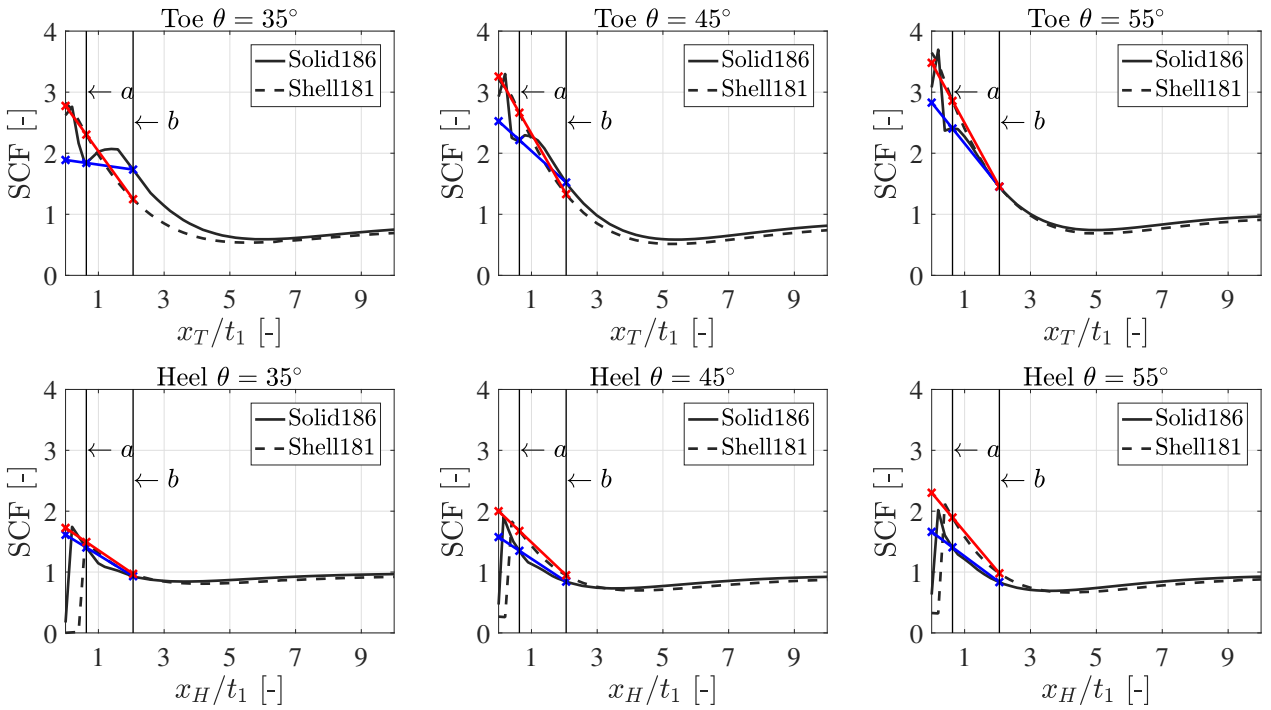

Figure 4.15: *Influence of θ in the brace plate clamping effect. BAL are applied at the brace ends and the following non-dimensional parameters are used to reproduce the data in this plot: $\beta = 0.4$, $\tau = 0.4$ and $\gamma = 10$.*

continued with the chord thickness. For high brace inclinations, this transition occurs within a longer extension. Nevertheless, this is not the case for the heel position. At this position, a path perpendicular to the brace walls does not have that continuation of the brace thickness with the chord thickness.

If the weld is not modelled, the original formulation of the extrapolation region does not properly capture the structural stress behavior. Moreover, it is seen that this effect yields non-conservative results for most situations. It is concluded that the read-out points ought to be reformulated. Previous to that, the spacial extension of this phenomenon is to be estimated. Note that, it is expected that this effect would disappear if the weld was modelled. This is going to be studied in more detail in Chapter 7, where a comparison between the hot-spot and notch methods is made including the weld geometry. The normal stress S_x and the displacement u_y, referenced to the Brace 1 LCS, are plotted along a path normal the weld over the geometry in Figure 4.14. It is observed that the effect starts taking place approximately where the inner wall of the brace intersects the chord wall. This corresponds to the brace thickness t_i projected to the outer wall, i.e. $t_i/\sin\theta_i$. Furthermore, it can be observed that the vertical displacements u_y of the outer and inner walls are not exactly the same. This means that the stresses in the direction of the wall thickness are non-zero. Regarding the cyclic nature of the applied loading, these stresses stretch and compress the plate section.

Reformulation of the read-out points

The definition of the read-out points fails to capture the structural stress tendency for some cases. This is specially true for the normal stress field at the toe position when using solid modelling. A discontinuity in the field is observed close to the intersection point. An explanation of this phenomenon is given above. Moreover, the location of the sudden change in the slope is found at a distance, measured from the intersection point of the outer faces of the brace and chord plates, of approximately $t_i/\sin\theta_i$. If no reformulation of the read-out points is performed, the extrapolation will not produce realistic results, tending to underestimate the SCF. This enhances the disagreement between the results obtained by the solid and plate theories.

Table 4.5: *Comparison of the results between the solid and shell models including the original formulation of the extrapolation read-out points and the corrected one. Results are computed at the crown toe position of the Brace 1. NC and C refer to the non-corrected and the corrected extrapolation region, respectively.*

Case	LC	Solid NC	Solid C	Shell	Difference NC	Difference C
CASE1	BAL	2.52	3.25	3.26	22.48%	0.24%
CASE1	IPB	1.31	1.43	1.61	18.96%	10.98%
CASE2	BAL	2.35	2.49	2.72	13.67%	8.47%
CASE2	IPB	1.49	1.46	1.67	10.74%	12.20%
CASE3	BAL	2.14	2.18	2.56	16.15%	14.78%
CASE3	IPB	1.56	1.51	1.68	7.29%	9.81%
CASE4	BAL	2.63	3.60	3.66	28.12%	1.60%
CASE4	IPB	1.25	1.35	1.57	20.65%	14.32%
CASE5	BAL	2.79	3.60	3.80	26.58%	5.16%
CASE5	IPB	1.28	1.24	1.54	16.66%	19.80%
CASE6	BAL	1.89	3.20	2.78	31.91%	-15.38%
CASE6	IPB	0.85	1.14	1.14	26.18%	0.43%
CASE7	BAL	2.83	3.06	3.48	18.75%	11.97%
CASE7	IPB	1.68	1.71	2.05	18.12%	16.60%

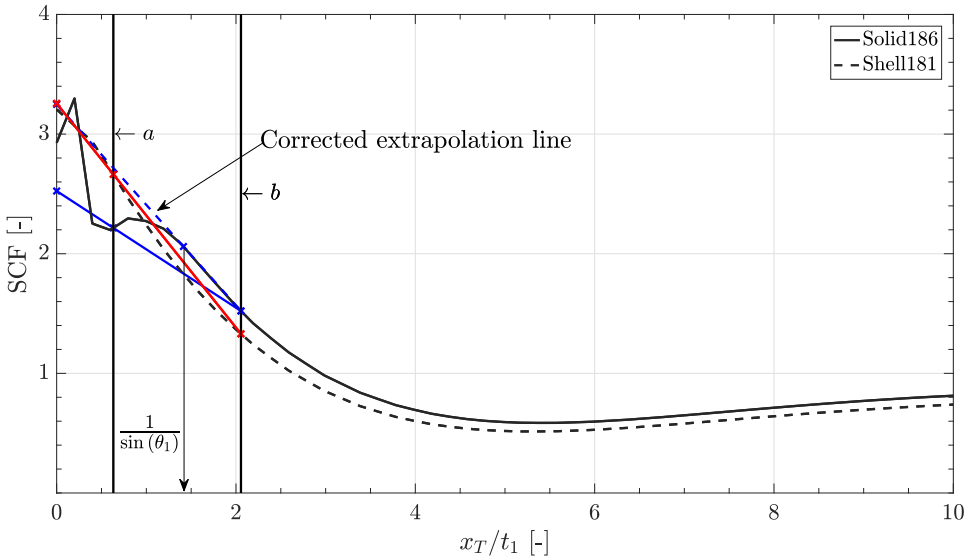

Figure 4.16: *Correction of the extrapolation region at the toe position. The extrapolation lines, as defined in DNVGL-RP-C203 [3], are plotted in blue and red for the solid and shell models, respectively. The corrected extrapolation line for the solid model is shown in dashed blue. These results are given at the Brace 1 toe position due to BAL for the geometrical CASE 1.*

A simple way of avoiding this problem in the definition of the read-out points is proposed hereafter. The second read-out point b is found to be in the structural stress region. Thus, the redefinition of the read-out points is chosen to only affect the first read-out point a. When a happens to be located within the stress discontinuity, i.e. $a < t_i/\sin\theta_i$, then a is redefined as $a \leftarrow t_i/\sin\theta_i$. This improvement places the point a away from the discontinuity. The redefined extrapolation region will therefore capture the structural stress tendency.

A comparison of the results, accounting and not accounting for the reformulation of the extrapolated region, is carried out. This is collected in Table 4.5 and exemplified in Figure 4.16. An average difference of ca. 20% exists between the results of the shell model and the non-corrected results of the solid model. The difference drops to ca. 8% when including the correction. It can be observed that, not accounting for the reformulation yields non-conservative results for most of the cases. The difference between the two is estimated to be of 12%. It is concluded that the difference is not negligible and that it should be considered in order to make a fair comparison between the two models.

The results are recalculated using the aforementioned reformulation of the extrapolation region. The results are collected in Appendix A. The SCF comparison is presented in Tables A.2 to A.4. Moreover, the extrapolation paths used to generate the results are shown in Figures A.1 to A.7. The results of the parametric investigation are plotted in Figure 5.3 in Chapter 5, including a comparison with the SCF results obtained using the Efthymiou equations. The analysis of the results is elaborated in that chapter.

4.5 Summary

The hot-spot method applied to the fatigue assessment of tubular joints can be approached using numerical methods. There are various ways of building the FE models, but there are no guidelines that address the differences between them. In this chapter, the plate and solid models are compared. First of all, the stress field across the thickness is studied for the solid model. The variation is observed to be linear within the extrapolation region and non-linear at the vicinity of the intersection. Secondly, the normal stress field, at paths perpendicular to the weld, is compared at three positions around the weld. This study is carried out within a parametric study of τ, β and θ, which comprised 42 simulations. A local phenomenon is seen to take place for the solid model at certain positions, predominantly at the crown toe position. This phenomenon is a shadow effect caused by the abrupt change in stiffness at the chord-brace intersection. Its extension is estimated to be ca. $t_i / \sin\theta_i$ from the intersection point. Due to this effect, the extrapolation region is displaced and its formulation, as given by the guidelines, provides unsatisfactory results. The extrapolation region is redefined so that the structural stress behavior is captured correctly.

5 | Investigation of Efthymiou Equations

There are several ways of performing a fatigue assessment following the structural stress approach. For instance, one can obtain the structural stress at the hot-spot from short scale testing, long scale testing, numerical methods or parametric formulae. Two ways of performing the assessment using numerical methods were investigated in Chapter 4. The use of parametric formulae is common in engineering practice, especially during the preliminary stages of the design. Therefore, it is worth comparing the results obtained in the previous chapter with the ones that these formulae predict. A brief discussion of the background of the Efthymiou equations is provided in Section 5.1. The results obtained in Chapter 4.4.2 are combined with the ones obtained from the Efthymiou equations in Section 5.2. A discussion of the results is included, together with the overall conclusions of the parametric investigation.

5.1 Background of the investigation

The Efthymiou equations are widely used in practice to assess the SCF of tubular joints. Formulae are given for tabulated joint and action configurations as a function of the geometrical non-dimensional parameters, cf. Eq. (3.1). The validity ranges of these equations are given in Eq. (5.1) [3]. The

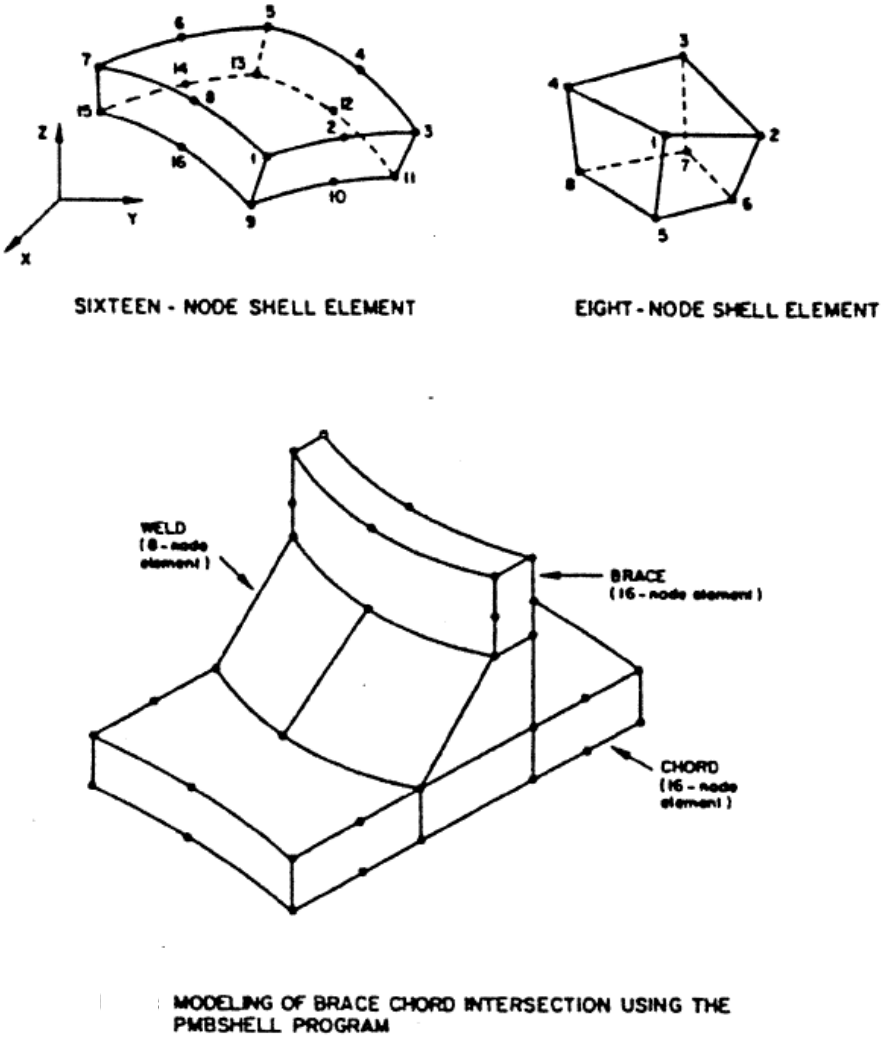

Figure 5.1: *Element type used by Efthymiou for the derivation of the parametric SCF formulae. This picture is taken from [4].*

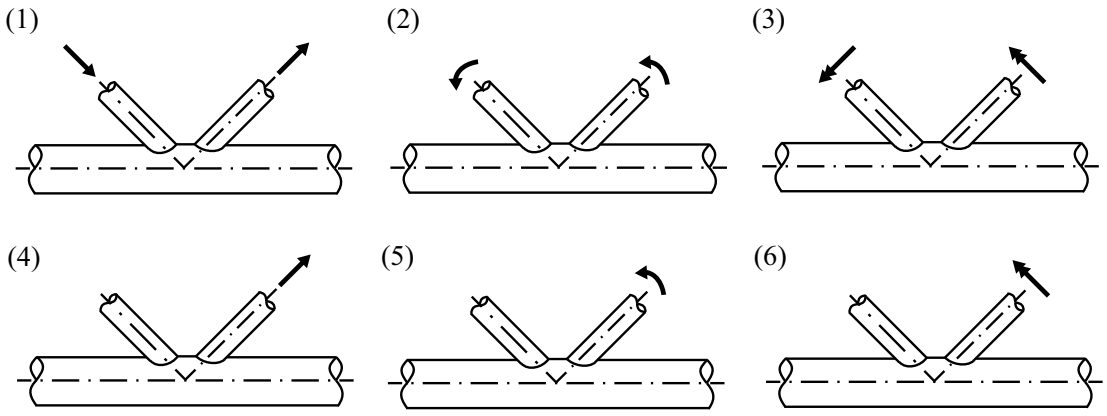

Figure 5.2: *Load cases covered by the Efthymiou formulae for the K-joint configuration.*

structural stress is obtained for various load cases as the nominal stress, magnified with the hot-spot SCF. The total structural stress around the weld can be estimated as the linear superposition of the structural stresses, as given in Eq. (2.5). For the particular case of K-joints, the equations are given for six load cases (cf. Fig. 5.2): (1) balanced axial loads (one brace compressed and one brace tensed); (2) one brace tensed only; (3) in-plane bending (both braces bending to the same direction); (4) bending moment applied to only one brace; (5) out-of-plane bending (both braces bending to the same direction); (6) out-of-plane bending moment applied to only one brace. Applying superposition from these cases, it is possible to find the remaining configurations of loading at the braces.

$$\begin{array}{lll} 0.2 & \leq \beta \leq & 1.0 \\ 0.2 & \leq \tau \leq & 1.0 \\ 8 & \leq \gamma \leq & 32 \\ 20^\circ & \leq \theta \leq & 90^\circ \\ \dfrac{-0.6\beta}{\sin\theta} & \leq \zeta \leq & 1.0 \end{array} \tag{5.1}$$

The Efthymiou equations can be found in Table B-3 and B-4 in Appendix B of DNVGL-RP-C203 [3]. Two equations are given for each load configuration, related to the chord and brace hot-spot. The parametric formulae were computed by polynomial fitting of massive amounts of data generated using FE models. The quality of the fitting is not equal for all the parameters combinations. An origin of combination was chosen. When moving further away from that origin, higher errors can be found. The element types used in the FE models are shown in Figure 5.1. It should be noted that, even though the element types are called shell elements, they are somehow more similar to solid elements. The reason for having that designation is that their distribution of nodes is not the same for all faces. For the sixteen-nodes shell element, mid-side nodes are found at the top and bottom shell faces but not at the through thickness direction. Therefore, they are meant to be used for geometries that have two dimensions predominantly higher than a third one; such as thin- or thick-wall structures.

Formulae are given to estimate the SCF at the hot-spot position only, for the chord and the braces. However, it is not established where the hot-spot is located. Hence, the application of the stress superposition in Eq. (2.5) results in quite conservative estimations. The SCF can only be computed where the maximum is found. The FEM results obtained in Chapter 4 present differences in the order of 50% between the toe, heel and saddle positions for the BAL case and in the order of 40% between the toe and heel position for the IPB case, see Tables A.2 to A.4. This is exemplified in Table 5.1 for the geometric CASE 1. It is concluded that the conservatism that results from the use of these equations is higher than the one implicit in the original fitting used for the derivation of the equations.

Table 5.1: *Example of the differences between the SCF at the hot-spot and at other positions. The data is extracted from the results of the solid model for the geometric CASE 1, which was described in Chapter 4.*

LC	Position	SCF	Diff. wrt. hot-spot SCF
BAL	**Toe**	**3.25**	0.00%
BAL	Heel	1.57	51.52%
BAL	Saddle	1.49	53.99%
IPB	Toe	1.43	39.06%
IPB	**Heel**	**2.35**	0.00%

5.2 Discussion of results

The parametric investigation carried out in Chapter 4.4.2 is extended with the results obtained using the Efthymiou equations. The SCF results computed by using the solid and shell FE models, and the ones produced applying the Efthymiou equations, are plotted in Figure 5.3. The results are organized per load case; balanced axial loads, in-plane moment and out-of-plane moment cases, respectively. For each figure, each row of subplots corresponds to a different position around the weld. Only the relevant positions are shown, i.e. the toe, heel and saddle positions for the BAL case; the toe and heel positions for the IPB case; and the saddle position for the OPB case. Each column corresponds to one of the investigated non-dimensional parameters, i.e. β, τ and θ. The values used to generate this plot are collected in Appendix A in Tables A.2, A.3 and A.4 and in Figures A.1 to A.7. The following observations and conclusions are drawn from the results:

- The solid and the shell models provide a similar tendency for the three parametric investigations for all the studied cases.
- The three models provide a similar tendency for the three parametric investigations for the majority of the cases. The reason that this does not happen for all the cases is that the Efthymiou equations only provide the SCF at the hot-spot position of the weld. Therefore, when analyzing the SCF at a different location, the Efthymiou equations yield a higher SCF and at some cases, a different tendency. An example of that can be found for the θ parametric study for the IPB case at the toe position. In this case, the Efthymiou equations predict a decreasing tendency for higher θ, while the solid and shell models predict the opposite. However, at the heel position, where the hot-spot is found, the three models estimate a similar tendency.
- The shell model provides more conservative results than the solid model for most of the studied cases. One reason for that could reside in the way of building the shell model. As explained in Chapter 4, the geometry of the shell element is defined at the outer wall of the members. The thickness of the shell element is set from there. This type of modelling has been compared with the option of modelling the shell from the plate mid-plane. The latter modelling option yields ca. 10% smaller results. Moreover, it was seen that the normal stress distribution across the thickness is not linear, at the vicinity of the intersection point. This cannot be captured by the plate theory. Since the stress field is erroneous at the intersection point, according to the Saint-Venant principle, the influence of the error is extended to a distance from that point which is presumably longer than the first read-out point a. Nevertheless, the stress field tends to be linear across the thickness within the extrapolation region. Due to that, the employment of a shell model is acceptable to some degree of accuracy.
- Regarding the BAL case, the highest results are found for the toe position. Thus, it is expected that the hot-spot is found either at this position or close to it. At this position, the SCF predicted by the solid model match relatively well to the ones given by the shell model. It should be noted that for large brace diameters, i.e. $\beta = 0.6, 0.8$; the Efthymiou equations provide non-conservative results. The equations, however, over-predict the results at the heel and saddle

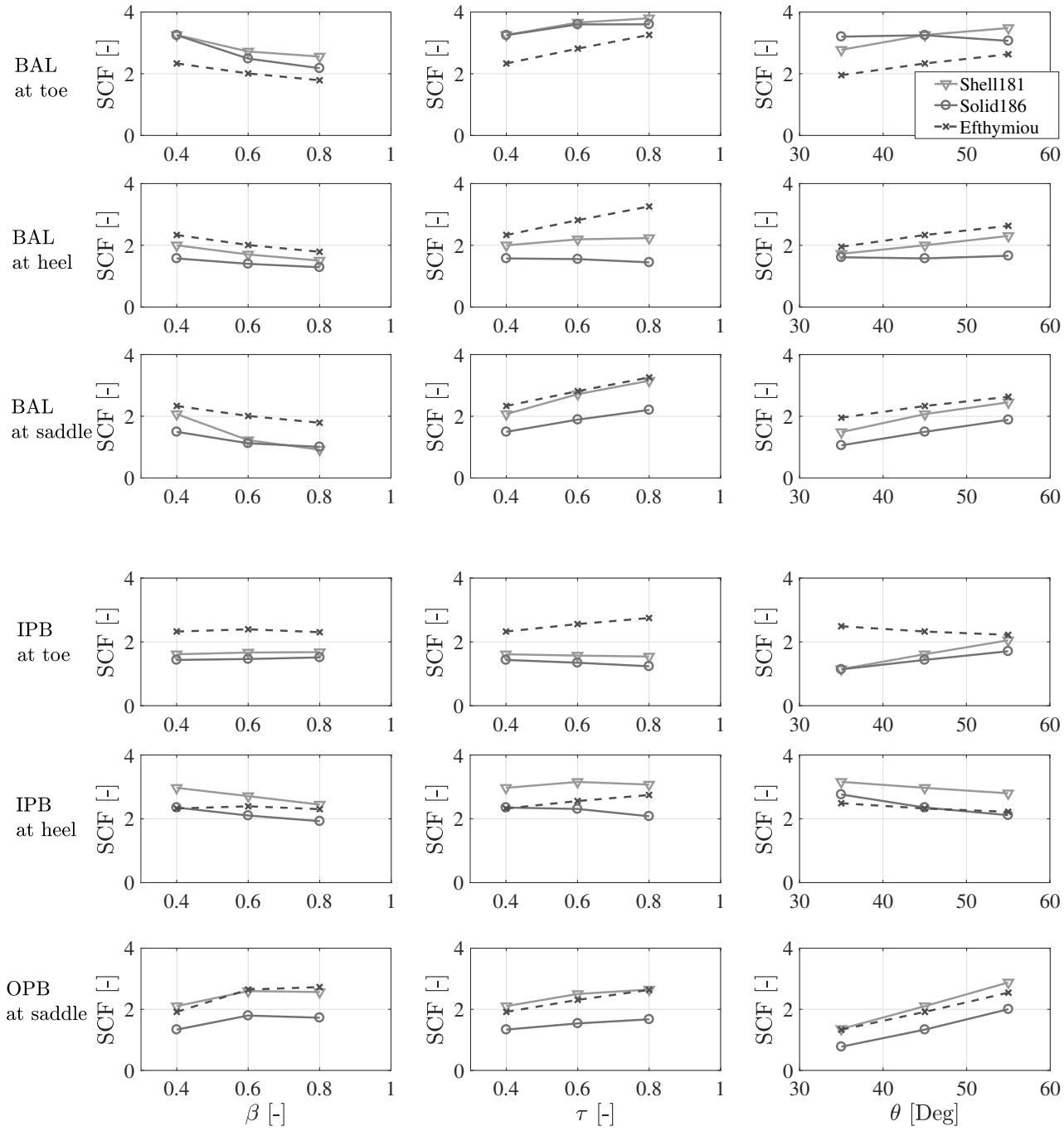

Figure 5.3: *SCF parametric comparison between shell and solid FE models and Efthymiou parametric formulae. The cases described in Table A.1 are used to generate the data in these plots. The Cases 1, 2 and 3 are used for the β comparison. The Cases 1, 4 and 5 are used for the τ comparison. The Cases 6, 1 and 7 are used for the θ comparison. The SCF results are tabulated in Tables A.2, A.3 and A.4.*

positions. Specially at the saddle position for large β values and at the heel position for high τ values.

- Regarding the IPB case, the highest values are found at the heel position. Large over-estimations of the Efthymiou equations are given at the toe position. At the heel, the Efthymiou results are in between the one obtained using the solid and shell models; being, generally speaking, closer to the solid model results. A particularly good match is found for the θ investigation. Within this study, the braces diameters and thicknesses are approximately half the chord ones. These ratios are conventionally used in OWT jacket members.

- Regarding the OPB case, it is seen that the Efthymiou results match the shell results better than the solid ones.

In general, it is concluded that generalizations are not easy to be made. An extensive parametric investigation is carried out, covering the SCF obtained by using solid and shell FE models and the Efthymiou equations for most of the K-joint configurations used in practice. In general, it is seen that using the solid model is favorable for the purpose of epitomizing the joint, since the shell model tends to overpredict the SCF.

5.3 Summary

In the previous Chapter 4, the comparison of the solid and plate models, used for the hot-spot fatigue assessment, was addressed. In this chapter, these results are combined with the ones estimated by the Efthymiou equations. This provides an overview of the accuracy inherent in its use. Some situations where these equations over-predict and underestimate the results are found. The equations only assess the HSS at the hot-spot position. When comparing the results at the other positions around the weld, where the stresses are not maximum, it is seen that the equations highly overestimate the SCF. Furthermore, it is concluded that the shell model yields higher SCFs for most of the cases.

6 | Carry-over Effect in KK-joints

In the previous Chapters 4 and 5, an investigation of various aspects of the structural stress approach regarding planar K-joints was presented. In this chapter, the study of this method is extended to cover the carry-over effect due to the out-of-plane braces in multiplanar KK-joints configurations. First of all, the problem is introduced in Section 6.1. The method used to investigate this problem is elaborated in Section 6.2. The characteristics of the models used to apply this methodology are described in Section 6.3. Finally, results are presented and discussed in Section 6.4.

6.1 Introduction to the problem

Most of the joints in offshore wind jackets are multiplanar KK-joint. The fatigue assessment of these joints is generally done neglecting any influence of the braces that are located at the contiguous face of the jacket. For instance, the KK-joints are assessed as planar K-joints, such as the ones analyzed so far in this project. The validity of this assumption is going to be investigated in this chapter.

It is expected to find situations where including this carry-over effect results in a beneficial or a detrimental contribution, i.e. reducing or magnifying the stresses at the hot-spot position. The aim of this study is to document the degree of accuracy of the omission of this effect. This is to be performed within a parametric study, covering an extensive range of braces and chord diameters and thicknesses.

6.2 Problem approach

In this chapter, the carry-over effect due to loading at the braces at the contiguous face of a multiplanar KK-joint is assessed using numerical methods. A parametric study is carried out to study this effect, covering several chord and brace diameter and thickness combinations. Several models are going to be developed within this investigation. The characteristics of the models used are described in Section 6.3.

Two parametric models are built, i.e. a planar K-joint model and a multiplanar KK-joint model. The SCF, computed at a reference brace, are to be compared between both parametric models. The influence of the loading at the out-of-plane braces, on the computation of the SCF at the reference brace, is defined as the carry-over effect. This effect is going to be studied for several load configurations. In addition to that, the influence of the magnitude of the applied loads is going to be quantified.

The parameter Ψ, defined in Figure 6.1, is introduced. This parameter measures the relative angle between the planes where the jacket braces are contained. In order to investigate the validity range of

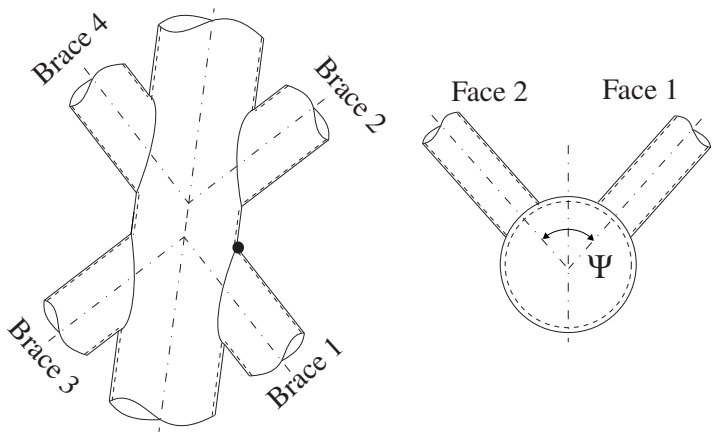

Figure 6.1: *Schematic representation of a multiplanar KK-joint.*

the assumption described in Section 6.1, this parameter is going to be varied. In order to extend the applicability of this study, Ψ is going to be varied from 60° to 105°. The case of having an opening Ψ of around 60° occurs for three leg jackets. A Ψ of around 90° is found for four leg jackets. Due to the considerations that were explained in Chapter 4.4.2, the influence of γ and ζ are neglected. In order to simplify the investigation, the braces are again kept identical in all the built models, i.e. $\tau_1 = \tau_2 = \tau_3 = \tau_4 = \tau$, $\beta_1 = \beta_2 = \beta_3 = \beta_4 = \beta$, $\theta_1 = \theta_2 = \theta_3 = \theta_4 = \theta$ and $\zeta_1 = \zeta_2 = \zeta_3 = \zeta_4 = \zeta$. Hence, a parametric study is performed regarding four parameters, i.e. Ψ, β, τ and θ.

In the definition of the SCF that is used within this investigation, the computation of the nominal stress at a brace i due to loading at a brace j, with $i \neq j$, is not accounted for. Therefore, the SCF is load dependent. This consideration is employed in order to make the comparison between the K-joint and the KK-joint models feasible. A better way of computing the influence of the loading at one brace on the nominal stress at the other braces would be through the definition of influence functions. However, the influence functions are not dimensionless. This would complicate the possibility of abstracting conclusions for the comparison of the two models.

The SCF at the reference brace is dominated by its own loading configuration and, to a certain degree, affected by the loading at the other braces. Since there is no source of non-linearity in the system, it is expected to find a linear correlation between the magnitude of the applied forces and the stresses. The same can be extended to the SCF. Due to the statement mentioned at the beginning of the paragraph, it is expected that the linear relation is shifted from the origin. Therefore, applying loading of double magnitude at the out-of-plane braces does not yield double stresses at the hot-spot of the reference brace. This is expressed mathematically in Eq. (6.1), where SCF is the stress concentration factor computed at the toe position of the reference brace. R_F is defined as the force magnitude ratio between the magnitude of the applied loads at Brace 2 and a reference load magnitude. The linear relation is plotted in Figure 6.2 for three Ψ values.

The reference load is chosen so that the nominal stress at the braces of Face 2 S_{F2} is equal to the one at the braces of Face 1 S_{F1}. Hence, $R_F = S_{F2}/S_{F1}$. This means that for $R_F = 1$ the same nominal stress, as the one applied to the braces of Face 1, is applied to the braces of Face 2. The coefficient $\tilde{K}_{LD}$ is introduced in Eq. (6.2). The subscript LD refers to the load dependency behavior that this parameter models. It is the slope of the linear relation between the loads at Face 2 and the SCF at the reference brace K_{LD}, normalized with SCF($R_F = 1$). Thus, it is a measurement of the carry-over effect provoked by the out-of-plane braces to the reference brace. For the same reason, this parameter is also a measurement of the influence of R_F in the quantification of the carry-over effect. Notice that, while the parameter $\tilde{K}_{LD}$ depends on the applied load case at each of the faces, K_{LD} depends on the applied load case (LC) at the out-of-plane pair of braces only. Moreover, they are a function of the geometry. Hence, $K_{LD}|_{LC} = K_{LD}|_{LC}(\Psi, \beta, \tau, \theta)$.

$$\mathrm{SCF}(R_F) = \mathrm{SCF}(R_F = 1)\left(1 + \tilde{K}_{LD} \cdot (R_F - 1)\right) \tag{6.1}$$

$$\tilde{K}_{LD} = \frac{\mathrm{SCF}(R_F = 2) - \mathrm{SCF}(R_F = 1)}{\mathrm{SCF}(R_F = 1)} = \frac{1}{\mathrm{SCF}(R_F = 1)} \cdot K_{LD} \tag{6.2}$$

Therefore, given a load case and a specific combination of non-dimensional geometry parameters, the carry-over effect of the out-of-plane braces can be quantified by K_{LD}. Knowing the SCF for a certain load ratio R_F, it is then possible to compute the SCF for any R_F. Furthermore, in order to compare the results between the K-joint and the KK-joint models, it is interesting to compute how much the loading of the out-of-plane braces contributes to the SCF at the reference brace. The stress at the toe position of the reference brace can be understood as a superposition of the stresses due to the loading at Face 1 and the loading at Face 2. Thus, the ratio between the contribution of Face 2 S_{cf2} over the one of Face 1 S_{cf1} can be expressed through the ratio S_R introduced in Eq. (6.3). In principle, $SCF(R_F = 0)$ does not necessarily have to be equal to the result obtained from the planar K-joint

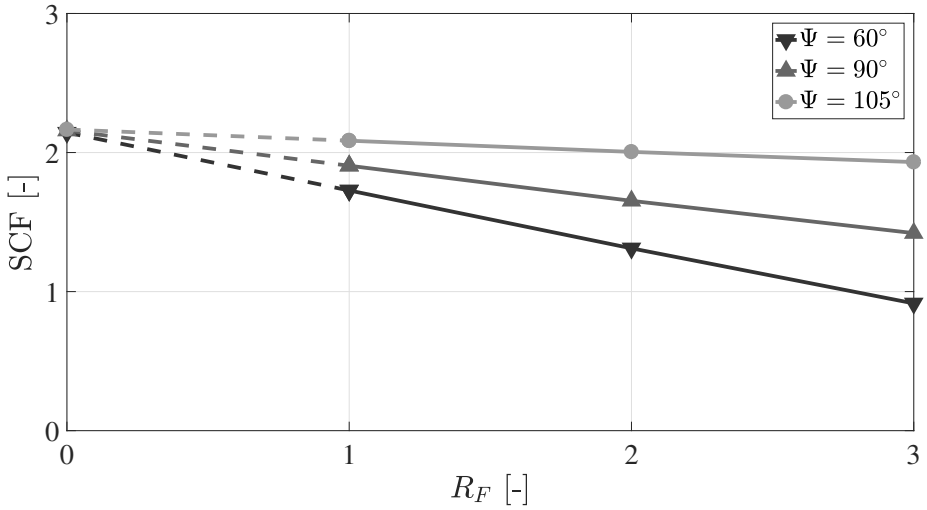

Figure 6.2: *Linear relation of the SCF at the crown toe position for varying R_F. This case corresponds to BAL1 as described in Table 6.1. The following non-dimensional parameters are used to create the data: $\tau = 0.4$, $\beta = 0.4$, $\gamma = 10$, $\theta = 45°$, $\zeta = 0.5$.*

model $SCF|_{KJ}$. Note that the subscript KJ refers to the results computed using the planar K-joint model. It can be expected that the inclusion of two extra members in the model will constrain the deformation of the chord, varying the SCF. This effect is going to be studied in Section 6.4. Note that if this effect was negligible, S_R would coincide with $\tilde{K}_{LD}$ for $R_F = 1$. Nevertheless, the latter expression of the equation is going to be used for the comparison.

$$S_R(R_F) = \frac{S_{cf2}}{S_{cf1}} = \frac{SCF(R_F = 1) - SCF(R_F = 0)}{SCF(R_F = 0)} \cdot R_F \approx \frac{SCF(R_F = 1) - SCF|_{KJ}}{SCF|_{KJ}} \cdot R_F \qquad (6.3)$$

Various load cases are defined to carry out this study. While the braces at Face 1 might be predominantly loaded by balanced axial actions, the braces at Face 2 might be seen in-plane bending, for instance. Thus, a combination of load situations at both faces shall be studied. Each brace can be subjected to axial, in-plane and out-of-plane actions. The influence of each loading on the stresses at the other three braces can be studied. Thus, 24 DOF can be identified for the KK-joint configuration. In order to reduce the extension of this investigation, some decisions are made. In reality, it is frequent that the braces at one face are loaded by the same type of action. The mentioned DOF can be superimposed to constitute linearly dependent DOF. Thus, instead of defining the degrees of freedom by single loads at each brace, they can be established by load cases constituted by pairs of forces or moments. The three most common load cases are the balanced axial load, in-plane bending and out-of-plane bending cases. Due to these considerations, six load cases are going to be regarded. This is pictured in Table 6.1, where a nomenclature is assigned to each case.

6.3 Characteristics of the models

Two parametric FE models are built in ANSYS© APDL. First of all, a KK-joint model is built. Secondly, a K-joint model, similar to the one used in Chapter 4, is built for comparison of the results. The brace under study is here called Brace 1. Brace 2 is the brace contained in the same face of the KK-joint as Brace 1. Braces 3 and 4 are thus, the braces in the contiguous face of the KK-joint. The face that contains Braces 1 and 2 is designated by Face 1. The face that contains Braces 3 and 4 is designated by Face 2. This nomenclature is shown in Figure 6.1. The GCS is defined with the x-axis in the direction of the chord, with Braces 1 and 2 contained in the xy-plane. The y-axis is defined so that the axis of Braces 1 and 2 lie in the positive y sector. The z-axis is then given in a Cartesian right-handed system. The directions of the axis of Braces 3 and 4 are defined by the vector $\vec{D}_{B3,4}$ in

Table 6.1: *Nomenclature of the load cases used in the investigation of the carry-over effect of multiplanar KK-joints.*

	BAL at Braces 1 and 2	IPB at Braces 1 and 2
BAL at Braces 3 and 4	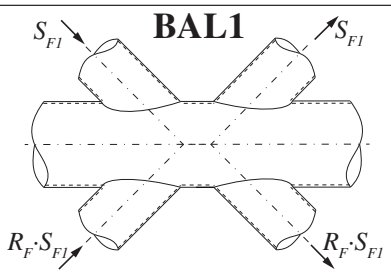	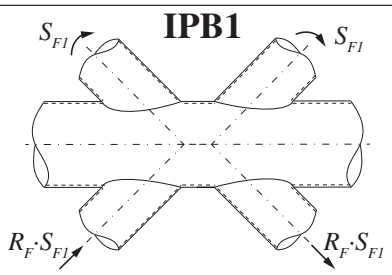
IPB at Braces 3 and 4	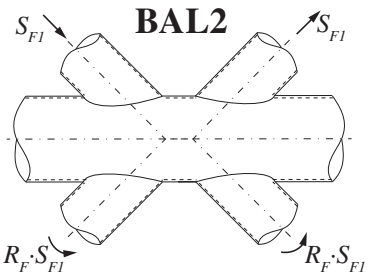	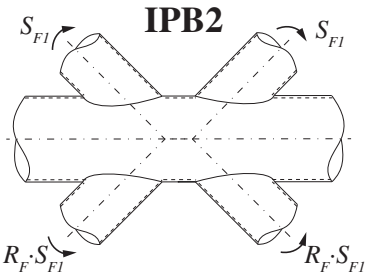
OPB at Braces 3 and 4	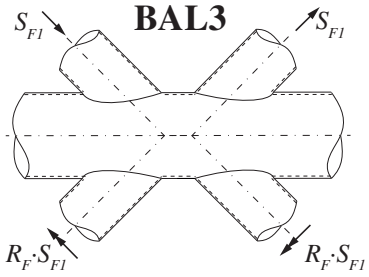	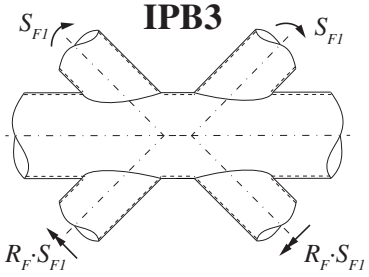

Eq. (6.4), referred to the GCS. If an eccentricity $ecc_{3,4}$ is set, the vectors are to be translated that distance in the GCS x direction.

$$\vec{D}_{B3,4} = \{\pm\cos\theta_{3,4}, \sin\theta_{3,4}\cdot\cos\Psi, \sin\theta_{3,4}\cdot\sin\Psi\} \tag{6.4}$$

The same material, element type and meshing scheme is used for both models. The same structural analysis is performed on both models. The same standard steel material properties and meshing scheme that are described in Section 4.3.2 for SHM are used. Shell elements are used for both models. This type of modelling is chosen since it requires a lower computational time to run a full case. Note that a parametric study is performed and thus, a great amount of simulations are performed. Therefore, the computational cost is a key factor in the selection of the model characteristics. Furthermore, since the aim of this study is to compare the K-joint model with the multiplanar KK-joint model, it is assumed that the conclusions drawn are relatively independent of the chosen element type, as long as the same one is used for both models. The employed element type is SHELL93. This element type follows the same plate theory as SHELL181, which was used and described in the aforementioned chapter. SHELL93 is characterized by 8 nodes: one at each corner and mid-sides of the element. It includes quadratic deformation at both in-plane directions and linear out-of-plane distribution through thickness.

The loads are applied at the ends of the braces. Simple supports are applied at the chord ends. For that purpose, rigid multi-point constraints (MPC) are defined at the members ends using the *cerig* subroutine. An auxiliary element type, i.e. MASS21, is defined for the application of the MPC. The mass of this element is set to a small magnitude, i.e. $1\cdot10^{-10}$ kg. Equations are not solved at the master nodes of the MPC. The use of this element type is just a requisite of the software to allow the application of the boundary conditions out of the tubes geometry.

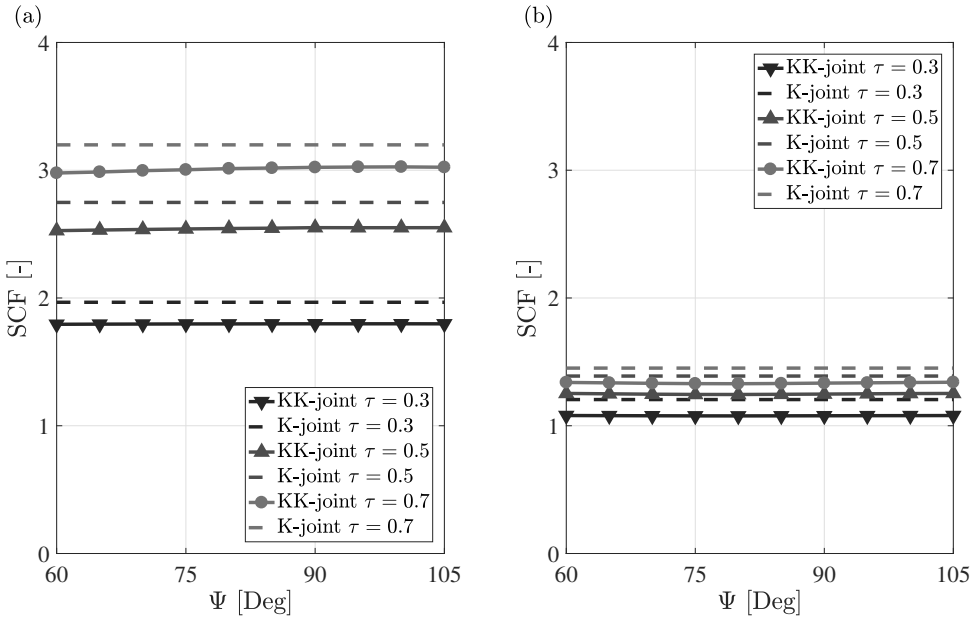

Figure 6.3: *Influence of the out-of-plane pair of braces in the rigidity of the joint. The results are presented for varying Ψ, various τ values and two load situations (a) BAL applied at Face 1. (b) IPB applied at Face 1. The following non-dimensional parameters are used to create the data:* $\beta = 0.4$, $\gamma = 10$, $\theta = 45°$, $\zeta = 0.5$.

The SCF is computed at the reference brace crown toe position, following the structural stress approach. The principal stress S_1 is read from the element solution at a path normal to the weld at that position. The stress field is interpolated at the read-out points a and b, defined in Chapter 2, using the element shape function. The structural stress is then computed as the linear extrapolation to the brace-chord intersection from the stresses at the two read-out points.

6.4 Discussion of the results

First of all, the change in stiffness due to the deformation constraint that the two new braces impose in the joint is studied. The SCF at Brace 1 is regarded when no loading is applied to the out-of-plane braces. This is compared with the results obtained from the K-joint model. The comparison is shown in Figure 6.3.(a) and (b) for having balanced axial and in-plane bending actions, respectively. Various values of τ are tested to make the conclusions broader. A difference exists between the results of both models. The additional two braces constrain the chord bending, reducing the SCF at the braces by ca. 10%. It is seen that the influence of Ψ in the stiffening of the joint is negligible, i.e. the difference in the SCF estimated by both models is almost constant with Ψ.

The first step to make the comparison, between the K-joint and KK-joint models, is to compute the SCF at the reference position, for the six load cases, setting $R_F = 1$. This is carried out for a parametric investigation of Ψ in combination with β, τ and θ. Additionally, this process is repeated for $R_F = 2$ in order to compute K_{LD} for each of the studied cases. Combining the results from the parametric investigation with the K_{LD} values, the SCF can be computed for any R_F ratio using Eq. (6.1). An example of the influence of R_F is shown in Figure 6.4. For the given case, it is inferred that R_F plays a bigger role for applying BAL or OPB at the out-of-plane pair of braces. However, as it is going to be observed from the computed K_{LD}, this is dependent on the non-dimensional geometry parameters combination. It is concluded that accounting for the carry-over effect of the out-of-plane braces is beneficial at this case. The loading at those braces reduces the tensile stress measured by the principal stress S_1. If loading of the opposite sign was applied, i.e. $R_F < 0$, the carry-over effect would be detrimental, i.e. it would increase the tensile stresses.

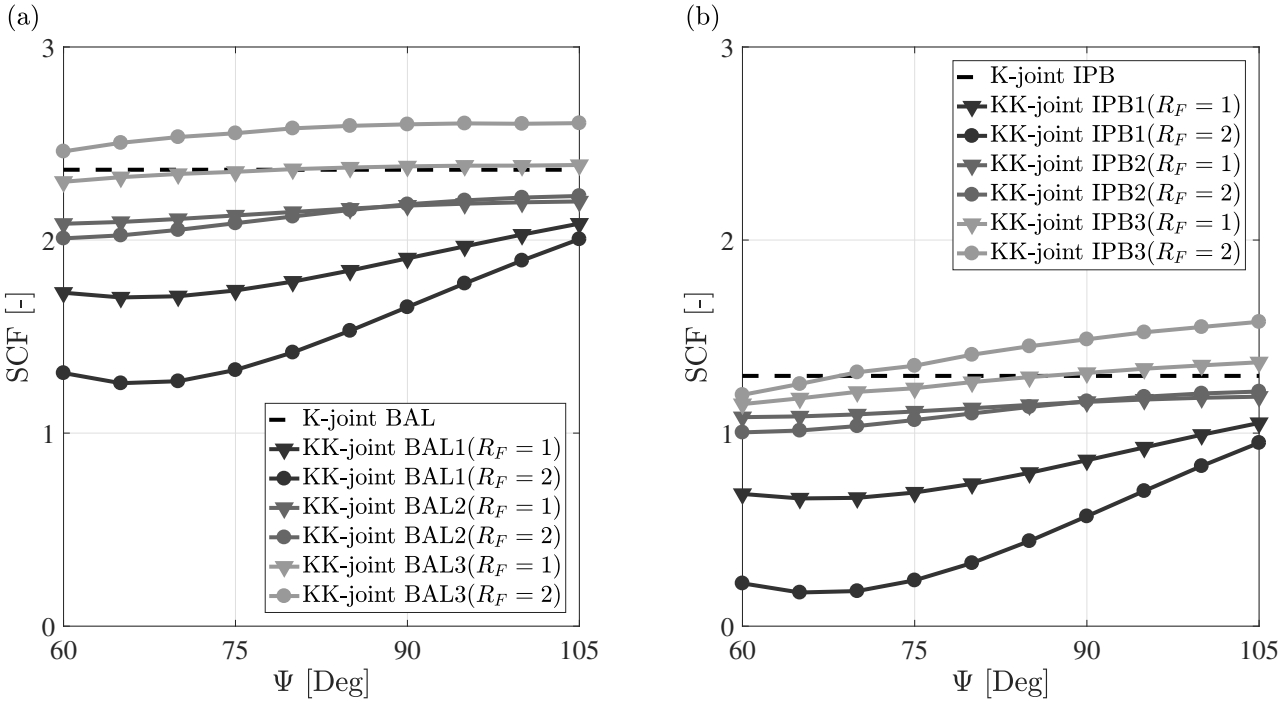

Figure 6.4: *Influence of Ψ and R_F in the computation of the SCF at the toe position of the reference brace of a tubular KK-joint for the studied six load cases collected in Table 6.1. (a) Face 1 subjected to BAL. (b) Face 1 subjected to IPB. The following non-dimensional parameters are used to produce the data: $\beta = 0.4$, $\tau = 0.4$, $\gamma = 10$, $\theta = 45°$, $\zeta = 0.5$.*

The influence on the reference brace due to subjecting the out-of-plane braces to BAL and IPB is represented in Figure 6.5(a) and (b), respectively. In these plots, the braces of Face 1 are not loaded. It is seen, that the BAL case yields a great bending of the chord plate. This results in significant structural stress magnification at the hot-spot region of the reference brace. Moreover, it is observed that this stress concentration is greater at the region close to the crown toe. On the contrary, the IPB provokes a slight chord bending. It should be noted that since the contour plots represent the maximum principal stress field S_1, the stress is high where the plates are tensed, and approximately zero where the bending results into compression. To capture the compression, the minimum principal stress S_3 should be regarded. The stress concentration is found to be maximum at the region in between the saddle and heel positions. Therefore, it would be recommendable to extend this investigation for more positions around the weld in future investigations.

In total, 396 simulations were carried out to produce the data of this investigation. This number results from having four Ψ values, which are combined with four τ, three β and four θ values. This is executed for six load cases. Furthermore, the cases BAL1, BAL2 and BAL3 are run for two R_F values, i.e. $R_F = 1$ and 2, in order to compute K_{LD}. As it is going to be seen, such an extensive parametric investigation is necessary, since the results have a high dependency on the geometry and the load cases. Therefore, in order to draw valid general conclusions, a high amount of simulations are to be performed. A typical combination of parameters for OWT jackets is $\tau = 0.4$, $\beta = 0.4$, $\theta = 45°$, $\gamma = 10$. The results are going to be discussed for this case, which will be here called the *typical case*.

The results of the parametric investigation are shown in Appendix B. The SCF comparison between the K-joint and KK-joint models is shown in Figures B.1 to B.2 for BAL applied to the members of Face 1, and in Figures B.3 to B.5 for IPB applied to the same members. An example of these plots is presented in Figure 6.6, for the τ investigation. The computed K_{LD} values are collected in Tables B.1 to B.3 for the various parametric investigations. The results obtained for $\tilde{k}_{LD}$ are presented in Figure 6.7 for the BAL1, BAL2 and BAL3 load cases. Notice that, for better display of the results, the negative value of this parameter is plotted. Furthermore, S_R/R_F is computed for each of the cases in order to

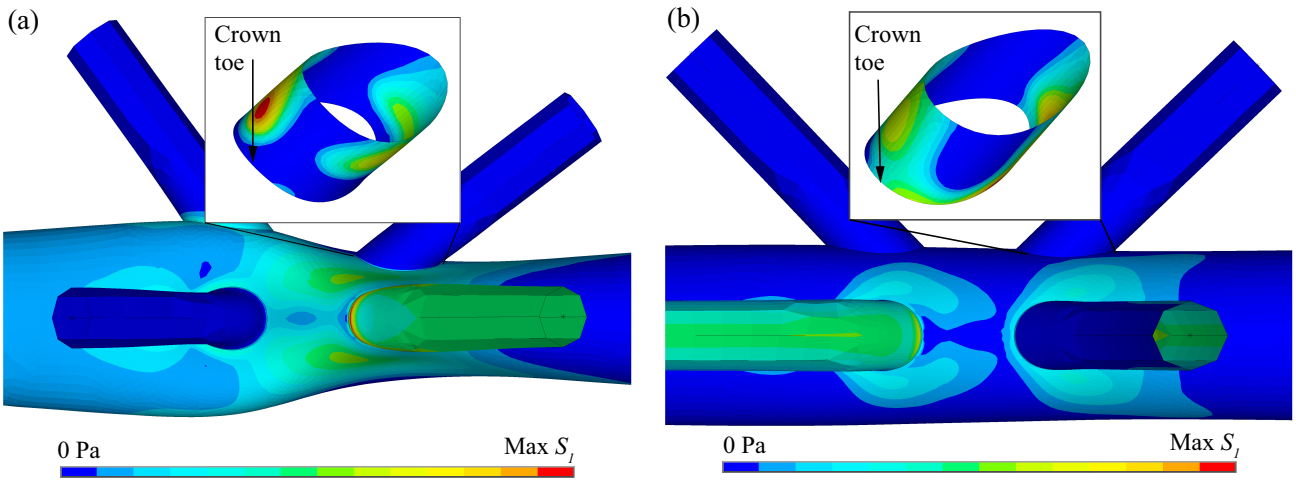

Figure 6.5: *Influences in the principal stress S_1 due to loading at the out-of-plane pair of braces. The subfigures correspond to the following two load situations: a) BAL applied to the braces at Face 2 b) IPB applied to the braces at Face 2. It should be noted that the stress contours of the details at the vicinity of the weld of Brace 1 are re-scaled with respect to the overall plots in order to have a better resolution of the stress field.*

have an overview of the importance of modelling the joint as a multiplanar KK-joint. These results also express the deviation of the KK-joint results from the K-joint results. The values are collected in Tables B.4 to B.9. The results are discussed hereafter.

The carry-over effect is highly influenced by the parameter Ψ, especially when BAL are applied at Face 2, i.e. the cases BAL1 and IPB1. For those cases, the loading at the out-of-plane braces becomes less relevant for higher Ψ values. Considering all the simulations performed for those two load cases, an average of 30% smaller K_{LD} is found for the four-leg jacket in comparison to the three-leg jacket configurations. When IPB are applied at the braces of Face 2, i.e. the cases BAL2 and IPB2, it is seen that K_{LD} changes its sign between the case of $\Psi = 60°, 75°$ and $\Psi = 90°, 105°$. This implies that, accounting for the carry-over effect when the out-of-plane braces are loaded with in-plane bending, would increase or decrease the hot-spot stresses at the Brace 1 toe position depending on the value of Ψ. The explanation can be observed from Figure 6.5. For small Ψ, the Brace 1 toe position gets into the area where the chord encounters high tensile stresses. Thus, this adds to those stresses provoked by the loading at that brace. For high Ψ values, the Brace 1 enters an area where the chord bending yields compressive stresses. Nevertheless, as it is going to be shown later, the carry-over effect at the reference position due to this type of loading, is relatively small. In the case of having OPB applied to Face 2, K_{LD} is not much influenced by Ψ.

The application of BAL to the out-of-plane braces, i.e. load cases BAL1 and IPB1, has a major influence on the SCF at the crown toe position of the reference brace. For all the studied cases, it yields an influence of the same sign, i.e. all the K_{LD} have the same sign. The geometrical parameter that influences the SCF the most is τ. The SCF estimated for $\tau = 0.8$ is ca. 90% higher than the ones obtained for $\tau = 0.2$. The difference is the highest for $\Psi = 105°$. For this case, the $\tilde{k}_{LD}$ is approximately 0.2 points larger in absolute value. An almost constant influence is found for the various brace inclinations θ, that are tested. The results do not seem to be much influenced by the parameter β, as well. The worst match between both models is found for $\tau = 0.8$, where a difference of ca. 43% exists between the models for $R_F = 1$ and $\Psi = 60°$. For that case, the contribution of the out-of-plane braces is $-0.57R_F$. It is also concluded that it is more acceptable to neglect the carry-over effect for the case of having small brace thicknesses and diameters, and a four-leg jacket configuration. For instance, when $\Psi = 105°$ and $\tau = 0.2$ or $\beta = 0.2$, differences in the order of 5% in the SCF are estimated with respect to the case of having no loading in the out-of-plane braces. For the OWT jacket aforementioned *typical case*, the results present a deviation from the K-joint model of 27% and 19% for the cases of three-leg and four-leg jackets, respectively, for the BAL1 case. For the IPB1 case, the

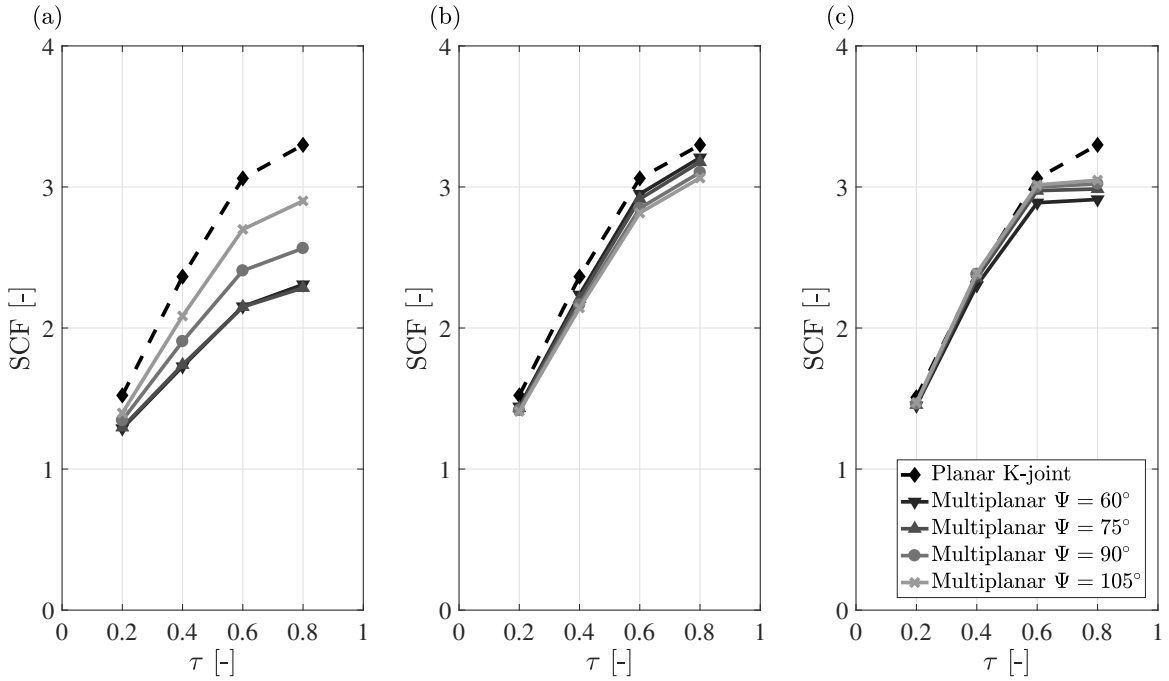

Figure 6.6: *Influence of Ψ in the computation of the SCF of a tubular KK-joint under application of BAL at the braces in face 1 within a parametric investigation of τ. The subfigures correspond to the following load cases, which are described in Table 6.1: (a) BAL1($R_F = 1$) (b) BAL2($R_F = 1$) (c) BAL3($R_F = 1$). The following non-dimensional parameters are used to produce the data: $\beta = 0.4$, $\gamma = 10$, $\theta = 45°$, $\zeta = 0.5$.*

same results show an even bigger deviation of 43% and 31%. Thus, it is concluded that for these load cases, the differences are high and the carry-over effect of the out-of-plane braces cannot be neglected.

The application of IPB to the out-of-plane braces, i.e. load cases BAL2 and IPB2, has a minor influence on the SCF at the crown toe position of the reference brace. As can be seen in Figures 6.6 to B.5, the results estimated by the KK-joint model present only a slight deviation from the K-joint model. For the OWT jacket aforementioned *typical case*, the results present a deviation from the K-joint model, in absolute value, of approximately 5% and 8% for the cases of three-leg and four-leg jackets, respectively, for the BAL2 case. For the IPB2 case, the same results present a difference of 4% and 11%. It is seen that the assumption of modelling a multiplanar KK-joint as a planar K-joint is relatively accurate for these cases. It should be noted that the results depend of R_F. However, it would be unreasonable to dimension the joint for a high R_F, since for that case the reference brace would be on the other face. Nevertheless, as it was mentioned above, it is recommended to extend this investigation to more positions around the weld, where it is expected to find a higher influence of the carry-over effect.

The application of OPB to the out-of-plane braces, i.e. load cases BAL3 and IPB3, has a considerable influence on the SCF at the crown toe position of the reference brace. The influence is, however, lower than for applying BAL to those members. Moreover, it affects the SCF in a positive and negative way, i.e. decreasing and increasing the SCF, respectively, depending on the geometrical parameters. The parameter that influences the carry-over effect the most is θ. For this parametric study, the carry-over effect has a stronger presence for highly inclined braces, i.e. $\theta = 60°$. For that case, K_{LD} results to ca. 0.4 in absolute value and the models deviate ca. 20% for both cases, BAL3 and IPB3. Regarding the β parametric study, it is seen that the influence is of the opposite sign between $\beta = 0.2, 0.3$ and $\beta = 0.4$. For the aforementioned *typical case*, the results present a deviation from the K-joint model, in absolute value, of approximately 3% and 1% for the cases of three-leg and four-leg jackets, respectively, for the BAL3 case. For the IPB3, the same cases present a deviation of 1% and 6%. Thus, for some of the practical situations of design of the OWT jacket tubular members, the carry-over effect due to the out-of-plane braces can be disregarded.

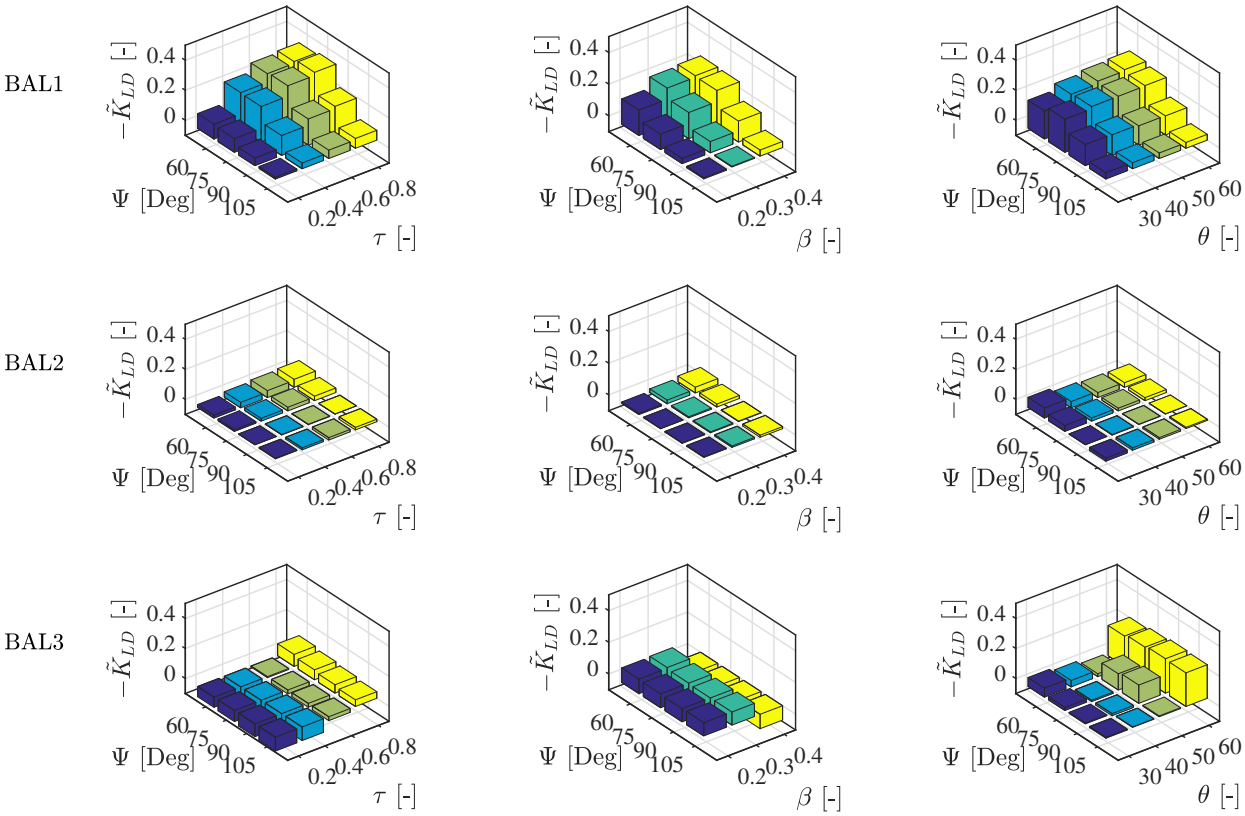

Figure 6.7: *Parametric study of $-\tilde{k}_{LD}$ for Ψ plotted together with τ, β and θ. Each row corresponds to a different load case, which are defined in Table 6.1.*

Generally speaking, it is seen that the carry-over effect due to the loading at the out-of-plane braces depends strongly on the geometrical parameters of the joint. It is difficult to abstract general conclusions from the presented results. Nevertheless, the results that have been produced for this investigation can be used as charts that assess the accuracy of modelling a multiplanar KK-joint as a planar K-joint. In general, it is seen that the carry-over effect should not be disregarded, specially for the BAL loading at the out-of-plane braces and for three-leg jackets.

6.5 Summary

In this chapter, the carry-over effect in multiplanar KK-joints is investigated. The impact of applying various load situations at the out-of-plane braces on the SCF at a reference brace is studied. An expression to predict the influence of varying the loading is presented. The influence is observe to be linear. Therefore, it can be assessed by the slope, here defined as k_{LD}. The conclusions are presented for a parametric investigation that comprises 396 FEM simulations that combines several combinations of τ, β, θ and Ψ. From this study, it can be seen for which cases the assumption of modelling a KK-joint as a K-joint is reasonable to be adopted.

7 | Fatigue Assessment of Joints using the Notch Stress Concept

In Chapter 4, some particularities of the hot-spot method were analyzed. This study was applied to the fatigue assessment of OWT jackets tubular joints. Three ways of approaching this method were regarded; i.e. (1) using a plate FE model; (2) using a solid FE model, in which the weld was not modelled; and (3) using the Efthymiou formulation [5]. The comparison among these variations was presented in Chapter 5. The limitations of the structural stress method were addressed. Due to the continuous pressure on the optimization of the design of OWT jacket, a more accurate method is required. Recommendation guidelines such as DNV-GL and IIW briefly introduce a third method that allows for a more detailed assessment, i.e. the so called effective notch stress method. In this chapter, an algorithm for the assessment of the notch stress, using the sub-modelling technique, is developed. The characteristics of this approach and the assumptions that are made are reported in Section 7.1. An example of a full assessment of the notch stress is presented in Section 7.2. The differences in the results obtained by using this method and the hot-spot approach are addressed in Section 7.3. This method allows for the optimization not only of the tubular members that conforms the joint, but also of the weld profile. A parametric study of the weld slope is carried out in Section 7.4.

7.1 Assessment of the NSCF using the sub-modelling technique

Fatigue failure occurs due to crack propagation, which results in a reduction of the fatigue resistance. The stresses that affect the crack propagation are the notch stresses. Generally speaking, a stress concentration exits in the vicinity of a welded connection of two structural components. The stress concentration can be understood as the superposition of a hot-spot stress component and a concentration due to the weld itself. The effective notch stress is a detailed fatigue assessment method which uses the notch stress for the estimation of the fatigue resistance. If the assessment is carried out using a numerical model, a fictitious notch radius is to be set in order to avoid sharp corners, which would yield theoretically infinite stresses.

The characteristic dimensions of the notch are drastically smaller than the dimensions of the members which are connected. There is a pronounced stress variation at the vicinity of the notch, which tends to the nominal stress as one moves further from it. In order to properly capture this behavior, an element size in the order of 0.0001 m is required at the notch influenced area. An element size in the order of 0.1 m is generally enough to capture the nominal stress behavior. An optimized mesh has to adapt to these requirements. Building a regular mesh that transitions among these element sizes is identified as a major problem. The computational requirements needed to solve a model of these characteristics are currently beyond the regular functionalities of a personal computer. For these reasons, it is decided to use the sub-modelling technique for the assessment of the NSCF.

Sub-modelling is a finite element technique that consists of reanalyzing an isolated region (sub-model) of a model (global model). The sub-model is set in equilibrium with the global model at the interface region that connects both. This technique is based on the Saint-Venant principle, which asserts that the effect of applying a self-equilibrated stress distribution to a structure has an impact on the preliminary stress state only locally. This technique is usually performed for the reassessment of the solution at a certain location, in which further refinement of the mesh or a more detailed modelling are desired.

The sub-modelling technique can be decomposed into a number of steps to be followed systematically. This is illustrated as a flow chart in Figure 7.1. First of all, the global model is to be built and solved. The solution is to be saved for later use. Secondly, the sub-model is defined. The interface between the sub-model and the rest of the global geometry is called the cut-boundary. The displacement

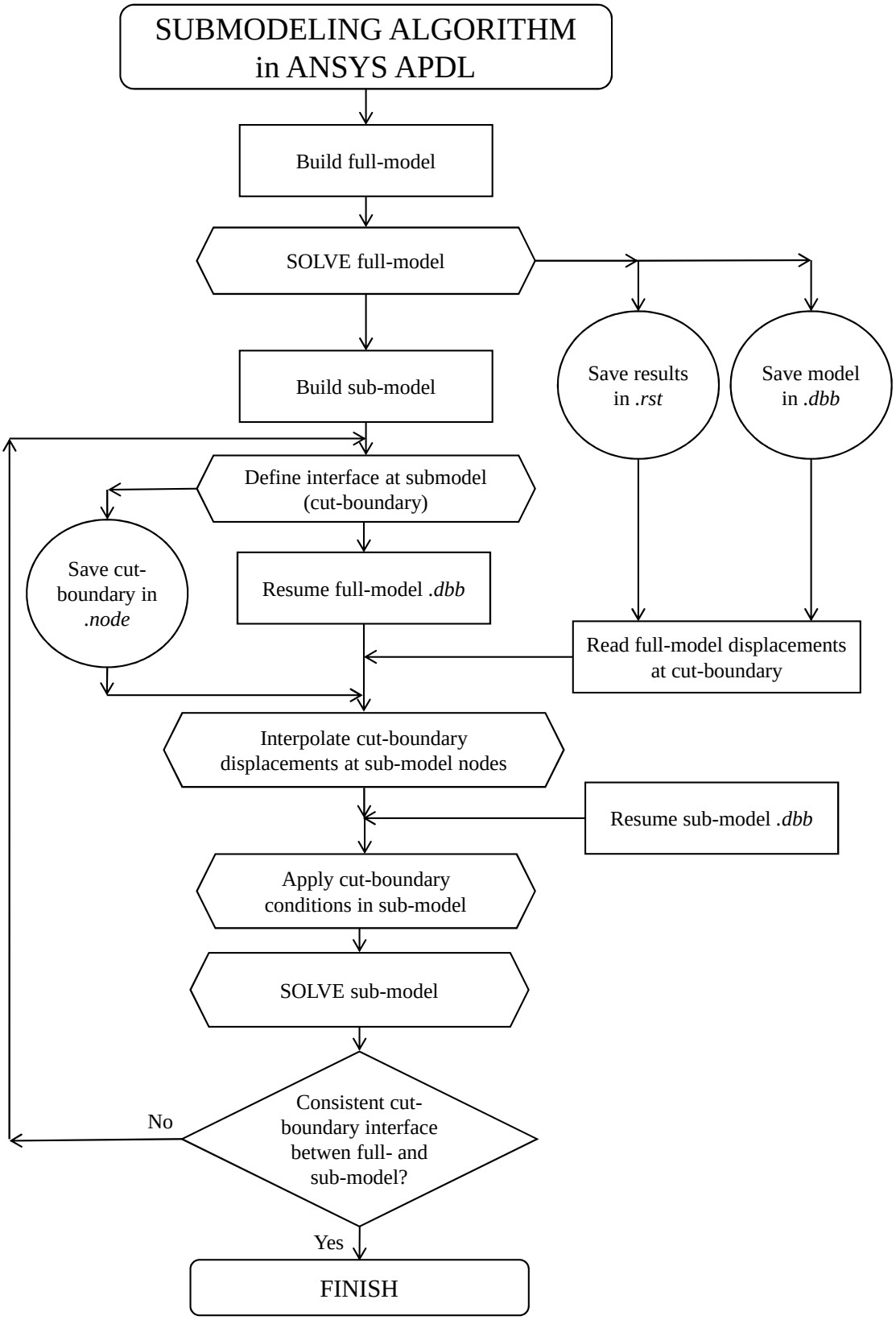

Figure 7.1: *Flow diagram of the sub-modelling algorithm.*

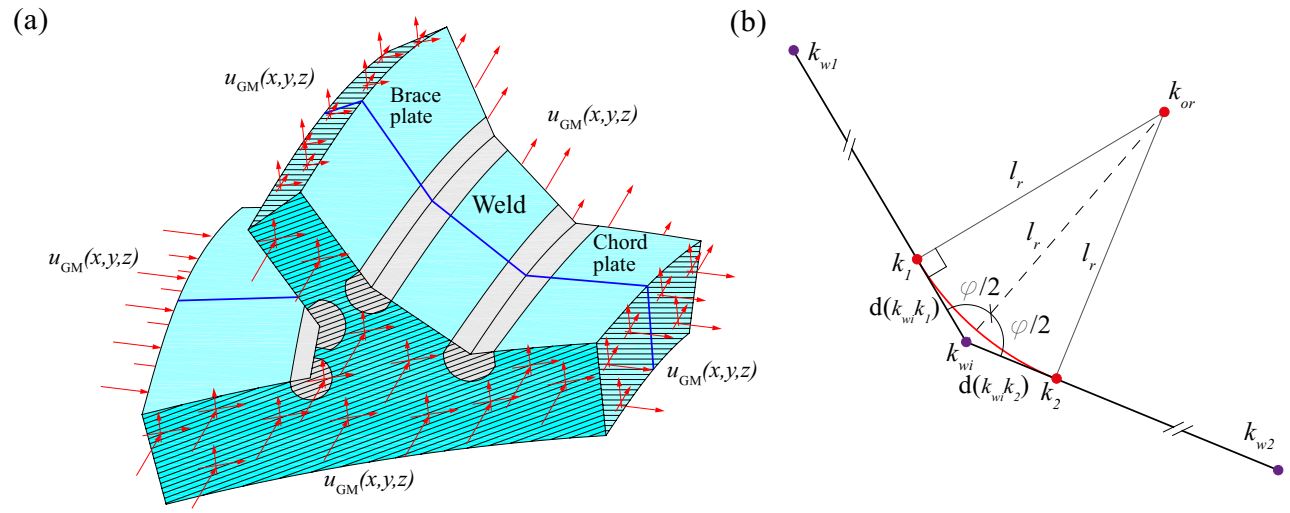

Figure 7.2: *(a) Sketch of the sub-model used in the assessment of the notch stress at a random location around the weld. The sub-model is set in equilibrium with the rest of the global model domain by applying the displacement field u_{GM} at the cut-boundary. (b) Relation between k_{wi}, k_{w1}, k_{w2} and the notch reference points.*

field, estimated by the global model, u_{GM} is read at the cut-boundary. In general, the meshes of the sub-model and the global model are different at the cut-boundary region. Thus, the displacements at the nodes of the global model are to be interpolated at the positions where the nodes of the sub-model are located. This interpolation is performed using the shape functions of the related elements of the global model. These displacements are the boundary conditions of the sub-model. In order to make the sub-model consistent with the global model, only additional boundary conditions that are in self-equilibrium can be applied. Once the sub-model is reassessed, it is important to follow the feedback loop which assures that the cut-boundaries that delimit the sub-model were chosen properly.

For the particular case of the assessment of the notch stress of a tubular joint, the following has to be considered. The cut-boundaries of the isolated region do include variations with respect to the geometry of the global model used to set the equilibrium, cf. Figure 7.2(a). This is due to the notch arc that is defined in the sub-model. This is contrary to the aforementioned Saint-Venant principle and therefore, the solution is not to be trusted at that region. The solution is to be assessed at the surroundings of the central section, highlighted with a dark blue line in the same figure. This yields the need of defining several sub-models around the weld. In the following subsection, the algorithm that is followed to build the sub-models is presented.

7.1.1 Parametric definition of the sub-model

The geometry of the sub-model is built based on parametric inputs read from the global model. The material and the analysis type of the sub-model have to be consistent with the global model. Linear elastic standard steel and static analysis are used. The properties of the material that is used are summarized in Table 4.1. The element type SOLID186 is used. A macro is written in ANSYS© APDL language to build the geometry and mesh of the FE sub-models. The script follows the algorithm shown in Figure 7.4. A common way to produce the sub-model geometry is to isolate it from the global model by performing Boolean operations. Nevertheless, a different approach is followed in order to make the sub-modelling algorithm robust. The sub-model geometry is built based on reference points read from the global-model.

First of all, the coordinates (referenced to the GCS) of the points marked in Figure 7.3(a) are read from an input file. These points are extracted at various sections around the region that constitutes the sub-model. The process of building the sub-model is illustrated in Figure 7.5. A function is created in APDL language to compute the points k_1, k_2 and k_{or}, i.e. the two tangent points of the notch arc and their centre of curvature, respectively. These points are here called notch reference points. A

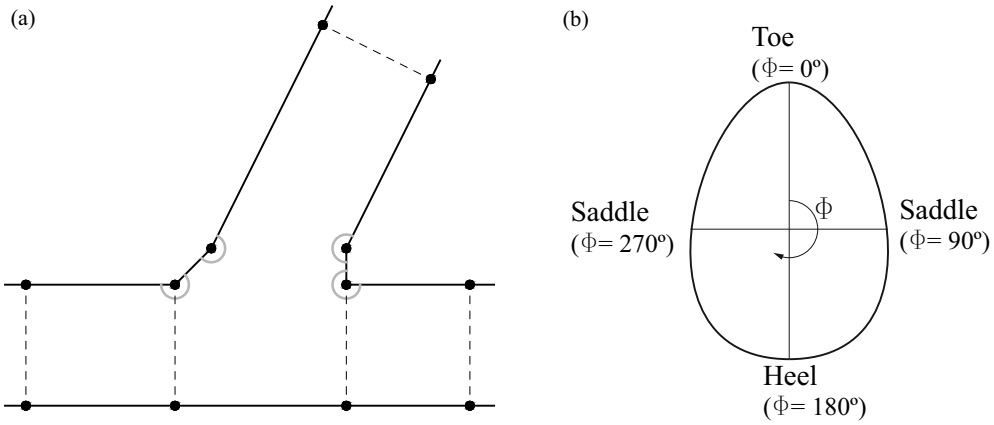

Figure 7.3: *(a) Reference points read from the global model to be input for the creation of the notch sub-model. (b) Reference used for the definition of* Φ.

sketch of the situation is illustrated in Figure 7.2(b). Each notch is defined in the global model by the intersection of two lines. These lines are represented by three points, i.e. k_{w1}, k_{w2} and k_{wi}. k_{w1} and k_{w2} are two points contained in those lines and different from the intersection point k_{wi}. k_1 and k_2 are computed knowing their distances to the intersection point, which are, respectively, $\mathrm{d}(k_{wi}k_1)$ and $\mathrm{d}(k_{wi}k_2)$, cf. Eq. (7.1). φ is the opening angle of the two intersecting lines and l_r is the radius of the notch.

$$\mathrm{d}(k_{wi}k_1) = \mathrm{d}(k_{wi}k_2) = \frac{l_r}{\tan(\varphi/2)} \tag{7.1}$$

It is pursued to build a regular fine mesh at the vicinity of each of the four notches. Given the notch reference points, a function is developed for the creation of the guiding lines, which are used to develop a regular mesh at each of the sections read from the global model. These lines are represented in grey in the same figure. Areas are formed using the guiding lines. Subsequently, areas are created to connect the various sections. This process is also sketched in Figure 7.5. Note that, since the members geometries are modelled by cylinders in the global model, there is always a cylindrical LCS in which the outer and inner walls can be expressed as planes. Thus, knowing those LCS, the curvature of the plates are known at each position. However, the weld profile is not continuous along the weld. Therefore, the latter cannot be applied to infer the weld geometry between sections. A 2D third order polynomial spline is used to define the interpolation of the weld geometry between sections. These areas are built using the built-in APDL function *askin*. Note that this function constrains the number of the sections to be used to nine.

Once all the areas are created, they are combined to create a volume for each notch. These volumes are meshed as follows. Firstly, a regular mapped mesh is built at the vicinity of each notch. In order to do that, an auxiliary 2D mesh is built at the areas that are highlighted in purple in Figure 7.5. The element type MESH200 is used. It is set to be coherent with SOLID186. This mesh is afterwards swept up to the last section. The mesh refinement requisites decrease when moving away from the notches. Therefore, a mesh transition is to be built. In the areas highlighted in yellow, the regular mesh transition is performed. An auxiliary mesh is built in this area and swept around, afterwards. This process produces a regular pattern at the outer areas of the volumes. This is crucial for the meshing of the rest of the sub-model geometry.

Once the volumes at the vicinity of the four notches are meshed, the rest of the geometry is to be built. The element size is increased when moving away from the notches. The mesh is created using the sweeping technique. In the following subsection, various parameters that characterize the sub-model mesh are tuned.

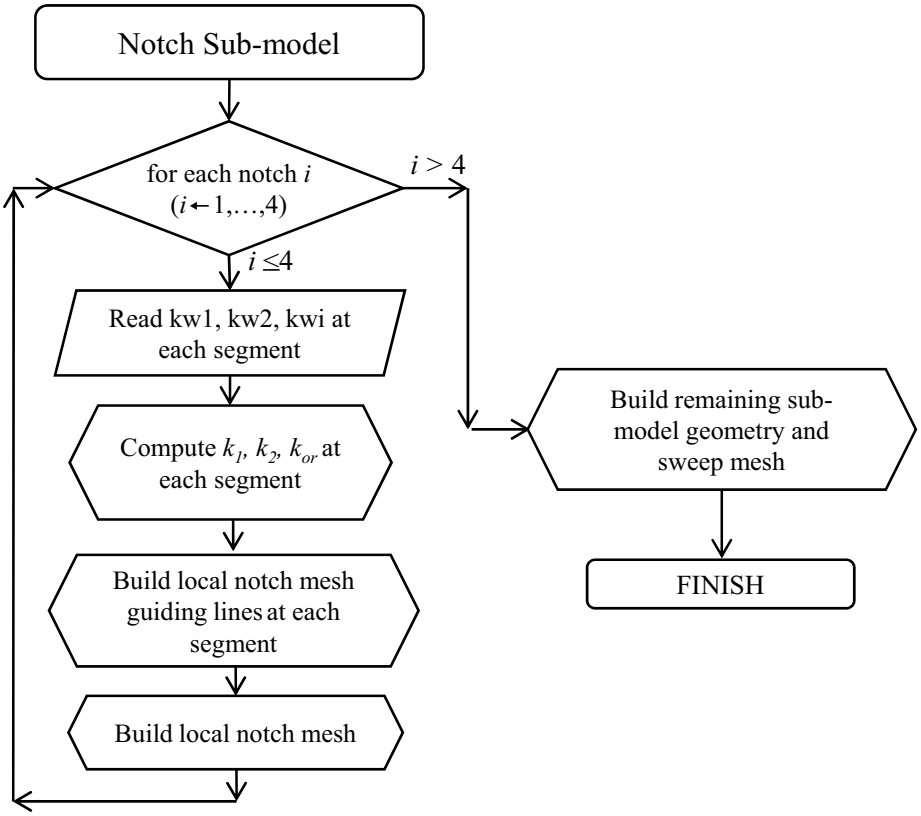

Figure 7.4: *Flow diagram of the algorithm used to build the FE sub-model.*

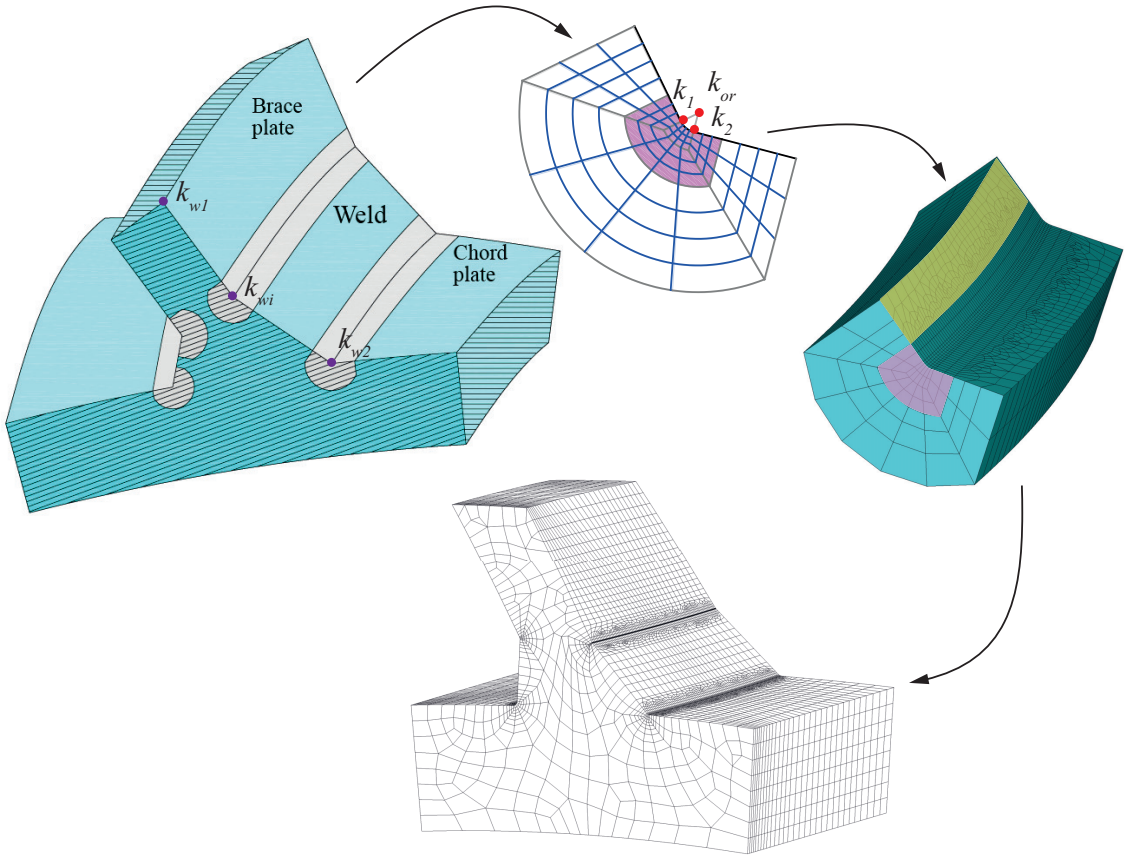

Figure 7.5: *Sketch of the process of building a regular mesh at the vicinity of a notch.*

Table 7.1: *Representative values of the characteristics of the FE sub-model. These values are averaged and rounded from the definition of several sub-models for several K-joint non-dimensional parameters combinations.*

	Elements [#]	Nodes [#]	t_b [s]	t_{bc} [s]	t_s [s]
Global model	22,900	126,000	16	-	15
Sub-model	38,000	161,000	15	4	25

Table 7.2: *Influence of the model extension, defined by $\Delta\Phi$, in the computation of the notch and the structural stresses.*

$\Delta\Phi$ [deg]	$\tilde{\sigma}_k/S$ [-]	σ_s/S [-]
5	3.03	2.36
10	3.03	2.35
15	3.03	2.35
20	3.04	2.35

Table 7.3: *Influence of the number of division at the notch arc $n_{div,c}$ in the computation of the notch and the structural stresses.*

$n_{div,c}$ [-]	$\tilde{\sigma}_k/S$ [-]	σ_s/S [-]
3	3.03	2.35
4	3.03	2.35
5	3.03	2.35
6	3.03	2.35
7	3.03	2.35
8	3.03	2.35

7.1.2 Mesh parametric study

Two parameters of the sub-model mesh are studied in this subsection, i.e. the model extension and the number of elements along the notch arc $n_{div,c}$. The model extension is measured by $\Delta\Phi$, with Φ defined in Figure 7.3. The influence of these parameters in the computation of the local stresses at the notch and at 2 mm from the notch is studied. The results are computed at the toe position, for applying balanced axial loads at the braces ends. The geometry is defined by $\beta = 0.5$, $\tau = 0.6$, $\gamma = 20$, $\theta = 45°$ and $\zeta = 0.3$. Various values of $\Delta\Phi$ and $n_{div,c}$ are used. The studied notch is modelled with a 160° arc. The results are collected in Tables 7.2 and 7.3.

It is observed that, none of the two parameters have much influence within the ranges studied. Variations in the results are found in the third decimal of the SCF. Considering the low influence of $\Delta\Phi$, the possibility of using a 2D sub-model, assuming plane strain conditions, should be studied in posterior works. In the following sections of this chapter, $\Delta\Phi$ and $n_{div,c}$ are going to be set to 10° and 3 divisions per quarter of an circle, respectively.

The different sub-models have different dimensions, depending on the global model and on the position around the weld at which they are created. Therefore, they will be characterized by a different amount of elements and nodes, and a different computational time of the building and solving processes. Nevertheless, the scatter of these values is considered to be small. Some representative values of these models are collected in Table 7.1. t_b is the computational time employed in building the geometry and the mesh. t_{bc} is the time required to set the cut-boundary conditions. t_s is the computational time employed for solving one load case. The characteristics of the global model are also shown in that Table. If six load cases are considered, the computational time required to compute the notch stress for each sub-model is $t_{CPU} = t_b + 6t_{bc} + 6t_s \approx 189$ s. Additionally, the global model is to be solved and built. Thus, the total computational time required to compute the solution is $t_{CPU} = 189 + 16 + 6 \cdot 15 = 295$ s ≈ 5 min.

7.2 Example of the notch approach using sub-modelling

In this section, an assessment of the notch stress around the welded connection of a tubular K-joint is performed. The sub-modelling approach described above is employed. Several sub-models are analyzed around the weld, following the algorithm presented in Figure 7.4. First of all, the global model is built

and solved for the considered load cases. The load cases are described below. The geometry of the joint is defined by the following non-dimensional parameters: $\beta = 0.5$, $\tau = 0.6$, $\gamma = 20$, $\theta = 45°$, $\zeta = 0.3$. Moreover, the weld profile is defined at various sections around the weld. This is presented in Table C.1 in Appendix C. Each weld profile is characterized by four dimensions z_{Bo}, z_{Co}, z_{Bi} and z_{Ci}. The subscript i and o refer to the inner and outer part of the weld, respectively. A sketch of these distances can be seen in Figure 7.11. Secondly, the sub-models are built for the regarded positions around the weld, described below. Once the volumes of the sub-models are meshed, the displacements of the global model u_{GM} are read for each of the solved load cases and applied at the cut-boundary of all the sub-models. Right after this, the sub-models are solved for each of the applied boundary conditions. Finally, the results are post-processed.

In order to compute the NSCF from the notch stress σ_k, the following is to be regarded. As mentioned in Chapter 2.1, a correction due to mild-notches has to be accounted for, cf. Eq. (7.2). This equation is a lower bound of the notch stress. The structural stress σ_s is estimated as the normal stress taken at a distance of 2 mm from the tangent point of the arc, i.e. k_1 or k_2, as suggested by IIW [25]. The stresses normal to the weld are regarded. The GCS and LCS are defined identically as in Chapter 4. Thus, the stresses normal to the weld, expressed in the LCS of the regarded member, are defined by S_x.

$$\text{NSCF} = \max\left\{\frac{\sigma_k}{S}; \frac{1.6\sigma_s}{S}\right\} \tag{7.2}$$

The K-joint has six DOF. The notch stress is assessed for the six load cases that were studied by Efthymiou [5], cf. Figure 5.2. From the results obtained, linear superposition can be applied to find the NSCF for any other load situation. By way of example, the case of having an axial load applied to the upper brace, can be found as the case in Figure 5.2(1) minus the case in Figure 5.2(2). According to DNV-GL [3], the solutions are to be computed in at least eight positions around the weld. Thus, eight sub-models are to be built. The angle Φ is introduced in Figure 7.3(b). The notch stress is assessed at the positions defined by the following Φ values: $\Phi = 0°$,45°,90°,135°,180°,225°,270° and 315°.

The full simulation takes ca. 25 min. The scatter in the computational times and number of elements of the sub-models have a standard deviation of 23 s and 848 elements, respectively. The simulation of the global model required approximately 107 s to be solved, i.e. ca. 7% of the total computational time. Therefore, the effective notch stress assessment takes 13 times more computational capacity than the hot-spot assessment. Therefore, this method might be impractical to be used in preliminary stages of the design. Nevertheless, once an optimized joint is achieved, it can be used for its reassessment.

The deformed shapes of the global model and the contour diagrams of the equivalent Von Mises stresses are shown in Figure 7.6 for the six studied load cases. Moreover, the principal stress S_1 is plotted for the global model and for the sub-models at three positions in Figure 7.7. It is seen that, considering the weld concentration yields high differences in the local stresses between the brace and the chord, for a given position around the weld.

The NSCF and the hot-spot SCF are presented for all the considered load cases and positions in Figure 7.8. The values are presented in Tables C.2 and C.3 at the Appendix C. The NSCF can be understood as the hot-spot SCF, magnified with the weld concentration k_w. It is seen that k_w depends on the position and on the load case. This factor is in average 2.25, for all considered load cases and positions. As it was mentioned previously, the ratio between the NSCF and the hot-spot SCF should be below ca. 2 if this method was used with the aim of providing a more optimized design. Nevertheless, the thickness correction is yet to be applied to the hot-spot damage estimation. Therefore, the fatigue life predicted by the effective notch stress assessment can still be higher. This will be addressed in further detail in the following Section 7.3. A thorough analysis of the weld concentration factor is elaborated below in this section.

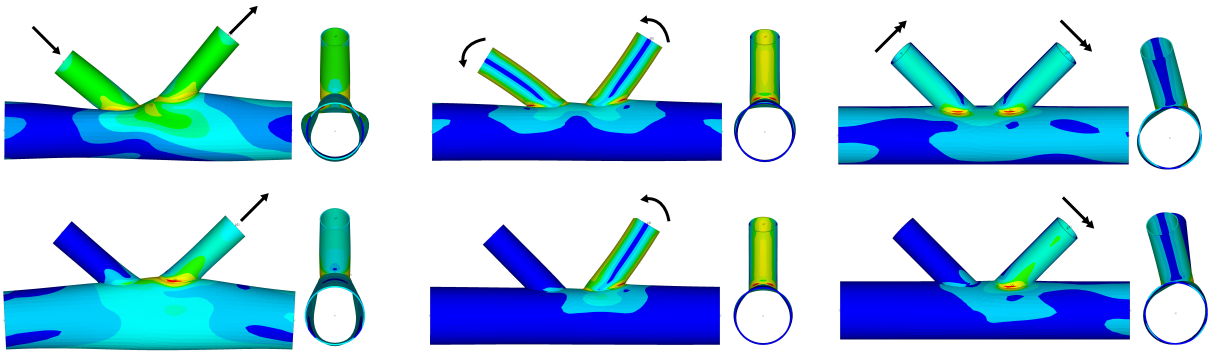

Figure 7.6: *Deformed shapes and equivalent Von Mises stresses of the global model for the six load cases.*

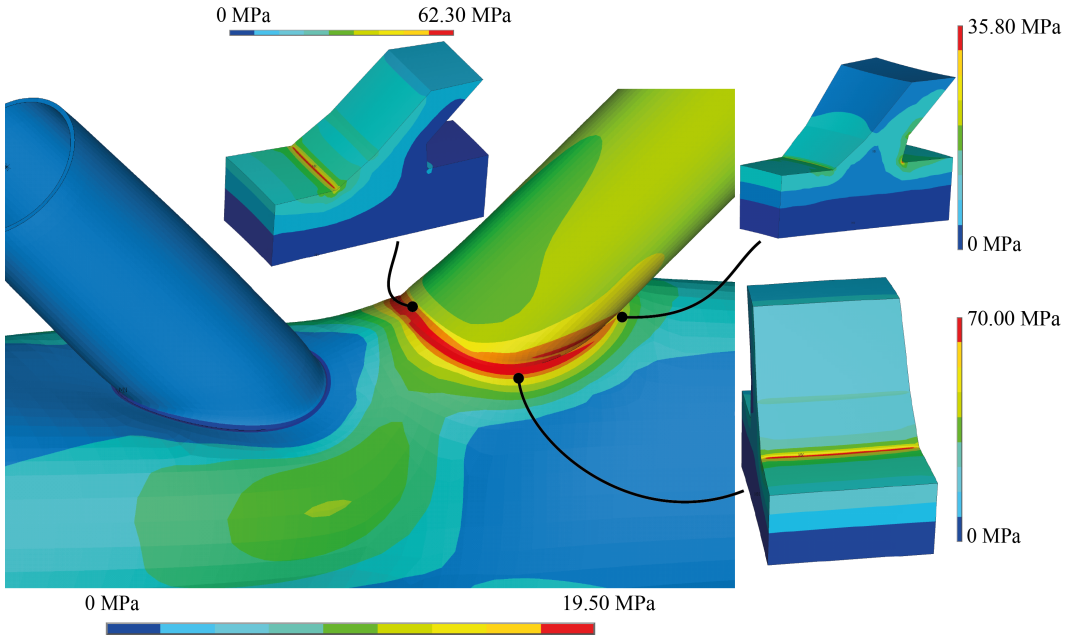

Figure 7.7: *Principal stress field S_1 due to BAL shown at the global model and at three sub-models located at the toe, saddle and heel positions. The applied nominal stress is 10 MPa.*

The maximum NSCF, the hot-spot SCF and the positions where they are found are collected in Table 7.4. Note that they are not necessarily found at the same weld positions for a given load case. The highest stress concentration is found at the saddle position for the LC4. This case is characterized by only one brace loaded axially. For this case, the effective notch methods predicts its maximum at $\Phi = 90°$, while the hot-spot method predicts it in an intermediate position. Notice that, the balanced axial load case (LC1) yields a higher NSCF at the toe position than for the LC4. Nevertheless, for the LC1, the additional axial load at Brace 2 significantly reduces the stresses at the saddle.

The weld concentration factor k_w is calculated for all the considered cases using Eq. (2.9). The results are presented in Table 7.5. Only the relevant results are presented. For instance, the local stresses at the crown toe and heel positions due to out-of-plane bending loading (LC3 and LC6) are mainly caused by the stress concentration due to the weld, since for these cases the nominal stress is zero at these positions. The same can be asserted for the saddle positions for the in-plane-bending cases (LC2 and LC5).

When following the structural stress approach, the same k_w is used for every situation. This factor is implicit in the formulation of the T-curve. Nevertheless, it is observed that this factor is different for each geometry, load case and position around the weld. The scatter of the computed k_w is relatively broad; i.e. around 1.6 to 3.7, with a standard deviation of 0.76. Therefore, the aim of optimizing a joint is limited if the hot-spot method is followed.

Table 7.4: *Maximum NSCF and hot-spot SCF computed for the six load cases and the position where they are found. The following non-dimensional parameters are used to produce the data:* $\beta = 0.5$, $\tau = 0.6$, $\gamma = 20$, $\theta = 45°$, $\zeta = 0.3$.

	Position	NSCF	Position	Hot-spot SCF
LC1	Toe ($\Phi = 0°$)	3.76	Toe ($\Phi = 0°$)	2.40
LC2	Heel ($\Phi = 180°$)	4.05	Toe ($\Phi = 0°$)	1.76
LC3	Saddle ($\Phi = 90°$)	5.98	Saddle ($\Phi = 90°$)	3.14
LC4	Saddle ($\Phi = 90°$)	6.66	Saddle ($\Phi = 45°$)	3.70
LC5	Heel ($\Phi = 180°$)	4.13	Toe ($\Phi = 0°$)	1.78
LC6	Saddle ($\Phi = 90°$)	5.12	Saddle ($\Phi = 90°$)	2.66

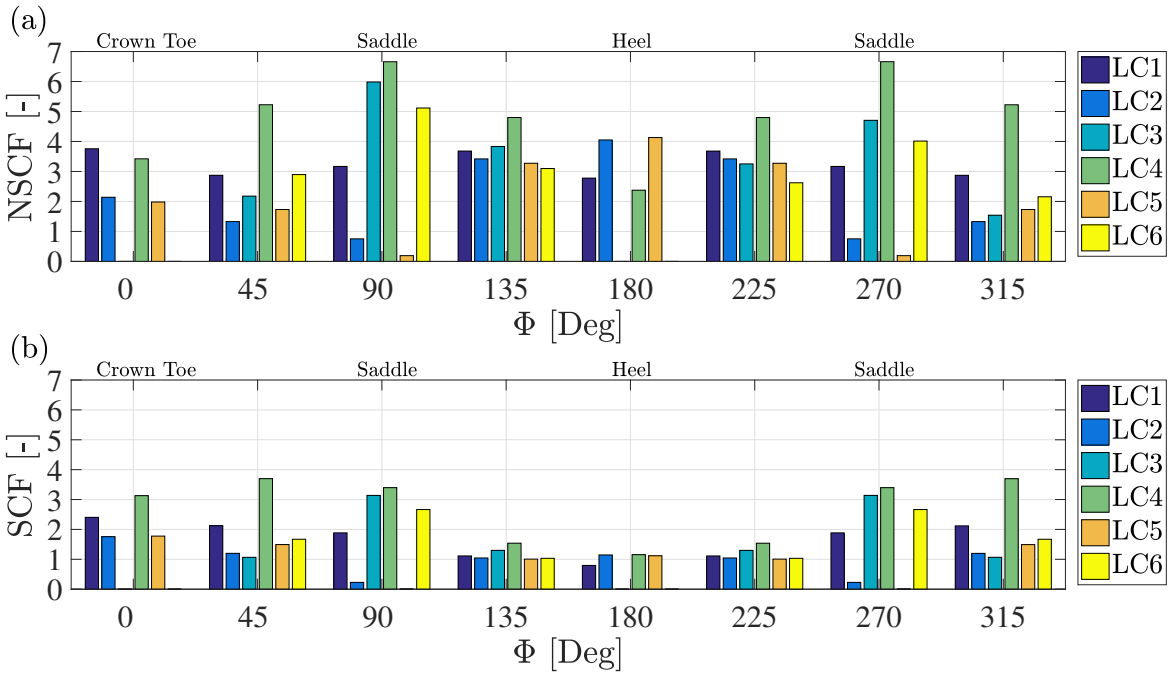

Figure 7.8: *Stress concentration factor of a K-joint computed for six load cases at eight positions around the brace part of the weld. (a) NSCF (b) Hot-spot SCF. The following non-dimensional parameters are used to produce the data:* $\beta = 0.5$, $\tau = 0.6$, $\gamma = 20$, $\theta = 45°$, $\zeta = 0.3$.

7.3 Comparison of the NSCF with the hot-spot SCF

In this section, two different fatigue assessment approaches are compared, i.e. the hot-spot and the notch stress methods. The comparison is going to be carried out within the same parametric investigation that was performed in Chapter 4. Thus, several brace and chord diameter and thickness combinations are to be tested within this parametric investigation. For each of them, a global model is built. From each global model, three sub-models are defined in order to find the NSCF at the toe, heel and saddle positions. The same algorithm that was used in Section 7.2 is followed here, cf. Figure C.1 in Appendix 7.1. Furthermore, the hot-spot SCF is computed using the global model. Thus, the comparison comprises the results of four different models, i.e. (1) a shell model, which was designated as SHM in Chapter 4; (2) a solid model in which the weld geometry is not modelled, that was called SM2 in the same chapter; (3) a solid model that includes the weld geometry, which is the global model used in the sub-modelling technique and (4) a notch model, which are the sub-models. Notice that the results of (1) and (2) have already been discussed previously in Chapter 5.

Some particularities have to be accounted for in order to compare their predicted stress concentration factors. First of all, the computation of the fatigue damage is based on different fatigue classes. The background of these fatigue classes is explained in Chapter 2.1. Therefore, inputting the same stresses

Table 7.5: *Weld concentration factor k_w computed at eight positions around the weld and for six different load cases (LC1-LC6). The following non-dimensional parameters are used to produce the data: $\beta = 0.5$, $\tau = 0.6$, $\gamma = 20$, $\theta = 45°$, $\zeta = 0.3$.*

Φ [Deg]	LC1	LC2	LC3	LC4	LC5	LC6
0	1.60	1.60	-	1.60	1.60	-
45	1.60	1.60	2.04	1.60	1.60	1.73
90	1.68	-	1.91	1.96	-	1.92
135	3.31	3.27	2.95	3.12	3.25	3.00
180	3.49	3.53	-	2.06	3.69	-
225	3.31	3.27	2.50	3.12	3.25	2.54
270	1.68	-	1.60	1.96	-	1.60
315	1.60	1.60	1.60	1.60	1.60	1.60

into their related SN-curves would yield different fatigue lives. Secondly, the thickness effect correction is to be considered for the hot-spot damage estimation, but not for the notch one. This reduction of the fatigue strength strongly decreases the fatigue life prediction of thick members, such as the tubular members used for the OWT jackets. The computed NSCF and SCF are to be corrected in order to compare them. These corrections are going to be elaborated hereafter.

The SN-curve to be used in the notch stress concept does not implicitly include any stress concentration. Thus, it corresponds to a higher fatigue class than the T-curve. The ratio between both fatigue classes is approximately 1.95, as shown in Chapter 2.1. An effective notch stress concentration factor NSCF_{eqv} is defined in order to be able to compare it with the hot-spot SCF, cf. Eq. (7.4). The mathematical derivation is elaborated in Eq. (7.3). To avoid confusion, the SN-curve constants of the notch and tubular joint SN-curves have been renamed to a_N and a_T, respectively. It is considered that the environment is seawater with cathodic protection. For this case, the correction factor yields $\left(\frac{a_T}{a_N}\right)^{1/m} = \left(\frac{10^{12.180}}{10^{12.958}}\right)^{1/3} \approx 0.55$.

$$\begin{aligned} N \cdot \sigma_k^m &= a_N = a_N \frac{a_T}{a_T} \\ N \cdot (\text{NSCF}_{eqv} \cdot S)^m &= a_T \end{aligned} \tag{7.3}$$

$$\text{NSCF}_{eqv} = \text{NSCF} \left(\frac{a_T}{a_N}\right)^{1/m} \tag{7.4}$$

The background of the thickness correction, cf. Eq. (2.2), was explained in Chapter 2.1. The thickness effect can be included implicitly into an equivalent hot-spot SCF, SCF_{eqv}, cf. Eq. (7.6). The mathematical logic followed to define the SCF_{eqv} is shown in Eq. (7.5). The constant k is set to 0.25 and the reference thickness t_{ref} is 16 mm.

$$\begin{aligned} N \cdot \left(HSS \cdot \left(\frac{t}{t_{ref}}\right)^k \right)^m &= a_T \\ N \cdot \left(\text{SCF} \cdot S \left(\frac{t}{t_{ref}}\right)^k \right)^m &= N \cdot (\text{SCF}_{eqv} \cdot S)^m \end{aligned} \tag{7.5}$$

$$\text{SCF}_{eqv} = \text{SCF} \left(\frac{t}{t_{ref}}\right)^k \tag{7.6}$$

These two corrections yield two equivalent stress concentration factor values, i.e. SCF_{eqv} and NSCF_{eqv}. They can be directly compared, avoiding the need to compute the fatigue damage. Notice that a local stress computed as $\text{NSCF}_{eqv} \cdot S$ is related to the T-curve. The results that were presented in Chapter 4 are corrected accordingly using Eq. (7.6).

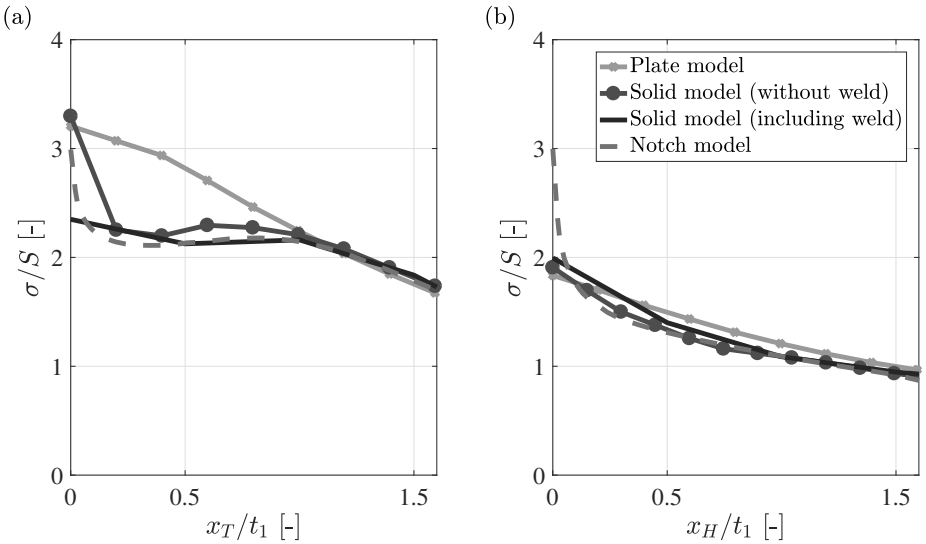

Figure 7.9: *Comparison between the four models of the normal stress S_x referred to the brace LCS. The results are computed for the BAL load case and the CASE 1 geometry. (a) Path at the crown toe position. (b) Path at the heel position.*

A comparison of the normal stresses at paths perpendicular to the weld at the toe and heel positions is plotted in Figure 7.9. It should be noted that, since the models SHM and SM2 do not model the weld, their brace-chord intersection point is different than for the other two models. Nevertheless, a relatively good match of the paths is found. The increase in the local stress due to the weld concentration is considerably higher at the heel position. At this position, the four models predict a similar structural stress tendency. This behavior is present in all four models within the range $0.5t_1$ to $1.5t_1$. At the vicinity of the notch, the non-linear stress peak yields an increase in the stresses of ca. 50%. At the toe position, the structural stress behavior happens at a further distance to the weld. The weld shape factor is of a lower magnitude due to the mild notch situation that is present at the crown toe. If the extrapolation region was properly selected, the three models used to assess the hot-spot SCF would predict a relatively similar value. However, they would overestimate the fatigue damage since they cannot benefit from the small stress concentration due to the weld.

The results of the parametric comparison are plotted in Figure 7.10. The first, second and third columns of plots are related to the β, τ and θ parametric investigations. Each row of plots refers to a different combination of load case and position around the weld. The following conclusions are drawn from the results:

- The $NSCF_{eqv}$ is, for most of the studied cases, smaller than the SCF_{eqv} predicted by the other three models. This means that the effective notch assessment would predict a higher fatigue life. Therefore, a more optimized design can be achieved if this fatigue assessment is followed.
- As will be discussed in the following section, differences in the notch stresses in the order of 30% can be expected, depending on the weld profile. Hence, the results of the effective notch model are to be interpreted within a certain scatter. Nevertheless, the weld profiles used in the comparison carried out in that section are rather extreme. Thus, the values are not expected to vary much from the presented situation.
- The SCF_{eqv} predicted by the solid model including the weld and the $NSCF_{eqv}$ present a good correlation with of the cases. If the notch results are considered to be the more accurate ones, it is concluded that modelling the weld remarkably improves the results.

Generally speaking, it is observed that the proposed approach to perform the effective notch stress fatigue assessment can be advantageous for the purpose of the optimization of the joint. Furthermore, the computational requisites are considered acceptable.

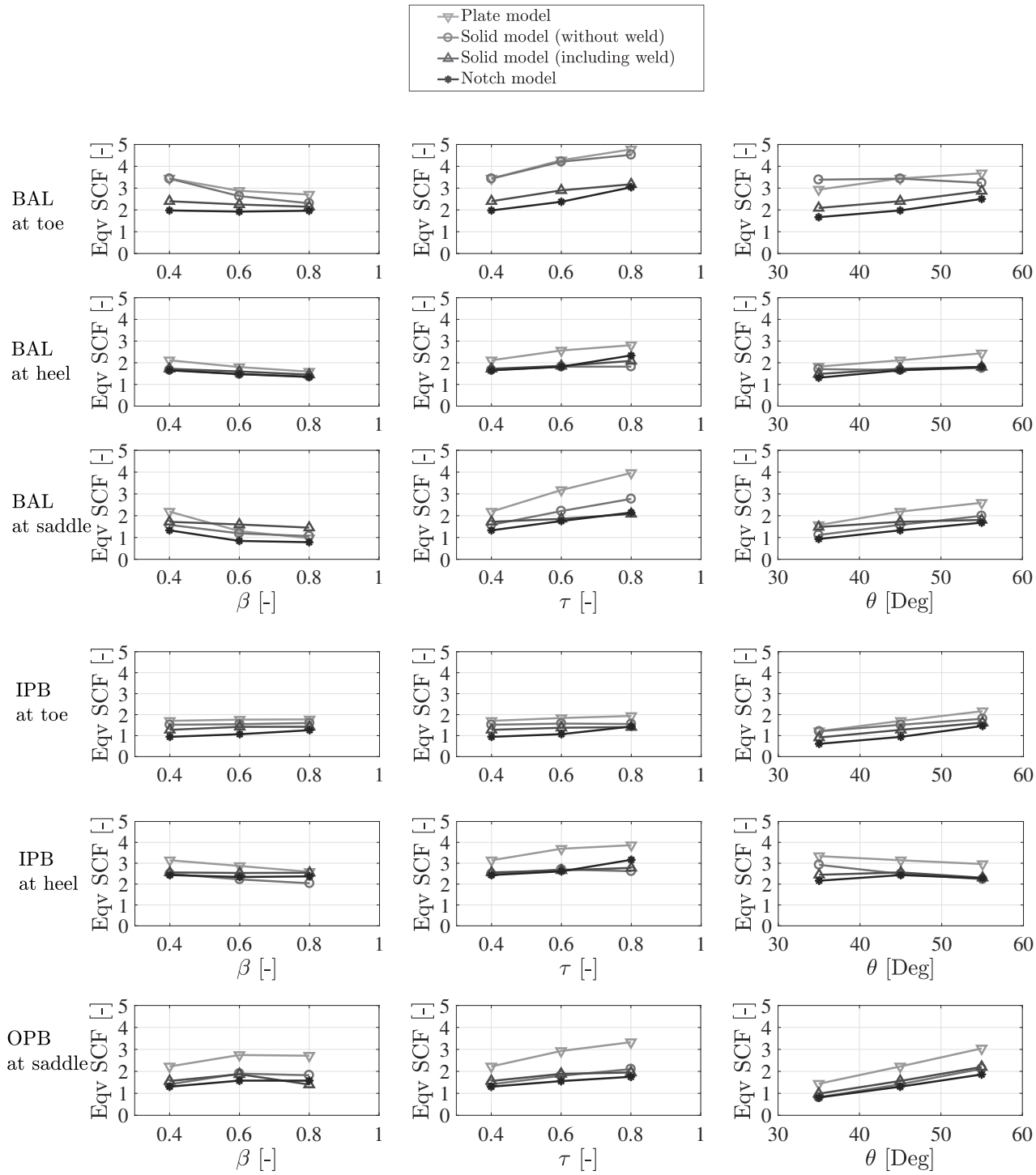

Figure 7.10: *Parametric comparison of the equivalent stress concentration factors as defined in Eqs. (7.4) and (7.6) between the shell, the solid (with and without modelling the weld) and the notch model. The same geometrical cases that were studied in Chapters 4 and 5 are used, cf. Table A.1. The Cases 1, 2 and 3 are used for the β comparison. The Cases 1, 4 and 5 are used for the τ comparison. The Cases 6, 1 and 7 are used for the θ comparison.*

7.4 Parametric study of the weld slope

In this section, a parametric study of the weld profile is carried out. Several weld profiles are defined around the connection for the characterization of the weld. The geometry is interpolated in between these profiles using a polynomial spline. The outer face of the weld profile is characterized by two parameters, i.e. z_{Bo} and z_{Co}, cf. Figure 7.11. For a given brace inclination θ, these parameters are directly related to the weld slope δ.

Table 7.6: *Parametric study of the influence of the weld slope. The following non-dimensional parameters are used to produce the data: $\beta = 0.5$, $\tau = 0.6$, $\gamma = 20$, $\theta = 45°$, $\zeta = 0.3$. The parameter z_{Bo} is set to 15 mm.*

		Balanced axial loads			In-plane bending		
δ [deg]	**z_{Co} [mm]**	**$\tilde{\sigma}_k/S$ [-]**	**NSCF [-]**	**$\tilde{\sigma}_k/\sigma_s$ [-]**	**$\tilde{\sigma}_k/S$ [-]**	**NSCF [-]**	**$\tilde{\sigma}_k/\sigma_s$ [-]**
20	19	4.58	4.58	1.66	2.74	3.05	1.44
25	12	4.10	4.22	1.56	2.51	2.93	1.37
30	8	3.68	4.04	1.46	2.28	2.80	1.31
35	5	3.22	3.84	1.34	2.05	2.66	1.23
40	2	2.60	3.56	1.17	1.72	2.46	1.12

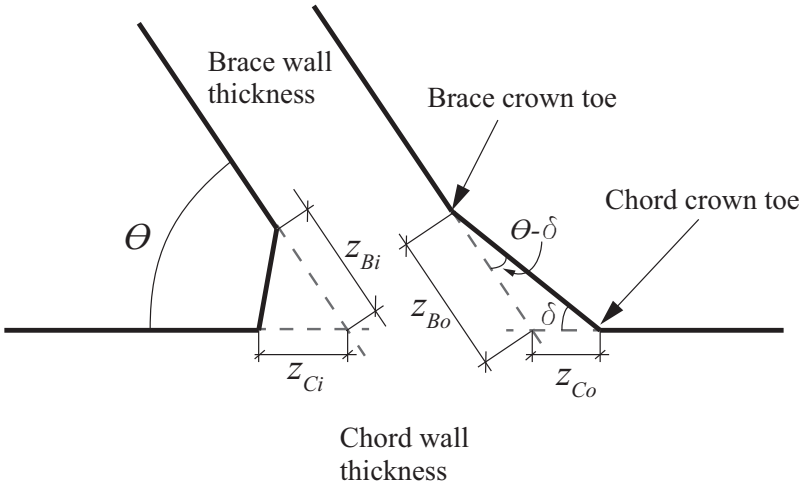

Figure 7.11: *Sketch of the parameters that define the weld geometry.*

The notch stress is influenced by the geometry of the weld. When the difference $\theta - \delta$ becomes small, the stress concentration due to the notch decreases. Nevertheless, as it was seen before, a correction for mild-notches applies, cf. 7.2, limiting this reduction. The inclination of the weld has a non negligible influence. This is going to be studied and quantified in this Section.

$$z_{Co} = z_{Bo} \cdot \left(\frac{\sin\theta}{\tan\delta} - \cos\theta \right) \tag{7.7}$$

A K-joint defined by the following non-dimensional parameters is regarded: $\beta = 0.5$, $\tau = 0.6$, $\gamma = 20$, $\theta = 45°$, $\zeta = 0.3$. Two load cases are considered, i.e. the balanced axial load and in-plane bending. Only the crown toe position is regarded. It is assumed that the conclusions drawn by this investigation can be extrapolated, in a qualitative way, to other positions and load cases. A distinction in the notation of the notch stress, including and not including the mild-notch correction is introduced. They are denoted as σ_k and $\tilde{\sigma}_k$, respectively. The results are computed for five slopes, $\delta = 20°$ to $40°$ in $5°$ steps. The results are presented in Table 7.6 and plotted in Figure 7.12.

It is observed that the variations of $\tilde{\sigma}_k$ and σ_s are approximately linear for varying δ. For the balanced axial loads case, the ratio $\tilde{\sigma}_k/\sigma_s$ is only higher than 1.6 for $\delta = 20°$. For the in-plane bending case, all weld slopes yield a ratio under 1.6. Therefore, it is concluded that for the toe position, most of the cases are penalized with the mild-notch correction. This can also be appreciated in the plot, where the curve of $\tilde{\sigma}_k$ lies for most of the studied cases under the curve of $1.6\sigma_s$.

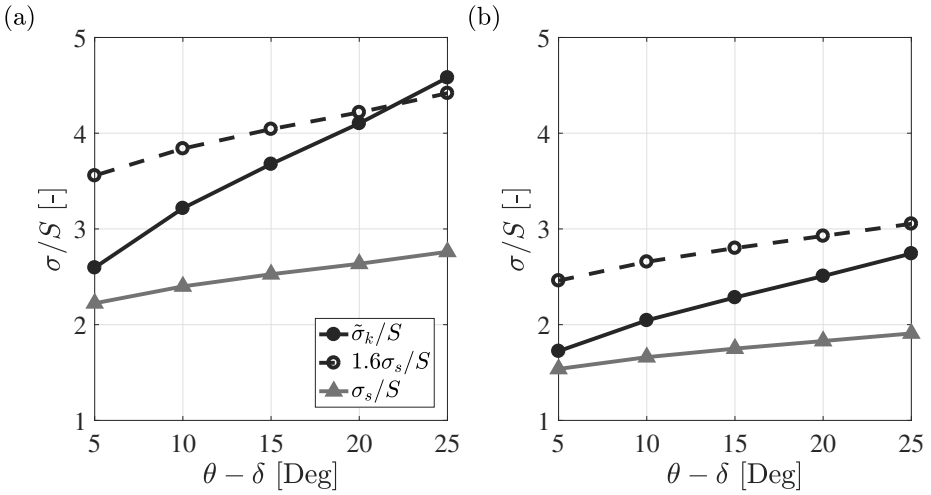

Figure 7.12: *Influence of the weld slope on the computation of the notch stress. The following non-dimensional parameters are used to produce the data:* $\beta = 0.5$, $\tau = 0.6$, $\gamma = 20$, $\theta = 45°$, $\zeta = 0.3$. *(a) is computed for the balanced axial load case. (b) is computed for the in-plane bending case.*

Additionally, the latter is also studied using the results of Section 7.3. From 63 evaluations of the notch stress, 28 of them were to be adjusted with the mild-notch correction. Regarding the influence of the slope on the results, it is concluded that it has a strong effect on the fatigue life of a K-joint. A difference of ca. 30% exists between the NSCF for $\delta = 20°$ and $\delta = 40°$ for the balanced axial load case. The same difference is approximately 24% for the in-plane bending case. This means that it can be optimized in order to significantly increase the fatigue resistance of a joint. The weld throat is designed by ULS. Using the effective notch stress approach, the weld slope could be designed in addition for the purpose of optimizing the fatigue resistance.

7.5 Summary

In this chapter, the use of the effective notch stress method, applied to tubular connections, is studied. In order to make this method computationally feasible, an approach that uses the sub-modelling technique is implement in ANSYS© APDL. An example of the assessment of the NSCF, using this approach, is presented for a K-joint. Furthermore, the parametric investigation carried out in Chapter 4 is combined with the NSCF results. Moreover, the results are complemented with the SCF provided by the global solid model, which explicitly models the weld. This investigation is not performed in terms of the fatigue damage. The complexities and assumptions made for carrying out the comparison in terms of the stress concentration values are addressed. Finally, a study of the weld slope is performed, in order to assess the potential material optimization of the weld profile that this method provides.

8 | Conclusions and Further Research

The aim of this project was to gain a better understanding of the various methods that can be used for the assessment of OWT jacket tubular joints. Four research topics that required further investigation were identified: (1) The difference between modelling a K-joint using plate and solid FE models; (2) a comparison between assessing the hot-spot method using FE models and the Efthymiou formulae; (3) the influence of the carry-over effect in multi-planar KK-joints; (4) the feasibility of assessing a tubular joint using the effective notch stress concept and the difference in the results with the hot-spot method. The conclusions drawn are presented below, separately for each of the studies. To conclude, some research topics that can follow this work are listed.

8.1 Conclusions

Two ways of approaching the hot-spot method by means of the FEM were compared, i.e. using solid and shell models. The assumptions and decisions made were justified and the characteristics of these models were reported. A mesh parametric study was performed for the solid model. Its outcome was the optimum mesh layout for the requisites given by the carried out investigations. A study of the stress distribution across the wall thickness was carried out for the solid model. It was concluded that several elements through thickness were to be used. Moreover, if the latter was fulfilled, reduced integration is acceptable to be employed. The normal stress distribution across the thickness was observed to be non-linear at the vicinity of the notch and linear within the extrapolation region. The non-linear stress distribution cannot be captured by using the shell model. This yields further differences between the models within the extrapolation region.

Furthermore, the element solution of the normal stresses to the weld was assessed for both models at three locations around the weld, i.e. the toe, heel and saddle positions. This study is carried out within a parametric study that comprises 42 simulations, in which several brace diameters and thicknesses, and brace inclinations are tested. A phenomenon was observed to take place for the solid model at some positions, particularly at the crown toe. This phenomenon is a shadow effect, which is related to the abrupt change in stiffness at the intersection point. The extension of this phenomenon is characterized by a distance of $t_i / \sin\theta_i$ from the intersection point. The first read-out point was reformulated considering this distance. In general, the shell model predicts higher SCF than the solid model.

The aforementioned parametric comparison was extended with the results of the Efthymiou equations. The SCF predicted by the three mathematical models were compared. The shell model predicted the highest results for most of the studied cases. The Efthymiou equations over-predicted the SCF at the locations where the SCF is not maximum. Situations where the Efthymiou equations underestimate the SCF were also found. The latter happened especially at the toe position, when balanced axial loads are applied at the braces ends.

The carry-over effect due to the loading at the out-of-plane braces of a KK-joint was investigated. Furthermore, the validity of modelling a KK-joint as a K-joint was studied. To carry out those investigations, two parametric models were built in ANSYS© APDL, i.e. one for the K-joint and one for the KK-joint. The study is carried out within a parametric investigation that comprises 396 FEM simulations. The simulations relate to several combinations of members diameters and thicknesses, braces inclinations θ, and face opening angles Ψ.

Generally speaking, the carry-over effect yields a high influence on the SCF. Therefore, it cannot be neglected for most cases. The highest carry-over effect was found for applying balanced axial loads at the out-of-plane braces. The carry-over effect was found maximum when the face opening angle

is small, i.e. for 3-leg jackets. It was found that applying in-plane bending loads to the out-of-plane braces yields a small influence on the in-plane braces SCF.

A method that makes the effective notch stress fatigue approach feasible, for the particular case of assessing tubular joints, was developed. The method is based on the employment of several sub-models around the weld in which the local stresses are estimated at the notch. The method was written in an ANSYS© APDL macro. The input of the macro are various reference points that are extracted from the global model.

An example of the use of this algorithm applied to the case of tubular K-joint was developed. The NSCF was estimated at eight positions around the weld for six load cases. The simulation required ca. 25 min in total. 93% of that time was employed in building and solving the sub-models. Therefore, the effective notch stress assessment demanded a computational dedication 13 times higher than the hot-spot method. The computed NSCF was ca. 2.13 times higher than the hot-spot SCF. The ratio between both factors was found to have a relatively large scatter. For the studied cases, the values belonged to the interval 1.1 to 3.7. The standard deviation of the scatter was 0.88. The hot-spot method uses the same concentration due to weld for all the cases, since this value is implicit in the formulation of the T-curve. This strongly limits the optimization of the joint.

The parametric investigation that was carried out between the solid and shell solid models was complemented with the results computed with the effective notch stress method. The comparison was made regarding the stress concentration factors and not in terms of the fatigue damage. In order to accomplish that, an equivalent hot-spot SCF SCF_{eqv} and an equivalent NSCF $NSCF_{eqv}$ were defined. The background of these definitions was based on two reasons: (1) The hot-spot method and the effective notch stress method belong to different fatigue classes, which means that the fatigue resistance is estimated using different SN-curves; (2) The thickness correction is to be applied only for the estimation of the hot-spot SCF. For most of the studied cases, the effective notch method predicted the highest fatigue life. In general, the results of the hot-spot method including the weld and the ones of the effective notch method presented a good match. Therefore, it is recommended to include the welding detail for the modelling of the hot-spot method.

A parametric study of the weld profile was performed. The influence of the weld slope on the NSCF was investigated at the crown toe position for two load cases, i.e. balanced axial loads and in-plane bending. The results were compared for five slopes δ in the range of 20° to 40°. This parameter was found to have a great influence on the results. The influence had an approximately linear tendency. The NSCF computed for the highest and lowest δ presented a difference of ca. 30%. Moreover, it was observed that the correction due to mild-notches is very likely to be applicable. Only for the balanced axial load and the case $\delta = 20°$, the read notch stress was larger than 1.6 times the hot-spot stress. It was concluded that the effective notch method can be used in order to optimize the weld profile.

8.2 Further Research

The studied research gaps yield further study questions. Moreover, the implementation of the effective notch stress concept for the fatigue assessment of tubular joints brings the possibility of studying some design aspects in further detail. Some of these topics are listed hereafter:

- ***Comparison of the fatigue life predictions using real load cases***. In this work, the comparison of the different methods was performed in terms of the SCF predictions. These values can be used to compute the fatigue damage for given design load time series. These would allow to perform the comparison in a more realistic way, in which the most important positions and load configurations would yield a stronger influence.
- ***Use of the effective notch model for a more detailed design of the joint, studying the impact of adding internal rigidization.*** The employment of wall rigidization is a known

solution for material optimization. The developed algorithm could be extended, allowing for the inclusion of the structural details. This can be used to quantify the potential benefits of the structural alternative.

- ***Use of the effective notch model to assess the economic importance of post-welding treatments.*** Since this method allows for the direct computation of the local stresses and the inclusion of the weld in the model, it can be used to study the impact of several defects in the weld surface and the potential benefits of eliminating them by using post-welding techniques.
- ***Use of the effective notch model to assess the relevance of the root fatigue failure.*** A parametric study can be carried out to find out for which situations this type of failure is prone to occur and how it can be prevented.

Bibliography

[1] J. Mendoza, S. Schafhirt, and M. Muskulus. Mesh Parametric Study for Fatigue Assessment of Tubular K-joints using Numerical Methods. *Energy Procedia*, (accepted) 2017.

[2] European Wind Energy Association. The European Offshore Wind Industry - key Trends and Statistics 2015, 2016.

[3] DNV GL AS. DNVGL-RP-C203. Fatigue Design of Offshore Steel Structures, 2016.

[4] M. Efthymiou and S. Durkin. Stress Concentrations in T/Y and Gap/Overlap K-Joints. *Proceedings of the 4th International Conference on Behaviour of Offshore Structures*, pages 429–440, 1985.

[5] M. Efthymiou. Development of SCF Formulae and Generalised Influence Functions for use in Fatigue Analysis. In *OTG 1988*, Surrey, UK, 1988.

[6] I. Lotsberg. On stress Concentration Factors for Tubular Y- and T-Joints in Frame Structures. *Marine Structures*, 24:60–69, 2011.

[7] S.J. Maddox. *Fatigue Strength of Welded Structures*. Abington Publishing, Cambridge, UK, 1969.

[8] S.J. Maddox. Hot-Spot Stress Design Curves for Fatigue Assessment of Welded Structures. *International Journal of Offshore and Polar Engineering*, 12(2):115–124, 2002.

[9] L. Fried, S. Shukla, S. Sawyer and S. Teske. Global Wind Energy Outlook, 2016.

[10] S. Berge. *Fatigue and Fracture Design of Marine structures*. NTNU, Trondheim, Norway, 2016.

[11] G.J.W. van Bussel and A.R. Henderson. State of the art and technology trends for offshore wind energy: Operation and maintenance issues, 2001.

[12] Almar-Naess. *Fatigue Handbook - Offshore Steel Structures*. Tapir Press, Trondheim, Noway, 1969.

[13] T.R. Gurney. *Fatigue of Welded Structures*. Cambridge University Press, Cambridge, UK, 1969.

[14] D.R.V. van Delft. A two dimensional analysis of the stresses at the vicinity of the weld toes of tubular structures, 1981.

[15] P.W. Marshall. Connections for Welded Tubular Structures. *IIW International Conference on Welding of Tubular Structures. Boston, USA*, pages 1–51, 1984.

[16] X.L. Zhao et al. Design Guide for Circular and Rectangular Hollow Section Welded Joints under Fatigue Loading, 2000.

[17] A.F. Hobbacher. Recommendations for Fatigue Design of Welded Joints and Components, 2016.

[18] A. Hobbacher and International Institute of Welding. *Recommendations for Fatigue Design of Welded Joints and Components*. Bulletin: Welding Research Council (U.S.). Welding Research Council, New York, 2009.

[19] W. Fricke. IIW Guideline for the Assessment of Weld Root Fatigue. *Welding in the World*, 57:753–791, 2013.

[20] Y. Cao, Z. Meng, S. Zhang, and H. Tian. FEM Study on the Stress Concentration Factors of K-joints with Welding Residual Stress. *Applied Ocean Research*, 43:195–205, 2013.

[21] T.R. Gurney. Fatigue Design Rules for Welded Steel Joints. *The Welding Institute Research Bulletin*, 17:115–124, 1976.

[22] E. Haibach. Discussion Paper. Technical report, The Welding Institute Conf. on Fatigue of Welded Structures, 1970.

[23] Det Norske Veritas AS. DNV-RP-C203. Fatigue Design of Offshore Steel Structures, 2011.

[24] D. Radaj. *Design and analysis of fatigue resistant welded structures.* Abington Publishing, 1990. Edition: Cambridge.

[25] W. Fricke. IIW Recommendations for the Fatigue Assessment by Notch Stress Analysis for Welded Structures, 2010.

[26] R. Tovo and P. Lazzarin. Relationship between Local and Structural Stress in the Evaluation of the Weld Toe Stress Distribution. *International Journal of Fatigue*, 21:1063–78, 1999.

[27] A. Romeijn. *Stress and Strain Concentration Factors of Welded Multiplanar Tubular Joints.* PhD dissertation, Delft University of Technology, Civil Engineering Department, November 1994.

[28] O. Doerk, W. Fricke, and C. Weissenborn. Comparison of Different Calculation Methods for Structural Stresses at Welded Joints. *International Journal of Fatigue*, 25:359–69, 2003.

[29] W. Fricke. Recommended Hot-Spot Analysis Procedure For Structural Details of Ships And FPSOs Based On Round-Robin FE Analyses. *International Journal of Offshore and Polar Engineering*, 12(1):40–47, 2002.

[30] I. Huther et al. Longitudinal non loaded welded joints geometrical stress approach. *Welding in the World*, 43(3):20–26, 1999.

[31] Wimpey Offshore Lloyd's Register of Shipping. Stress Concentration Factors for Simple Tubular Joints. Assessment of Existing and Development of New Parametric Formulae, 1997.

[32] B.H. Hammerstad, S. Schafhirt, and M. Muskulus. On Fatigue Damage Assessment for Offshore Support Structures with Tubular Joints. *Energy Procedia. 13th Deep Sea Offshore Wind R&D Conference, EERA DeepWind 2016*, 94:339–346, 2016.

[33] S. Yong-Bo, D. Zhi-Fu, and L. Seng-Tjhen. Prediction of hot spot stress distribution for tubular K-joints under basic loadings. *Journal of Constructional Steel Research*, 65:2011–2026, 2009.

[34] S. Yong-Bo. Geometrical effect on the stress distribution along weld toe for tubular T- and K-joints under axial loading. *Journal of Constructional Steel Research*, 1(63):1351–1360, 2007.

[35] *Computation of Stress Concentration Factors for Tubular Joints*, OMAE2013-10934, Nantes, France, 2013. Proc. ASME 2013 32nd International Conference on Ocean, Offshore and Arctic Engineering.

[36] L. Tang. Stress Concentration Factors (SCFs) for Partial Joint Penetration Plus (PJP+) welds for tubular joints. Master's thesis, Eindhoven University of Technology, Eindhoven, The Netherlands, sep 2010.

[37] S.A. Karamanos, A. Romeijn, and J. Wardenier. Stress Concentrations in Tubular Gap K-joints: Mechanics and Fatigue Design. *Engineering Structures*, 22:4–14, 2000.

[38] Wimpey Offshore Lloyd's Register of Shipping. Stress concentration factors for tubular complex joints, 1992.

[39] N.M. Irvine. Comparison of the Performance of modern semi-empirical Parametric Equations for Tubular Joint Stress Concentration Factors. *International Conference on Steel in Marine Structures, France.*, 1981.

[40] A.C. Wordsworth. Aspects of the Stress Concentration Factors at Tubular Joints. In *3rd International Offshore Conference on Steel in Marine Structures*, Delft, The Nehterlands, 1987.

[41] A.M. van Wingerde, J.A. Packer, and J. Wardenier. Simplified SCF formulae and graphs for CHS and RHS K- and KK-connections. *Journal of Constructional Steel Research*, 57:221–252, 2001.

[42] S.A. Karamanos, A. Romeijnb, and J. Wardenier. SCF Equations in Multi-planar Welded Tubular DT-joints including Bending effects. *Marine Structures*, 1(15):157–173, 2002.

[43] H. Ahmadi and E. Zavvar. The effect of Multi-planarity on the SCFs in Offshore Tubular KT-Joints subjected to in-plane and out-of-plane Bending Loads. *Thin-Walled Structures*, 1(106):148–165, 2016.

[44] H. Petershagen, W. Fricke, and T. Massel. Application of the Local Approach to the Fatigue Strength Assessment of Welded Structures in Ships. *Annual Assembly of International Institute of Welding*, IIW-Doc(XIII-1409-91):11, 1991.

[45] W. Fricke and R. Bogdan. Determination of Hot Spot Stress in Structural Members with In-Plane Notches Using a Coarse Element Mesh. *Annual Assembly of International Institute of Welding*, IIW-Doc(XIII-1870-01):7, 2001.

[46] W. Fricke. Evaluation of Hot Spot Stresses in Complex Welded Structures. *Proc. of the IIW Fatigue Seminar, Commission XIII, Int. Institute of Welding*, 1:12, 2002.

[47] D. Radaj, C.M Sonsino, and W. Fricke. *Fatigue assessment of Welded Joints by local Approaches.* Woodhead Publishing Limited, Cambridge, England, 2006.

[48] J. Schönherr. Comparison of Different Structural- and Notch Stress Approaches on the Example of the Fatigue Strength of a Tubular K-joint. *STG Jahrbuch*, pages 70–77, 2009.

[49] E. Reissner. The Effect of Transverse Shear Deformation on the Bending of Elastic Plates. *ASME Journal of Applied Mechanics*, 12:68–77, 1945.

[50] R.D. Mindlin. Influence of Rotatory Inertia and Shear on Flexural Motions of Isotropic, Elastic Plates. *ASME Journal of Applied Mechanics*, 18:31–38, 1951.

[51] A.E.H. Love. On the Small Free Vibrations and Deformations of Elastic Shells. *Philosophical trans. of the Royal Society*, 17:491–549, 1888.

[52] S. Timoshenko. *History of Strength of Materials.* McGraw-Hill, 1953. Edition: New York.

[53] ANSYS Mechanical APDL User's Guide. Technical report, Ansys, Inc., November, 2013.

A | Results of the investigation of the Hot-spot Method

In Chapters 4 and 5, an investigation of the structural stress approach was elaborated. Some features of the possible ways of approaching this method were investigated. Some of the results used in the discussion are presented in this part of the Appendix. The geometry of the cases used for the parametric investigation is described by non-dimensional parameters in Table A.1. The SCF comparison between the solid and shell FE models and the Efthymiou equations is shown in Tables A.2 to A.4. The extrapolation paths used to compute these SCFs are shown in Figures A.1 to A.7.

Table A.1: *Definition of the cases created for the parametric investigation carried out in Chapter4.*

CASE 1			
$\gamma =$	10	$\tau =$	0.4
$\theta =$	45°	$\beta =$	0.4
$e =$	0	$\zeta =$	0.434

CASE 5			
$\gamma =$	10	$\tau =$	0.8
$\theta =$	45	$\beta =$	0.4
$e =$	0	$\zeta =$	0.434

CASE 2			
$\gamma =$	10	$\tau =$	0.4
$\theta =$	45°	$\beta =$	0.6
$e =$	0	$\zeta =$	0.151

CASE 6			
$\gamma =$	10	$\tau =$	0.4
$\theta =$	35°	$\beta =$	0.4
$e =$	0	$\zeta =$	0.731

CASE 3			
$\gamma =$	10	$\tau =$	0.4
$\theta =$	45	$\beta =$	0.8
$e =$	0.15	$\zeta =$	0.169

CASE 7			
$\gamma =$	10	$\tau =$	0.4
$\theta =$	55°	$\beta =$	0.4
$e =$	0	$\zeta =$	0.212

CASE 4			
$\gamma =$	10	$\tau =$	0.6
$\theta =$	45°	$\beta =$	0.4
$e =$	0	$\zeta =$	0.434

Table A.2: *SCF results for Cases 1 to 3 (described in Table A.1).*

				SCF					
				FEM			Efthymiou		
				Solid186	Shell181	Difference	SCF_{Efth}	Dif_{Solid}	Dif_{Shell}
CASE1	B1	BAL	t	3.25	3.26	0.24%	2.33	-39.22%	-39.55%
			h	1.57	2.00	21.26%	2.33	32.51%	14.29%
			s	1.49	2.07	27.77%	2.33	35.95%	11.33%
		IPB	t	1.43	1.61	10.98%	2.32	38.28%	30.67%
			h	2.35	2.97	20.76%	2.32	-1.29%	-27.83%
		OPB	s	1.34	2.10	36.50%	1.92	30.29%	-9.79%
	B2	BAL	t	3.22	3.80	15.07%	2.33	-38.17%	-62.70%
			h	1.56	2.23	30.05%	2.33	33.26%	4.59%
			s	1.30	2.36	45.05%	2.33	44.32%	-1.33%
		IPB	t	1.44	1.84	21.86%	2.32	38.08%	20.76%
			h	2.36	2.99	21.01%	2.32	-1.45%	-28.44%
		OPB	s	1.33	2.07	35.81%	1.92	30.48%	-8.30%
CASE2	B1	BAL	t	2.49	2.72	8.47%	2.01	-23.95%	-35.42%
			h	1.40	1.70	17.85%	2.01	30.37%	15.24%
			s	1.12	1.22	8.15%	2.01	44.04%	39.07%
		IPB	t	1.46	1.67	12.20%	2.39	38.88%	30.39%
			h	2.10	2.71	22.41%	2.39	12.09%	-13.30%
		OPB	s	1.80	2.60	30.84%	2.65	32.14%	1.87%
	B2	BAL	t	2.56	2.69	4.73%	2.01	-27.35%	-33.66%
			h	1.34	1.84	27.41%	2.01	33.39%	8.23%
			s	0.79	1.58	49.78%	2.01	60.55%	21.45%
		IPB	t	1.47	1.66	11.86%	2.39	38.77%	30.53%
			h	2.09	2.74	23.74%	2.39	12.72%	-14.44%
		OPB	s	1.79	2.60	31.23%	2.65	32.46%	1.79%
CASE3	B1	BAL	t	2.18	2.56	14.78%	1.79	-21.77%	-42.89%
			h	1.29	1.50	14.28%	1.79	27.96%	15.96%
			s	1.01	0.92	-10.00%	1.79	43.70%	48.82%
		IPB	t	1.51	1.68	9.81%	2.30	34.27%	27.13%
			h	1.93	2.45	21.22%	2.30	16.31%	-6.24%
		OPB	s	1.72	2.56	32.75%	2.73	36.76%	5.96%
	B2	BAL	t	2.40	2.38	-0.95%	1.79	-34.25%	-32.99%
			h	1.17	1.71	31.72%	1.79	34.83%	4.55%
			s	0.69	1.43	51.79%	1.79	61.43%	19.99%
		IPB	t	1.51	1.68	10.45%	2.30	34.59%	26.96%
			h	1.90	2.49	23.72%	2.30	17.61%	-8.01%
		OPB	s	2.10	2.57	18.14%	2.73	22.83%	5.73%

Table A.3: *SCF results for Cases 4 to 6 (described in Table A.1).*

				SCF					
				FEM			Efthymiou		
				Solid186	**Shell181**	**Difference**	**SCF$_{Efth}$**	**Dif$_{Solid}$**	**Dif$_{Shell}$**
CASE4	**B1**	**BAL**	t	3.60	3.66	1.60%	2.81	-27.86%	-29.93%
			h	1.55	2.19	29.20%	2.81	44.85%	22.10%
			s	1.89	2.72	30.36%	2.81	32.82%	3.52%
		IPB	t	1.35	1.57	14.32%	2.56	47.38%	38.59%
			h	2.31	3.16	26.83%	2.56	9.68%	-23.43%
		OPB	s	1.54	2.50	38.52%	2.31	33.37%	-8.38%
	B2	**BAL**	t	3.55	3.79	6.43%	2.81	-26.12%	-34.78%
			h	1.58	2.29	31.07%	2.81	43.80%	18.47%
			s	1.68	2.91	42.30%	2.81	40.37%	-3.34%
		IPB	t	1.35	1.56	13.22%	2.56	47.12%	39.07%
			h	2.31	3.17	27.11%	2.56	9.76%	-23.80%
		OPB	s	1.53	2.50	38.77%	2.31	33.63%	-8.39%
CASE5	**B1**	**BAL**	t	3.60	3.80	5.16%	3.26	-10.54%	-16.56%
			h	1.45	2.23	35.18%	3.26	55.55%	31.43%
			s	2.20	3.15	30.00%	3.26	32.32%	3.32%
		IPB	t	1.24	1.54	19.80%	2.75	55.02%	43.91%
			h	2.08	3.07	32.29%	2.75	24.26%	-11.86%
		OPB	s	1.67	2.65	36.82%	2.64	36.55%	-0.44%
	B2	**BAL**	t	3.53	4.00	11.72%	3.26	-8.32%	-22.70%
			h	1.65	2.29	28.14%	3.26	49.41%	29.60%
			s	2.01	3.33	39.50%	3.26	38.17%	-2.20%
		IPB	t	1.24	1.53	18.59%	2.75	54.81%	44.49%
			h	2.21	3.08	28.35%	2.75	19.66%	-12.12%
		OPB	s	1.69	2.64	36.13%	2.64	35.91%	-0.35%
CASE6	**B1**	**BAL**	t	3.20	2.78	-15.38%	1.95	-63.89%	-42.05%
			h	1.61	1.73	6.54%	1.95	17.47%	11.70%
			s	1.06	1.49	28.88%	1.95	45.89%	23.92%
		IPB	t	1.14	1.14	0.43%	2.49	54.21%	54.02%
			h	2.76	3.16	12.50%	2.49	-11.04%	-26.91%
		OPB	s	0.78	1.36	42.88%	1.33	41.81%	-1.88%
	B2	**BAL**	t	3.13	2.92	-7.33%	1.95	-60.45%	-49.49%
			h	1.59	1.87	14.92%	1.95	18.61%	4.34%
			s	0.83	1.70	51.47%	1.95	57.72%	12.86%
		IPB	t	1.15	1.13	-1.10%	2.49	53.92%	54.42%
			h	2.76	3.17	12.92%	2.49	-10.83%	-27.28%
		OPB	s	0.77	1.36	43.19%	1.33	42.23%	-1.68%

Table A.4: *SCF results for Case 7 (described in Table A.1).*

				SCF					
				FEM			Efthymiou		
				Solid186	**Shell181**	**Difference**	**SCF$_{Efth}$**	**Dif$_{Solid}$**	**Dif$_{Shell}$**
CASE7	**B1**	**BAL**	t	3.06	3.48	11.97%	2.63	-16.51%	-32.34%
			h	1.66	2.30	27.90%	2.63	36.88%	12.45%
			s	1.89	2.45	23.11%	2.63	28.33%	6.79%
		IPB	t	1.71	2.05	16.70%	2.22	23.13%	7.72%
			h	2.11	2.80	24.49%	2.22	4.73%	-26.16%
		OPB	s	2.00	2.88	30.39%	2.54	21.23%	-13.16%
	B2	**BAL**	t	3.06	3.49	12.16%	2.63	-16.50%	-32.63%
			h	1.64	2.36	30.24%	2.63	37.50%	10.41%
			s	1.74	2.59	33.09%	2.63	34.02%	1.39%
		IPB	t	1.71	2.04	16.29%	2.22	23.04%	8.06%
			h	2.11	2.81	24.78%	2.22	4.91%	-26.42%
		OPB	s	2.00	2.88	30.48%	2.54	21.34%	-13.15%

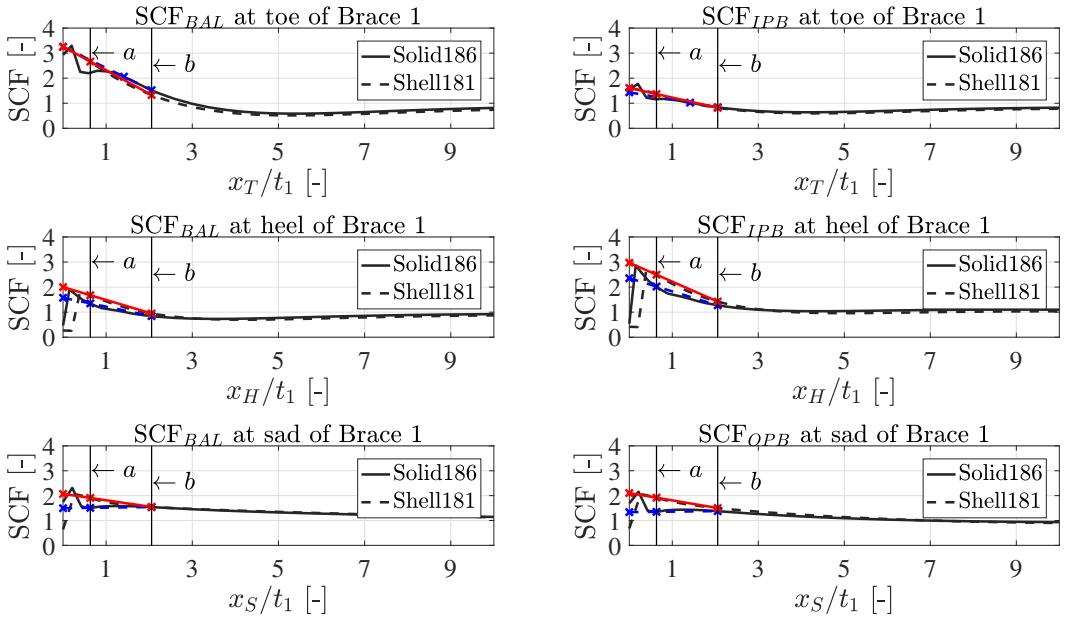

Figure A.1: *Stress field results CASE 1, cf. Table A.1, including lines of extrapolation to the weld toe (in blue for the solid model and red for the shell model).*

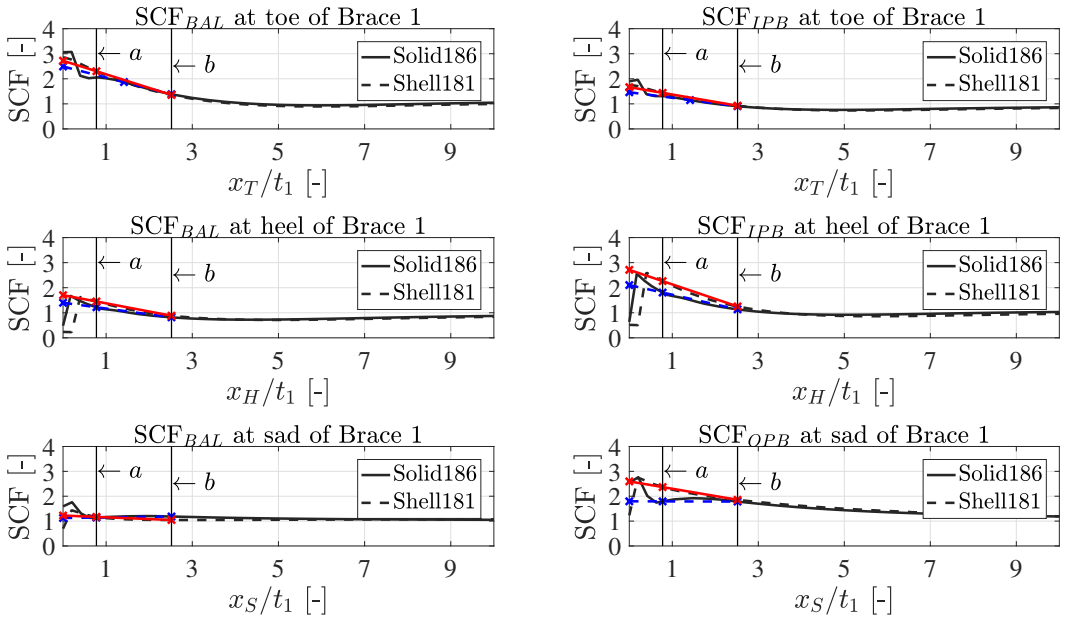

Figure A.2: *Stress field results CASE 2, cf Table A.1, including lines of extrapolation to the weld toe (in blue for the solid model and red for the shell model).*

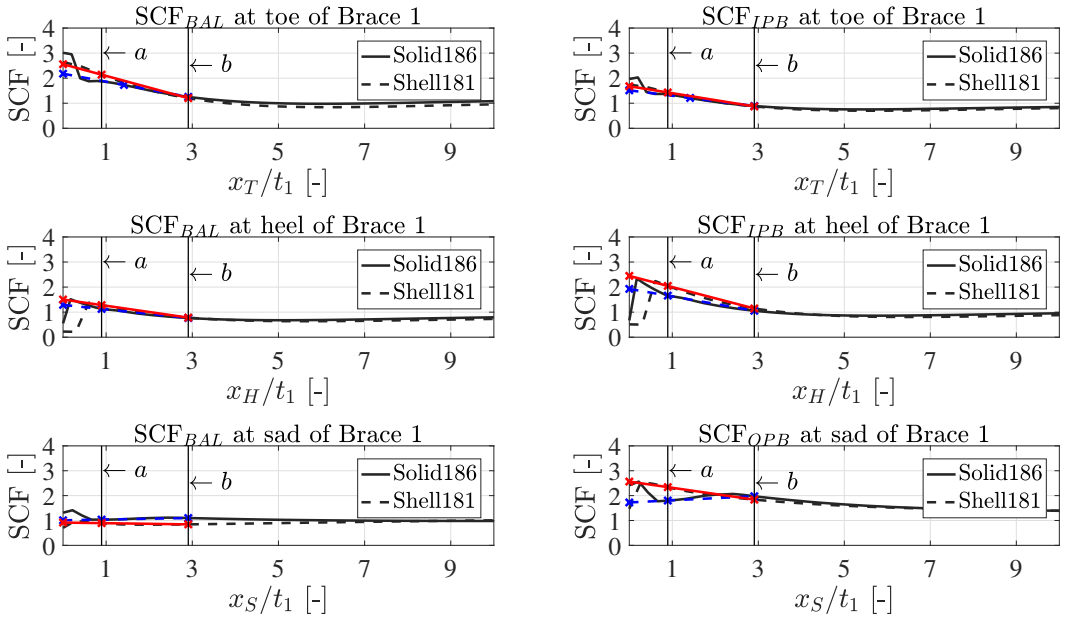

Figure A.3: *Stress field results CASE 3, cf. Table A.1, including lines of extrapolation to the weld toe (in blue for the solid model and red for the shell model).*

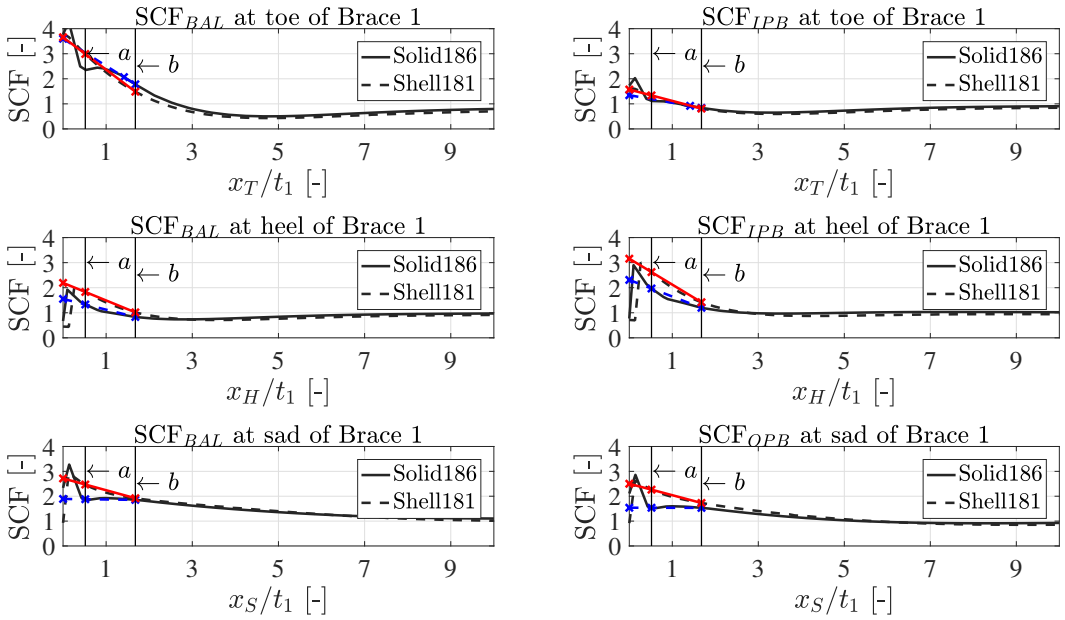

Figure A.4: *Stress field results CASE 4, cf. Table A.1, including lines of extrapolation to the weld toe (in blue for the solid model and red for the shell model).*

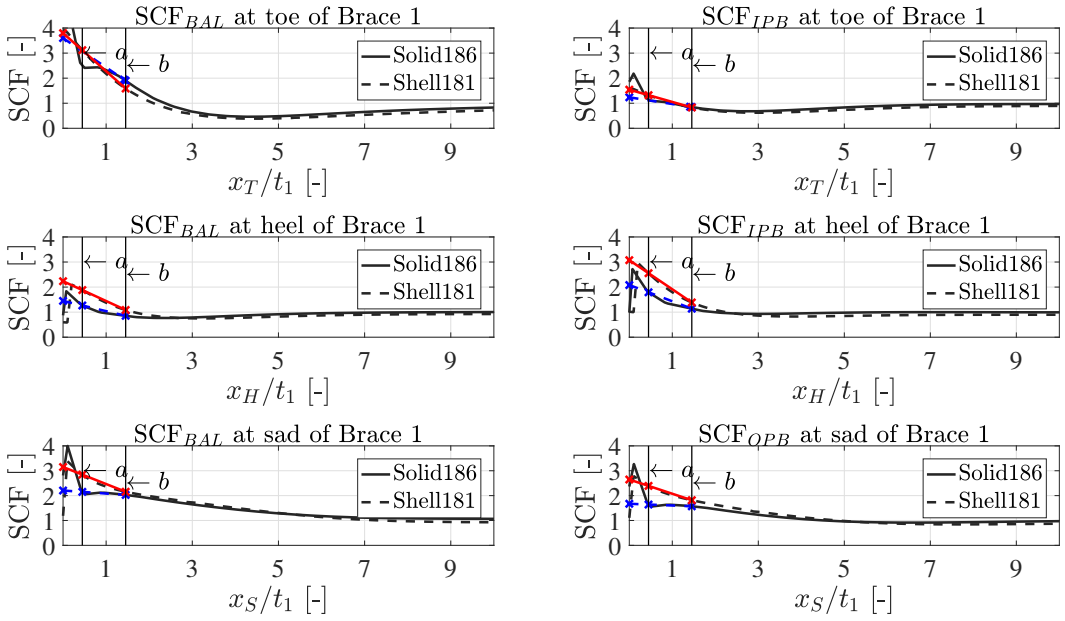

Figure A.5: *Stress field results CASE 5, cf. Table A.1, including lines of extrapolation to the weld toe (in blue for the solid model and red for the shell model).*

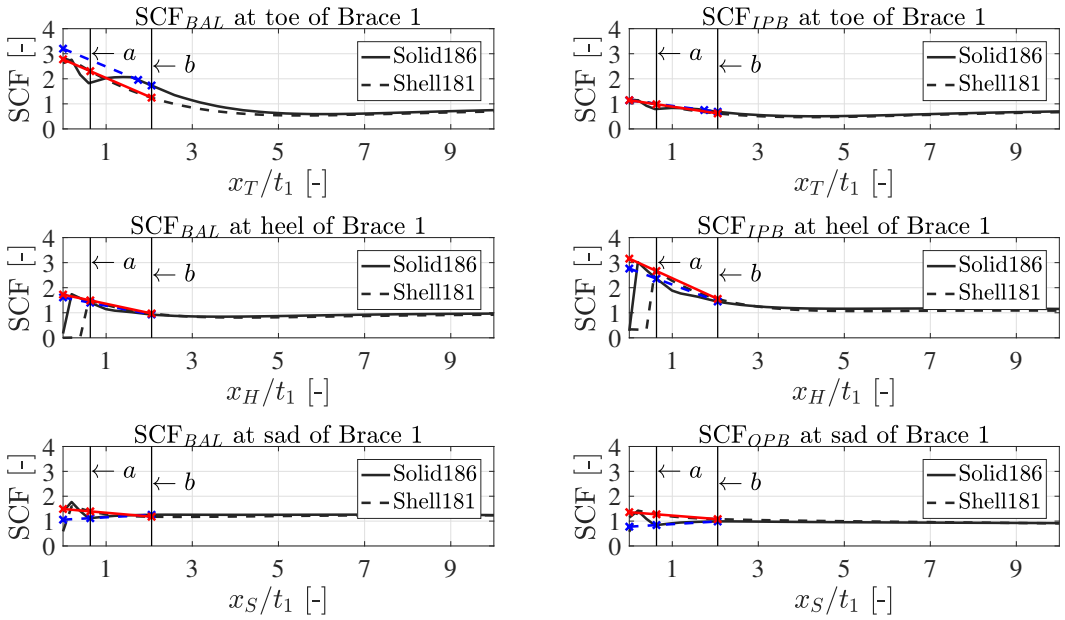

Figure A.6: *Stress field results CASE 6, cf. Table A.1, including lines of extrapolation to the weld toe (in blue for the solid model and red for the shell model).*

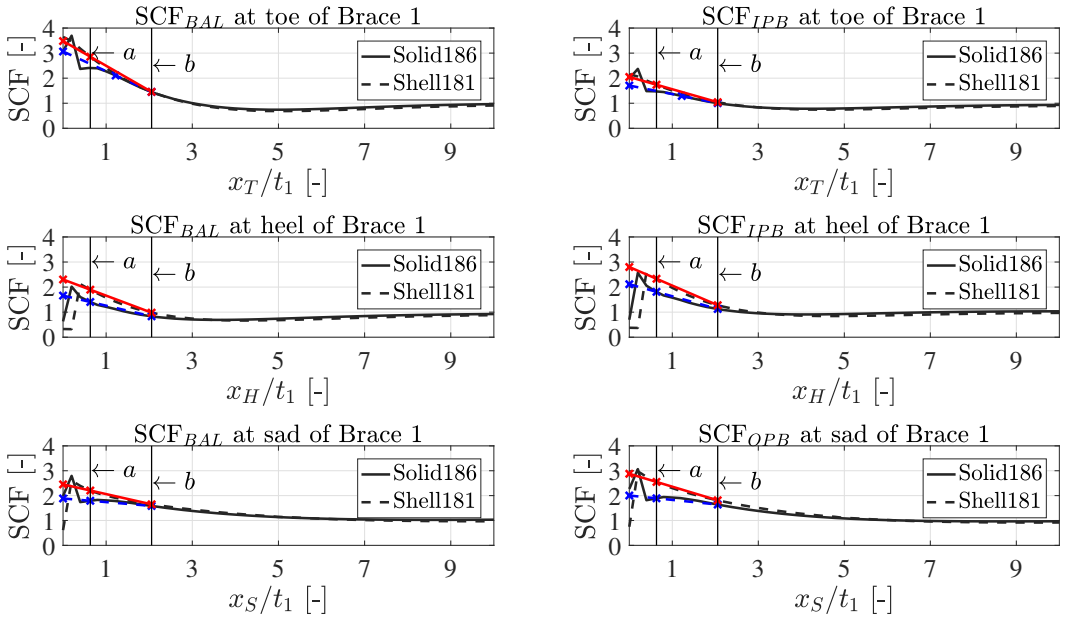

Figure A.7: *Stress field results CASE 7, cf. Table A.1, including lines of extrapolation to the weld toe (in blue for the solid model and red for the shell model).*

B | Results of the KK-joint investigation

Some of the results produced for the investigation of the carry-over effect of the out-of-plane braces of multiplanar KK-joints are collected in this chapter of the Appendix. Tables B.1 to B.3 show the a quantification of the carry-over effect due to loading at the out-of-plane braces. The importance of the contribution of the out-of-plane braces into the SCF is measured through the, here called, S_R parameter. S_R/R_F is tabulated for the studied cases in Tables B.4 to B.9. Figures B.1 to B.5 show the SCF comparison done between the K-joint and the KK-joint models within the parametric investigation of Ψ, τ, β, θ. The discussion of the results can be found in Chapter 6.4.

Table B.1: *Carry-over effect of a KK-joint at the crown toe position of the reference brace measured through K_{LD} for the τ parametric investigation for various Ψ values. K_{LD} is given for the BAL, IPB and OPB loading in the out-of-plane pair of braces. The following non-dimensional parameters are used to produce the data: $\beta = 0.4$, $\gamma = 10$, $\theta = 45°$, $\zeta = 0.5$.*

	$\tau = 0.2$			$\tau = 0.4$			$\tau = 0.6$			$\tau = 0.8$		
Ψ	BAL	IPB	OPB	BAL	IPB	OPB	BAL	IPB	OPB	BAL	IPB	OPB
60°	-0.13	-0.03	0.10	-0.42	-0.08	0.16	-0.64	-0.14	0.02	-0.72	-0.17	-0.23
75°	-0.12	-0.02	0.11	-0.41	-0.04	0.20	-0.66	-0.07	0.08	-0.75	-0.10	-0.20
90°	-0.07	0.00	0.12	-0.25	0.01	0.22	-0.42	0.01	0.08	-0.49	0.00	-0.17
105°	-0.02	0.01	0.14	-0.08	0.03	0.22	-0.15	0.05	0.08	-0.19	0.05	-0.13

Table B.2: *Carry-over effect of a KK-joint at the crown toe position of the reference brace measured through K_{LD} for the β parametric investigation for various Ψ values. K_{LD} is given for the BAL, IPB and OPB loading in the out-of-plane pair of braces. The following non-dimensional parameters are used to produce the data: $\tau = 0.4$, $\gamma = 10$, $\theta = 45°$, $\zeta = 0.5$.*

	$\beta = 0.2$			$\beta = 0.3$			$\beta = 0.4$		
Ψ	BAL	IPB	OPB	BAL	IPB	OPB	BAL	IPB	OPB
60°	-0.28	-0.02	-0.17	-0.40	-0.05	-0.20	-0.42	-0.08	0.16
75°	-0.18	0.00	-0.17	-0.31	-0.02	-0.18	-0.41	-0.04	0.20
90°	-0.07	0.01	-0.16	-0.14	0.01	-0.17	-0.25	0.01	0.22
105°	0.01	0.01	-0.16	-0.01	0.02	-0.17	-0.08	0.03	0.22

Table B.3: *Carry-over effect of a KK-joint at the crown toe position of the reference brace measured through K_{LD} for the θ parametric investigation for various Ψ values. K_{LD} is given for the BAL, IPB and OPB loading in the out-of-plane pair of braces. The following non-dimensional parameters are used to produce the data: $\tau = 0.4$, $\gamma = 10$, $\theta = 45°$, $\zeta = 0.5$.*

	$\theta = 30°$			$\theta = 40°$			$\theta = 50°$			$\theta = 60°$		
Ψ	BAL	IPB	OPB	BAL	IPB	OPB	BAL	IPB	OPB	BAL	IPB	OPB
60°	-0.13	-0.12	-0.09	-0.42	-0.09	-0.08	-0.64	-0.07	-0.04	-0.72	-0.07	-0.38
75°	-0.12	-0.07	-0.03	-0.41	-0.04	0.02	-0.66	-0.04	-0.21	-0.75	-0.04	-0.41
90°	-0.07	0.00	-0.01	-0.25	0.01	0.03	-0.42	0.00	-0.24	-0.49	0.00	-0.43
105°	-0.02	0.03	0.01	-0.08	0.03	0.01	-0.15	0.02	-0.01	-0.19	0.02	-0.41

Table B.4: *Ratio between the contribution of the out-of-plane braces over the reference braces to the SCF at the crown toe position of the reference brace S_R/R_F defined in Eq. 6.3. These results correspond to the case of having BAL loading at the reference braces for the τ parametric study. The loading cases BAL1, BAL2 and BAL3 are described in Table 6.1. The following non-dimensional parameters are used to produce the data: $\beta = 0.4$, $\gamma = 10$, $\theta = 45°$, $\zeta = 0.5$.*

	$\tau = 0.2$			$\tau = 0.4$			$\tau = 0.6$			$\tau = 0.8$		
Ψ	BAL1	BAL2	BAL3	BAL1	BAL2	BAL3	BAL1	BAL2	BAL3	BAL1	BAL2	BAL3
60°	-0.15	-0.05	-0.04	-0.27	-0.05	-0.03	-0.30	-0.04	-0.06	-0.30	-0.03	-0.12
75°	-0.15	-0.06	-0.04	-0.26	-0.07	0.00	-0.30	-0.05	-0.03	-0.31	-0.04	-0.09
90°	-0.12	-0.07	-0.03	-0.19	-0.08	0.01	-0.21	-0.07	-0.02	-0.22	-0.06	-0.08
105°	-0.08	-0.07	-0.02	-0.12	-0.09	0.01	-0.12	-0.08	-0.02	-0.12	-0.07	-0.08

Table B.5: *Ratio between the contribution of the out-of-plane braces over the reference braces to the SCF at the crown toe position of the reference brace S_R/R_F defined in Eq. 6.3. These results correspond to the case of having BAL loading at the reference braces for the β parametric study. The loading cases BAL1, BAL2 and BAL3 are described in Table 6.1. The following non-dimensional parameters are used to produce the data: $\tau = 0.4$, $\gamma = 10$, $\theta = 45°$, $\zeta = 0.5$.*

	$\beta = 0.2$			$\beta = 0.3$			$\beta = 0.4$		
Ψ	BAL1	BAL2	BAL3	BAL1	BAL2	BAL3	BAL1	BAL2	BAL3
60°	-0.18	-0.04	-0.11	-0.25	-0.05	-0.12	-0.27	-0.05	-0.03
75°	-0.13	-0.04	-0.11	-0.20	-0.06	-0.11	-0.26	-0.07	0.00
90°	-0.08	-0.05	-0.10	-0.13	-0.07	-0.11	-0.19	-0.08	0.01
105°	-0.04	-0.05	-0.10	-0.07	-0.07	-0.11	-0.12	-0.09	0.01

Table B.6: *Ratio between the contribution of the out-of-plane braces over the reference braces to the SCF at the crown toe position of the reference brace S_R/R_F defined in Eq. 6.3. These results correspond to the case of having BAL loading at the reference braces for the θ parametric study. The loading cases BAL1, BAL2 and BAL3 are described in Table 6.1. The following non-dimensional parameters are used to produce the data: $\beta = 0.4$, $\tau = 0.4$, $\gamma = 10$, $\zeta = 0.5$.*

	$\theta = 30°$			$\theta = 40°$			$\theta = 50°$			$\theta = 60°$		
Ψ	BAL1	BAL2	BAL3	BAL1	BAL2	BAL3	BAL1	BAL2	BAL3	BAL1	BAL2	BAL3
60°	-0.27	-0.06	-0.15	-0.27	-0.05	-0.13	-0.27	-0.05	-0.12	-0.26	-0.05	-0.19
75°	-0.29	-0.08	-0.12	-0.27	-0.07	-0.09	-0.26	-0.06	-0.18	-0.25	-0.05	-0.20
90°	-0.23	-0.11	-0.10	-0.20	-0.09	-0.08	-0.19	-0.08	-0.18	-0.18	-0.07	-0.21
105°	-0.15	-0.13	-0.08	-0.12	-0.10	-0.08	-0.11	-0.09	-0.09	-0.11	-0.08	-0.21

Table B.7: *Ratio between the contribution of the out-of-plane braces over the reference braces to the SCF at the crown toe position of the reference brace S_R/R_F defined in Eq. 6.3. These results correspond to the case of having IPB loading at the reference braces for the τ parametric study. The loading cases IPB1, IPB2 and IPB3 are described in Table 6.1. The following non-dimensional parameters are used to produce the data: $\beta = 0.4$, $\gamma = 10$, $\theta = 45°$, $\zeta = 0.5$.*

	$\tau = 0.2$			$\tau = 0.4$			$\tau = 0.6$			$\tau = 0.8$		
Ψ	IPB1	IPB2	IPB3	IPB1	IPB2	IPB3	IPB1	IPB2	IPB3	IPB1	IPB2	IPB3
60°	-0.19	-0.05	0.12	-0.43	-0.04	0.01	-0.55	0.00	-0.05	-0.57	0.04	-0.14
75°	-0.19	-0.06	0.14	-0.44	-0.07	0.04	-0.57	-0.05	-0.01	-0.61	-0.01	-0.11
90°	-0.14	-0.07	0.16	-0.31	-0.11	0.06	-0.40	-0.10	0.00	-0.43	-0.07	-0.09
105°	-0.09	-0.08	0.18	-0.17	-0.12	0.07	-0.20	-0.12	0.02	-0.20	-0.10	-0.07

Table B.8: *Ratio between the contribution of the out-of-plane braces over the reference braces to the SCF at the crown toe position of the reference brace S_R/R_F defined in Eq. 6.3. These results correspond to the case of having IPB loading at the reference braces for the β parametric study. The loading cases IPB1, IPB2 and IPB3 are described in Table 6.1. The following non-dimensional parameters are used to produce the data: $\tau = 0.4$, $\gamma = 10$, $\theta = 45°$, $\zeta = 0.5$.*

	$\tau = 0.2$			$\tau = 0.4$			$\tau = 0.6$			$\tau = 0.8$		
Ψ	IPB1	IPB2	IPB3	IPB1	IPB2	IPB3	IPB1	IPB2	IPB3	IPB1	IPB2	IPB3
60°	-0.19	-0.05	-0.82	-0.43	-0.04	0.01	-0.55	0.00	-0.05	-0.57	0.04	-0.14
75°	-0.19	-0.06	-0.55	-0.44	-0.07	0.04	-0.57	-0.05	-0.01	-0.61	-0.01	-0.11
90°	-0.14	-0.07	-0.87	-0.31	-0.11	0.06	-0.40	-0.10	0.00	-0.43	-0.07	-0.09
105°	-0.09	-0.08	-0.58	-0.17	-0.12	0.07	-0.20	-0.12	0.02	-0.20	-0.10	-0.07

Table B.9: *Ratio between the contribution of the out-of-plane braces over the reference braces to the SCF at the crown toe position of the reference brace S_R/R_F defined in Eq. 6.3. These results correspond to the case of having IPB loading at the reference braces for the θ parametric study. The loading cases IPB1, IPB2 and IPB3 are described in Table 6.1. The following non-dimensional parameters are used to produce the data: $\beta = 0.4$, $\tau = 0.4$, $\gamma = 10$, $\zeta = 0.5$.*

	$\theta = 30°$			$\theta = 40°$			$\theta = 50°$			$\theta = 60°$		
Ψ	IPB1	IPB2	IPB3	IPB1	IPB2	IPB3	IPB1	IPB2	IPB3	IPB1	IPB2	IPB3
60°	-0.77	-0.03	-0.27	-0.46	-0.04	-0.20	-0.40	-0.04	-0.15	-0.36	-0.03	-0.19
75°	-0.79	-0.09	-0.20	-0.48	-0.08	-0.12	-0.40	-0.06	-0.27	-0.35	-0.05	-0.20
90°	-0.73	-0.17	-0.16	-0.35	-0.13	-0.10	-0.28	-0.09	-0.26	-0.24	-0.07	-0.21
105°	-0.64	-0.21	-0.13	-0.19	-0.15	-0.11	-0.15	-0.11	-0.11	-0.13	-0.09	-0.21

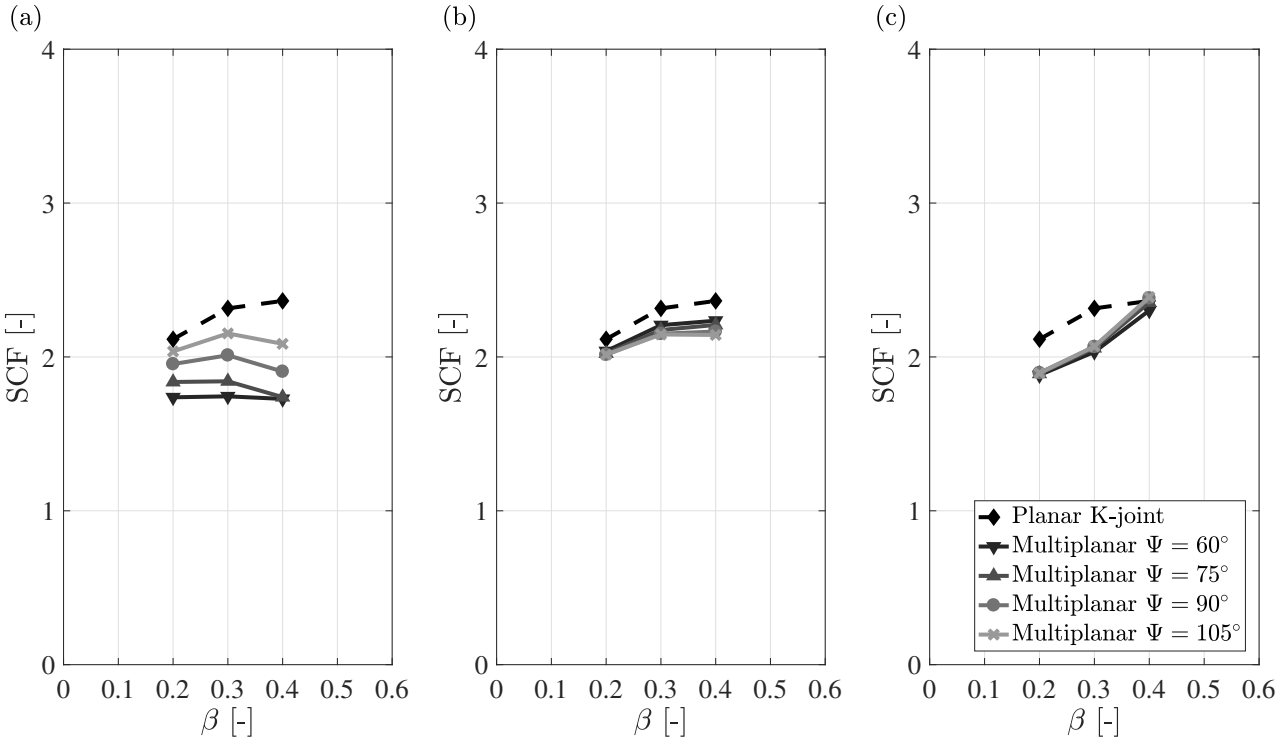

Figure B.1: *Influence of Ψ in the computation of the SCF of a tubular KK-joint under application of BAL at the braces in face 1 within a parametric investigation of β. The subfigures correspond to the following load cases, which are described in Table 6.1: (a) BAL1($R_F = 1$) (b) BAL2($R_F = 1$) (c) BAL3($R_F = 1$). The following non-dimensional parameters are used to produce the data: $\tau = 0.4$, $\gamma = 10$, $\theta = 45°$, $\zeta = 0.5$.*

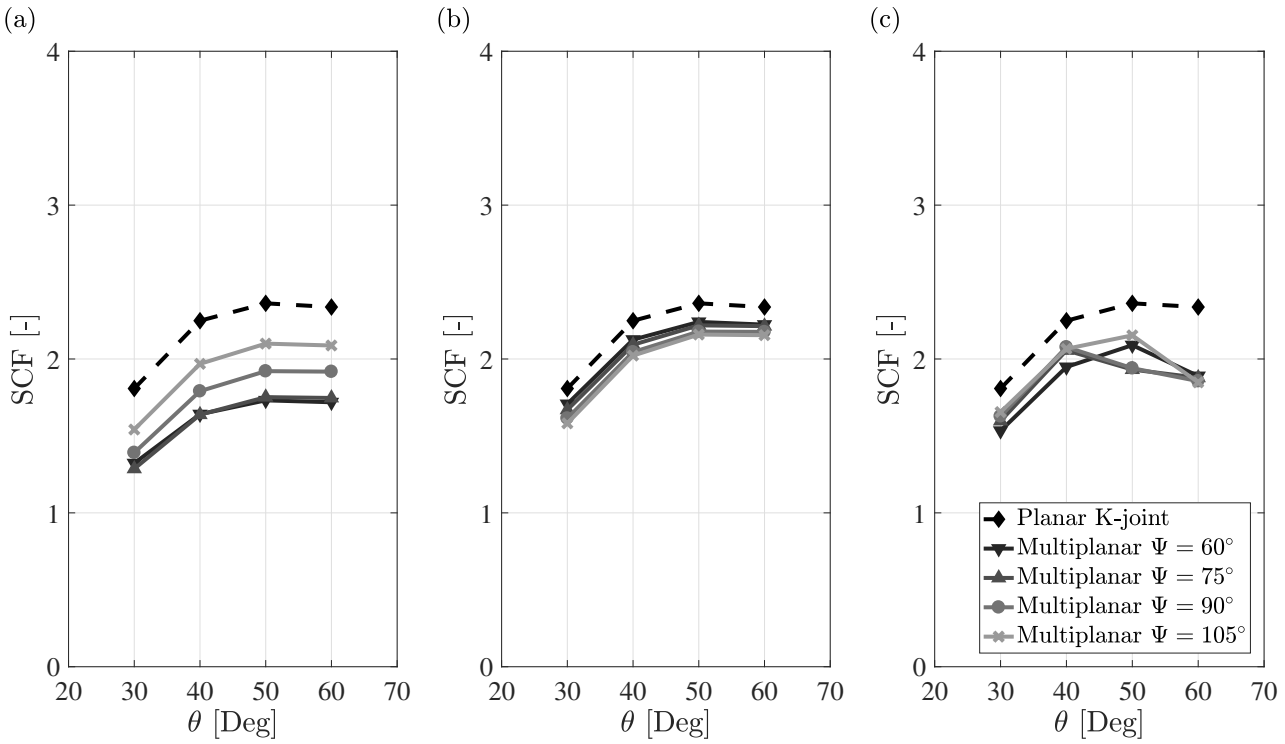

Figure B.2: *Influence of Ψ in the computation of the SCF of a tubular KK-joint under application of BAL at the braces in face 1 within a parametric investigation of θ. The subfigures correspond to the following load cases, which are described in Table 6.1: (a) BAL1($R_F = 1$) (b) BAL2($R_F = 1$) (c) BAL3($R_F = 1$). The following non-dimensional parameters are used to produce the data: $\beta = 0.4$, $\tau = 0.4$, $\gamma = 10$, $\zeta = 0.5$.*

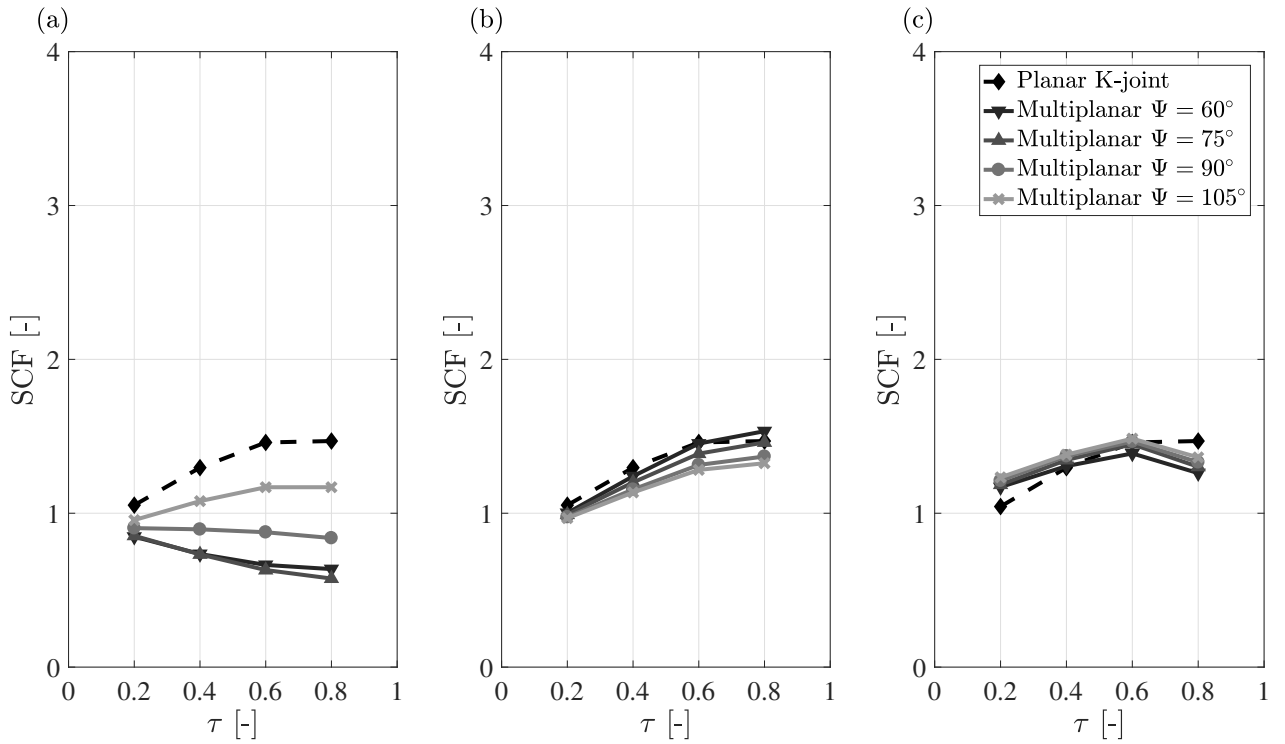

Figure B.3: *Influence of Ψ in the computation of the SCF of a tubular KK-joint under application of IPB at the braces in face 1 within a parametric investigation of τ. The subfigures correspond to the following load cases, which are described in Table 6.1: (a) IPB1($R_F = 1$) (b) IPB2($R_F = 1$) (c) IPB3($R_F = 1$). The following non-dimensional parameters are used to produce the data: $\beta = 0.4$, $\gamma = 10$, $\theta = 45°$, $\zeta = 0.5$.*

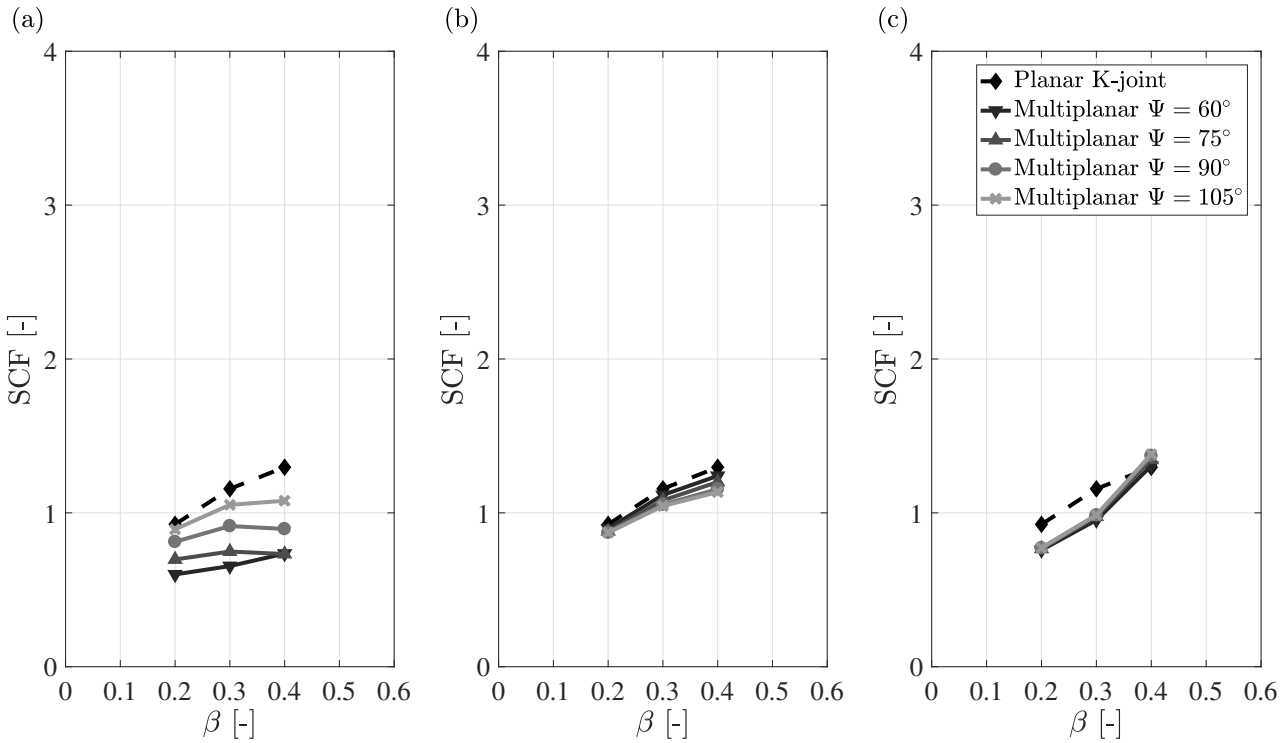

Figure B.4: *Influence of Ψ in the computation of the SCF of a tubular KK-joint under application of IPB at the braces in face 1 within a parametric investigation of β. The subfigures correspond to the following load cases, which are described in Table 6.1: (a) IPB1($R_F = 1$) (b) IPB2($R_F = 1$) (c) IPB3($R_F = 1$). The following non-dimensional parameters are used to produce the data: $\tau = 0.4$, $\gamma = 10$, $\theta = 45°$, $\zeta = 0.5$.*

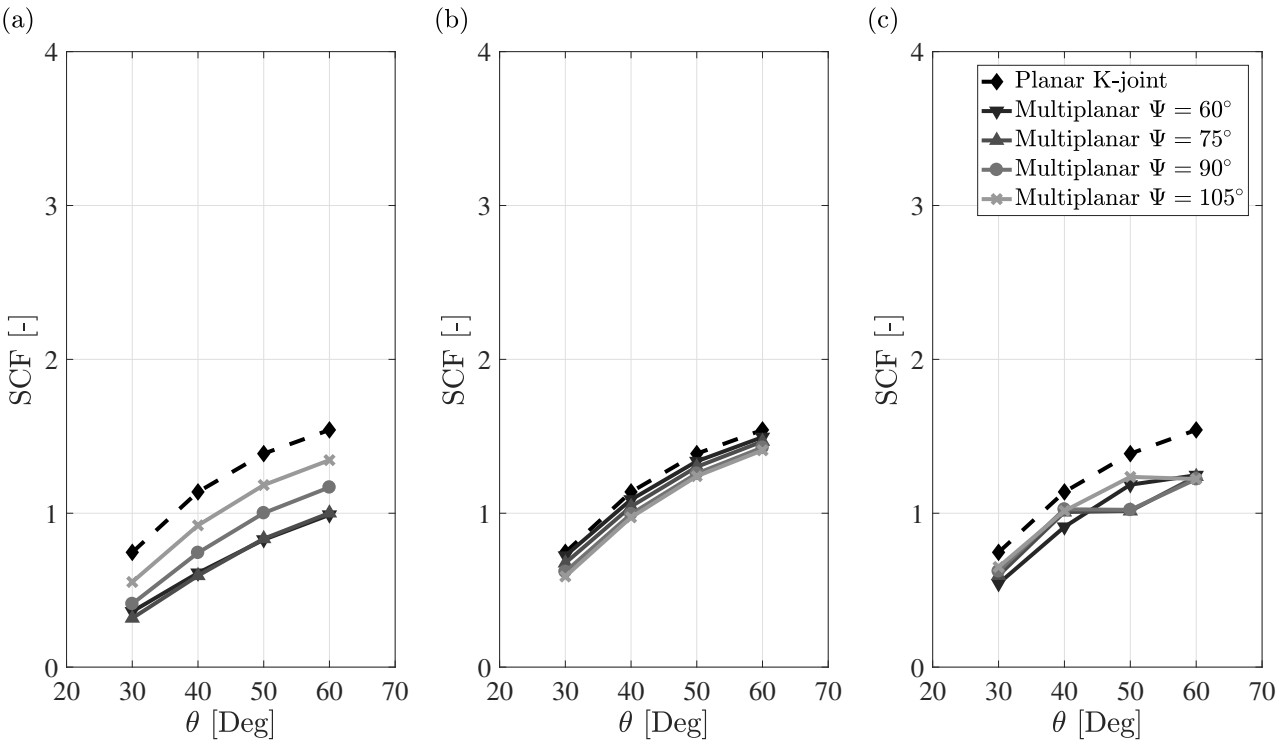

Figure B.5: *Influence of Ψ in the computation of the SCF of a tubular KK-joint under application of IPB at the braces in face 1 within a parametric investigation of θ. The subfigures correspond to the following load cases, which are described in Table 6.1: (a) IPB1($R_F = 1$) (b) IPB2($R_F = 1$) (c) IPB3($R_F = 1$). The following non-dimensional parameters are used to produce the data: $\beta = 0.4$, $\tau = 0.4$, $\gamma = 10$, $\zeta = 0.5$.*

C | Results of the NSCF investigation

In Chapter 7, the effective notch stress approach was investigated. An algorithm for the employment of this concept in the fatigue assessment of tubular joints was developed, making use of the sub-modelling technique. A flow diagram used for the explanation of this method is collected in this Chapter of the Appendix, cf. Figure C.1. Moreover, some of the results that were discussed in that chapter are presented here. Table C.1 shows the dimensions of the weld profiles, used to build the global model analyzed in Section 7.2. Tables C.2 and C.3 collect, respectively, the NSCF and hot-spot SCF results of that section.

Table C.1: *Definition of the weld profile at various sections around the weld for the creation of the global model that is studied in Section 7.2. The parameters used in the definition are described in Figure 7.11.*

Φ [Deg]	**z_{Co} [mm]**	**z_{Bo} [mm]**	**z_{Ci} [mm]**	**z_{Bi} [mm]**
-180	8	15	4	15
-150	6	15	4	15
-120	6	15	8	15
-90	6	15	8	15
-50	4	15	8	15
-30	4	15	10	15
0	4	15	12	15
30	4	15	10	15
50	4	15	8	15
90	6	15	8	15
120	6	15	8	15
150	6	15	4	15
180	8	15	4	15

Table C.2: *NSCF computed at eight positions around the weld and for six different load cases (LC1-LC6). The following non-dimensional parameters are used: $\beta = 0.5$, $\tau = 0.6$, $\gamma = 20$, $\theta = 45°$, $\zeta = 0.3$.*

Φ [Deg]	LC1	LC2	LC3	LC4	LC5	LC6
0	3.76	2.14	0.00	3.42	1.98	0.00
45	2.87	1.33	2.18	5.23	1.73	2.90
90	3.17	0.75	5.98	6.66	0.19	5.12
135	3.68	3.42	3.83	4.80	3.27	3.10
180	2.78	4.05	0.00	2.38	4.13	0.00
225	3.68	3.42	3.25	4.80	3.27	2.62
270	3.17	0.75	4.71	6.66	0.19	4.01
315	2.87	1.33	1.54	5.22	1.73	2.16

Table C.3: *Hot-spot SCF computed at eight positions around the weld and for six different load cases (LC1-LC6). The following non-dimensional parameters are used: $\beta = 0.5$, $\tau = 0.6$, $\gamma = 20$, $\theta = 45°$, $\zeta = 0.3$.*

Φ [Deg]	LC1	LC2	LC3	LC4	LC5	LC6
0	2.40	1.76	0.00	3.13	1.78	0.00
45	2.12	1.20	1.07	3.70	1.49	1.67
90	1.89	0.23	3.14	3.40	0.00	2.66
135	1.11	1.04	1.30	1.54	1.01	1.03
180	0.80	1.15	0.00	1.15	1.12	0.00
225	1.11	1.04	1.30	1.54	1.01	1.03
270	1.89	0.23	3.14	3.40	0.00	2.66
315	2.12	1.20	1.07	3.70	1.49	1.67

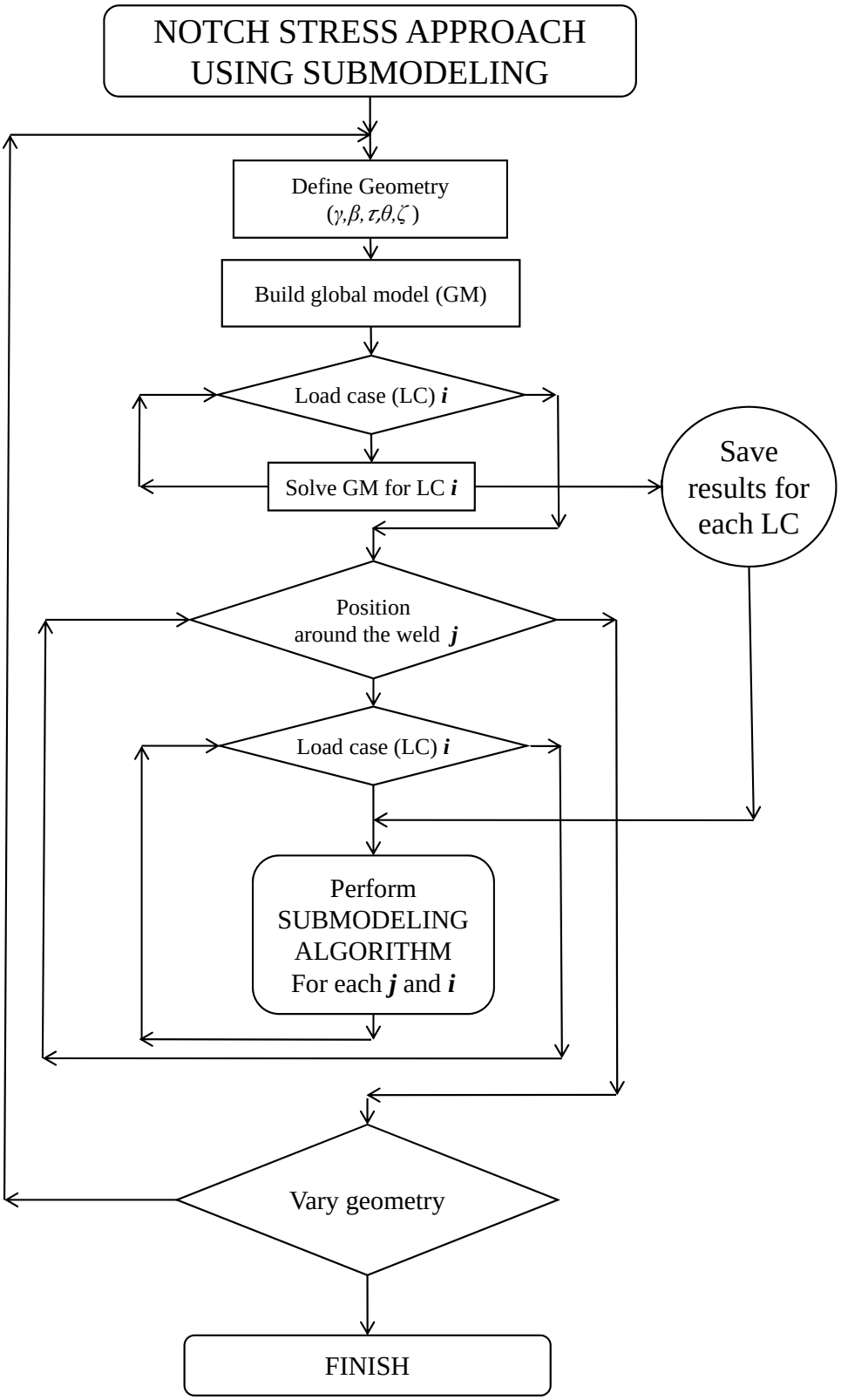

Figure C.1: *Flow diagram of the approach followed to assess the notch stress concentration factor using the sub-modelling technique.*